Reservoir Quality of the Stø Formation in the Hammerfest Basin, Southwestern Barents Sea

The role of initial composition of sediments and diagenesis

Kristoffer Løvstad

Master Thesis in Geosciences
Petroleum Geology and Petroleum Geophysics
30 credits

Department of Geoscience
Faculty of Mathematics and Natural Sciences

UNIVERSITY OF OSLO

01.06.2016

Reservoir Quality of the Stø Formation in the Hammerfest Basin, Southwestern Barents Sea

The role of initial composition of sediments and diagenesis

Kristoffer Løvstad

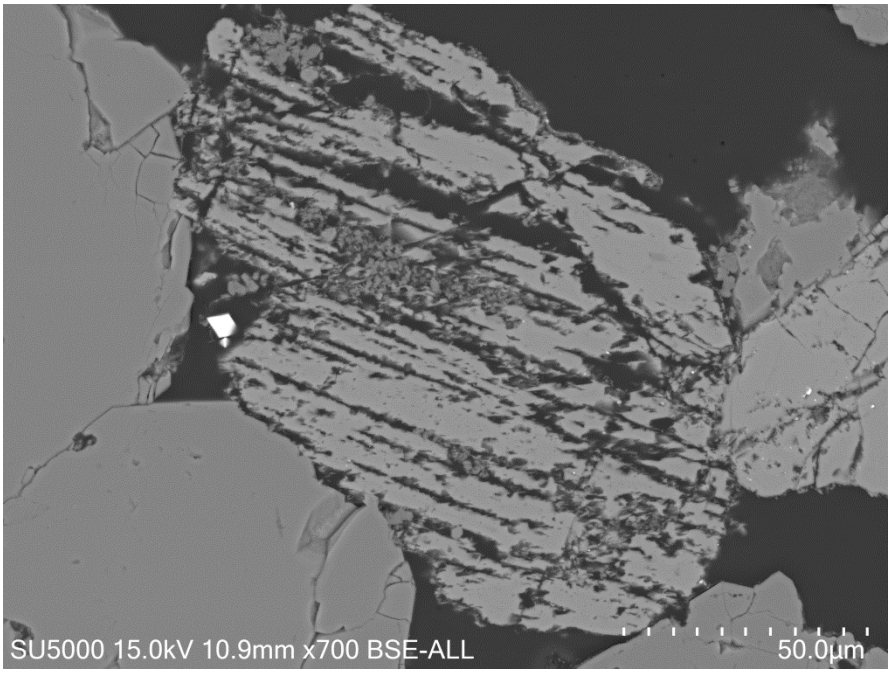

Master Thesis in Geosciences
Petroleum Geology and Petroleum Geophysics
30 credits

Department of Geoscience
Faculty of Mathematics and Natural Sciences

UNIVERSITY OF OSLO

01.06.2016

Reservoir quality of the Stø formation in the Hammerfest basin, Southwestern Barents sea – the role of initial composition of sediments and diagenesis

Kristoffer Løvstad

Supervisor: Jens Jahren

http://www.duo.uio.no/

Print: Reprosentralen, University of Oslo

Acknowledgements

First and foremost I would like to thank my supervisor, Professor Jens Jahren for his guidance in writing this thesis.

Further I would like to thank Lina Hedvig Line for her valuable support with the optical microscopy of thin sections, and Berit Løken Berg for the assistance with the SEM analyses.

The importance of the support and encouragement from my good friends at the geology department cannot be understated. I would especially like to thank Henrik N. Hansen, Jørgen A. Hansen and Hans Martin Kaspersen for their close friendship that has lasted from our first week of studies.

A big thank you to my family for all their support.

June 2016

Kristoffer Løvstad

Abstract

Reduction of porosity in sandstones with increasing burial is a function of mechanical compaction causing reorganization and crushing of grains with increasing pressure, and chemical compaction, mainly precipitation of authigenic quartz cement as temperatures reaches 70-80 ºC and above. The amount of mechanical compaction is governed by the initial lithological and textural features of the sediments. The precipitation of authigenic quartz can be reduced if efficient grain coats exist on detrital quartz grains.

This study investigates the parameters related to the reservoir quality of the Stø formation, the processes occurring during burial, the initial composition of the sediments and how they relate.

Well data and thin section samples from the Stø formation the two wells, 7120/2-3S and 7120/12-2, situated in the western parts of the Hammerfest basin in the Southwestern Barents Sea were examined using a petrographical and petrophysical approach. The well logs were utilized in a petrophysical investigation, and thin sections were investigated using optical microscopy and scanning electron microscope.

The sandstones of the Stø formation were seen to consist of highly matures quartz arenites with the major difference in initial composition between the units being the clay content, related to the depositional setting. The depositional settings observed ranged from upper shoreface beach/barrier bar deposits to more distal offshore deposits.

The Stø formation in well 7120/2-3S have been subjected to more extensive burial and higher temperatures resulting in the formation of more quartz cement than the formation in well 7120/12-2. The Stø formation in well 7120/2-3 consisted of a lower unit of consistently clean sands with porosities around 12-15% and significant quartz cement, and an upper unit with higher porosities of around 15-18% and less quartz cement interpreted to be caused by allogenic grain coats corresponding to the higher clay content. The Stø formation in well 7120/12-2 consisted of two clean sandstone units in the upper and lower parts of the formation with good porosities of 20-25% and a more extensive unit with higher clay content and frequent clay laminated horizons most likely reducing vertical permeability.

Table of contents

Chapter 1: Introduction

1.1 Introduction

The aim of this master thesis is to gain an understanding of the reservoir quality, and its distribution, within the Stø formation in the Hammerfest basin in the Southwestern Barents Sea area. This thesis is one of two master thesis related to the reservoir quality of the Stø formation. The work on this thesis has been undertaken over 5 months in the spring of 2016.

The properties of a sandstone reservoir at depth are the result of its initial composition governed by provenance, climate, transport and depositional setting, and subsequent alteration by mechanical and chemical compaction. The Barents Sea area is structurally complex with an intricate geological history. The uplift during the Cenozoic means that potential reservoirs that can presently be situated at shallow to intermediate depth may previously have been subjected to extensive chemical compaction at greater depth. Understanding the factors governing the ultimate reservoir quality at depth will mean that better predictions of the reservoir properties can be made prior to drilling.

1.2 Purpose and methods

The purpose of this thesis is to provide an estimate of the reservoir quality of the Stø formation and its correlation with the burial history and initial composition of the sediments. The characterization of the Stø formation was performed by the analysis of petrophysical well log data and petrographical analysis of thin section samples. The petrographical analysis consisted of the use of optical microscopy and scanning electron microscope with cathode luminescence ability.

1.3 Study area

The study area is located within the Hammerfest basin in the Southwestern Barents Sea on the Norwegian continental shelf. The data available for this thesis comes from two wells drilled in the Western parts of the Hammerfest basin; 7120/2-3S and 7120/12-2. Well 7120/2-3S is situated in the Northwestern end of the Hammerfest Basin close to the Loppa High and the Asterias fault complex, well 7120/12-2 lies towards the southwestern end of the Hammerfest basin towards the Finnmark Platform and the Troms Finnmark fault complex (fig.1-1)

Petrophysical well logs and a total of 20 thin section samples where available from the two wells (table B1 in appendix B and tables C1 & C2 in appendix C).

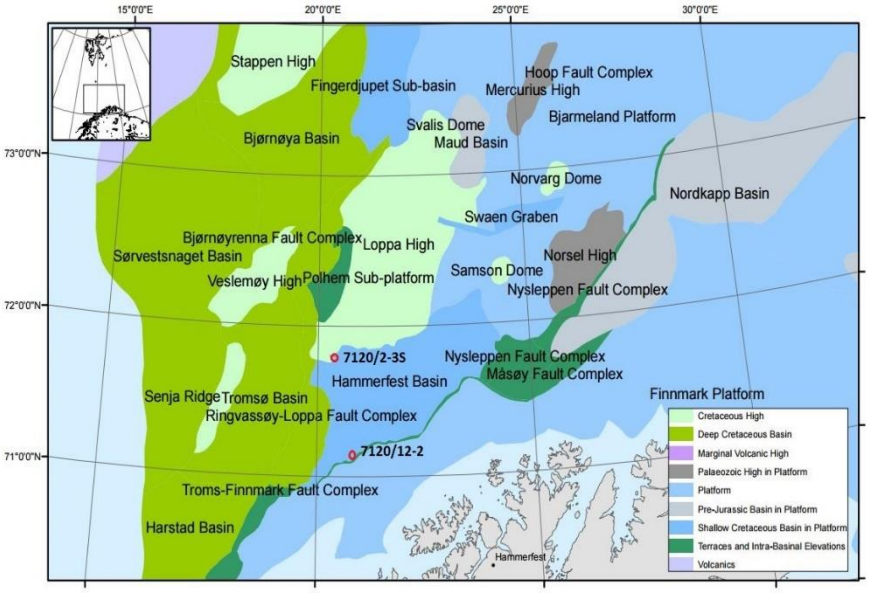

Figure 1-1. The Southwestern Barents Sea with major structural elements and location of wells. Modified from (Halland et al., 2013)

Chapter 2: Geological Setting

2.1 Introduction

This chapter provides an overview of the present geological setting and the structural evolution of the Southwestern Barents Sea, as well as a brief summary of the stratigraphy of the study area.

Several papers exist regarding the structural evolution of the Southwestern Barents Sea e.g. (Faleide et al., 1984); (Gabrielsen et al., 1990); (Gudlaugsson et al., 1998); (Worsley, 2008). Furthermore, the ATLAS – geological history of the Barents Sea (Smelror et al., 2009) and references given therein provide further reading on this topic.

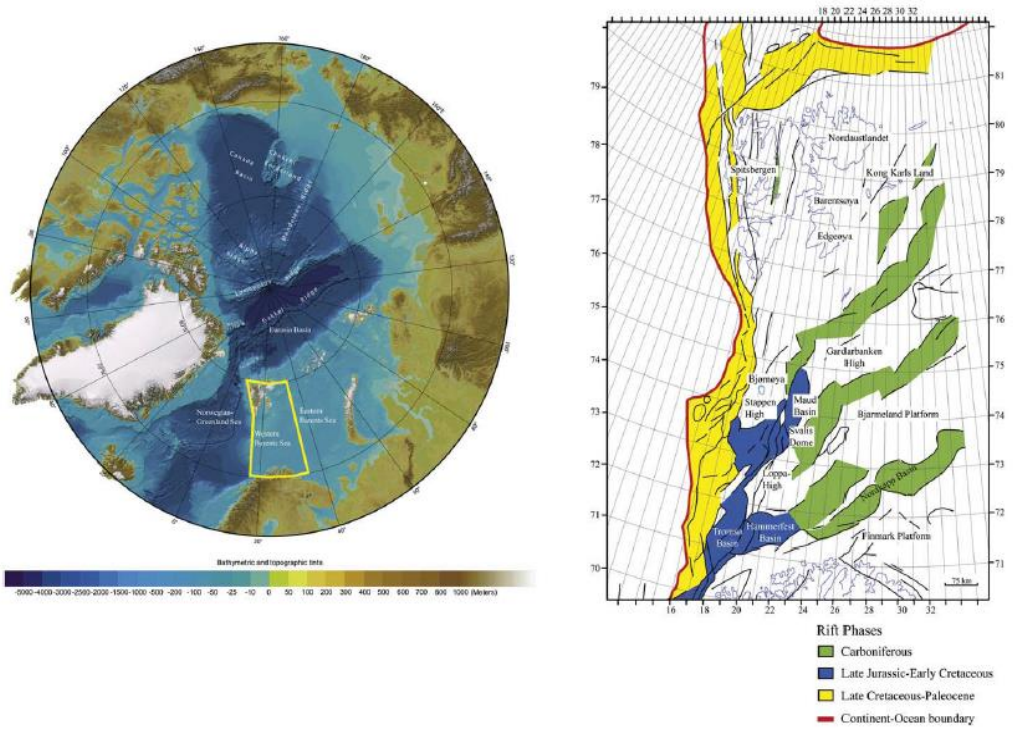

Figure 2-1. The location of the Western Barents Sea showed with yellow outline in left of the figure. The location and timing of major rift events on the right. (Glørstad-Clark et al., 2010)

2.2 Present Setting

The Barents Sea is an epicontinental platform situated on the Northwestern flank of the Eurasian continental shelf. The shelf area is bounded by two passive margins in the North and West, The Eurasian basin and Norwegian – Greenland Sea respectively. The Barents Sea is situated between Svalbard and Franz Josef Land to the North and the Northern Norwegian coast and Kola Peninsula to the South. It continues in the east to the Russian island of Novaya Zemlya, and to the continental slope of the Norwegian – Greenland Sea in the West. (Faleide et al., 1984). The western Barents Sea (fig. 2-1) has a more complex geometry than the eastern part (Henriksen et al., 2011). The western Barents Sea can be further divided into three geological settings: 1: an E-W trending province with several smaller basins and highs between Northern Norway and up to ca. 74°N. 2: An elevated platform area to the north up to the Svalbard archipelago and 3: Western continental margin (Faleide et al., 1984).

Between Norway and Svalbard, the Barents Sea consists of a continuous shelf area that is mainly covered by thick upper Paleozoic to Cenozoic sediments overlying metamorphic basement of Caledonian origin (Larssen et al., 2002). Generally upper Paleozoic sediments consists of mixed carbonates, evaporates and clastics, and Mesozoic to Cenozoic deposits consists of mainly clastic deposits (Faleide et al., 2015)

2.2.1 The Hammerfest Basin

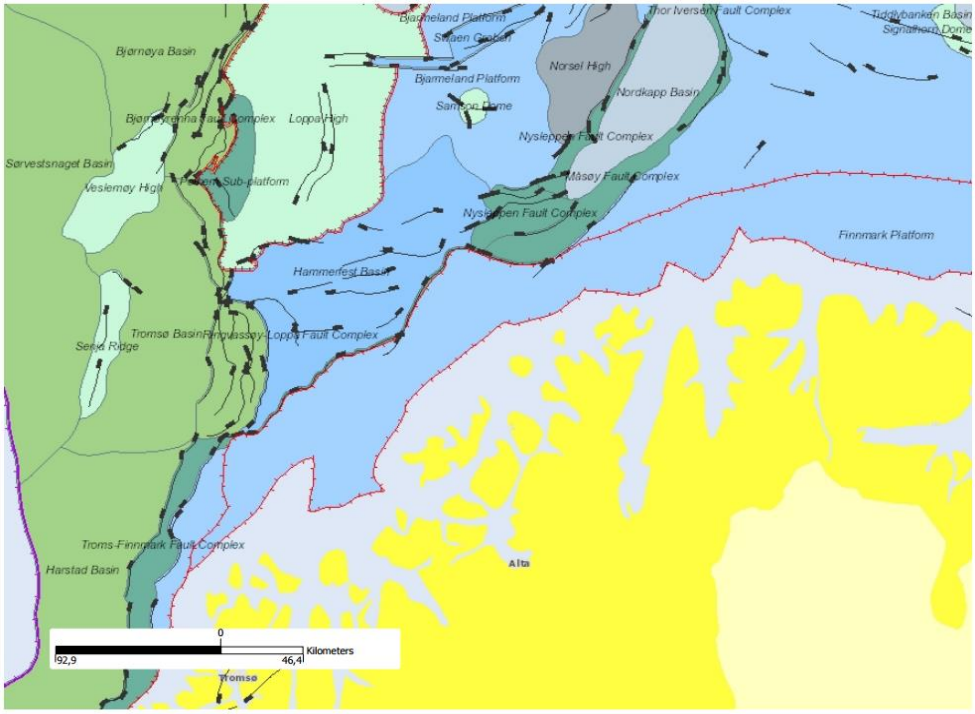

Figure 2-2. The location of the Hammefest basin and surrounding structures. Acquired from NPD fact maps (http://gis.npd.no/factmap)

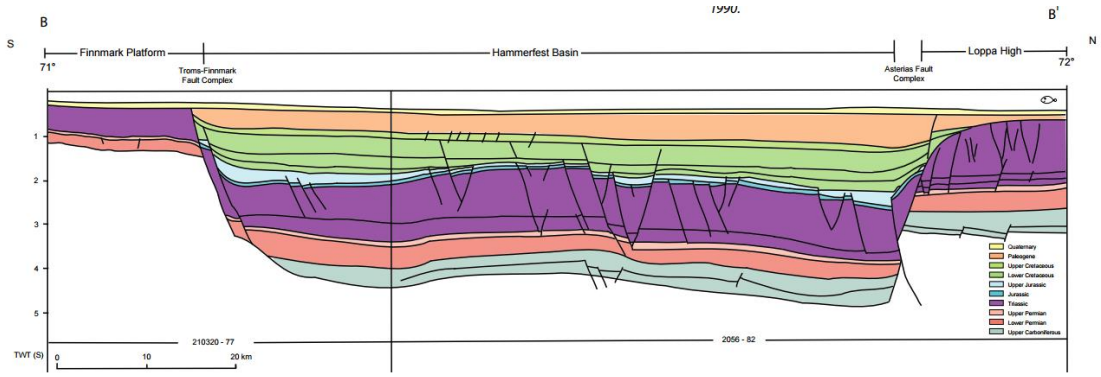

Figure 2-3. Cross section of the Hammerfest basin; from the Finnmark platform in the south to the Loppa High in the North from (Halland et al., 2013); modified from (Gabrielsen et al., 1990)

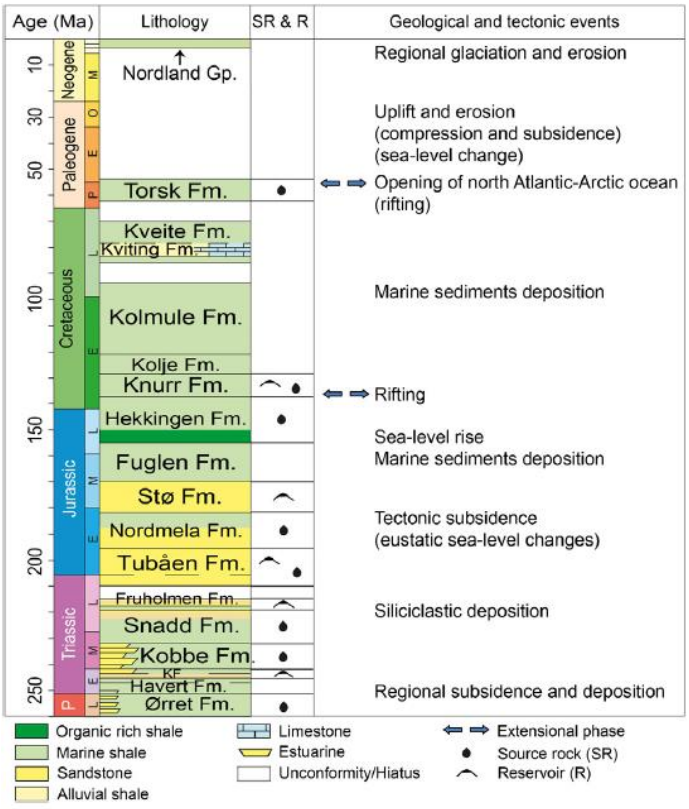

Figure 2-4. Lithostratigraphic chart of the Hammerfest basin with potential source rocks and reservoirs marked. On the right is an overview of major geological events (Rodrigues Duran et al., 2013) modified from (Ohm et al., 2008).

The Hammerfest basin is situated in the southern parts of the Barents Sea, just to the North-west of the Norwegian mainland, approximately 100 kilometers to the north of the town of Hammerfest (fig. 2-2). The Hammerfest basin has a general strike trend of ENE-WSW (Faleide et al., 1984, Gabrielsen et al., 1990) and is approximately 150km long and 70km wide and shows a graben like feature (Faleide et al., 1984). It is situated between the Finnmark platform in the south – separated by the Troms-Finnmark fault complex, and the Loppa high to the north – separated by the Asterias fault complex. In the west its limit with the Tromsø basin consists of the southern segment of the Ringvassøy-Loppa fault complex. The eastern limit is a flexure against the Bjarmaland platform (Gabrielsen et al., 1990). The Hammerfest basin is a relatively shallow basin with an estimated depth to basement averaging around 6-7 kilometers and containing a stratigraphy as showed in figure 2-4.

The basin can be further separated into a western and eastern sub basin, separated by the Trollfjord-Komagelv fault system. With the eastern parts appearing to be less affected by

faulting and showing more characteristics of a sag basin (Gabrielsen et al., 1990). The basin contains a complex geometry of W-NW trending faults, and these along with a central dome running along the strike of the basin make up the basins large scale internal structure (fig. 2-3) (Larssen et al., 2002).

The basin was probably established by late Carboniferous, but with main subsidence and formation of present tectonic features occurring in Triassic to early Cretaceous (Larssen et al., 2002). Basin development most likely peaked around mid-Cretaceous. A thin condensed section of shales from upper-Cretaceous and lower Tertiary is also preserved in spite of the Tertiary uplift (Larssen et al., 2002). The complex geometry of W-NW trending faults, and the central dome running along the strike of the basin are most likely remnant of late Jurassic tectonism (Larssen et al., 2002).

2.3 Evolution of the Southwestern Barents Sea

The structure of the present day Southwestern Barents Sea with its intricate geometry of highs, platforms and smaller basins is the result of a complex geological history, from the Caledonian orogeny in Devonian – Permian time and subsequent orogenic collapse (Smelror et al., 2009), to the several episodes of extensional rifting and lithospheric thinning occurring over a large time period from late Paleozoic to Early Tertiary (Faleide et al., 2015). Large scale processes from several hundred million years of continental drift, with the Barents Sea region of the Eurasian plate having moved from equatorial zones in middle Devonian – early Carboniferous to present day high latitudes Worsley (2008), has also exerted a massive influence on the evolution leading to the present day geometry and stratigraphy of the Barents Sea area (Worsley et al., 1988, Smelror et al., 2009).

2.3.1 Paleozoic

The Caledonian orogeny started in the middle Ordovician and reached a maximum in the Silurian, closing the Iapetus Ocean that once separated Eurasia from Laurentia (Henriksen et al., 2011). Following the compressional setting of the Caledonian Orogeny, Devonian to early Carboniferous was characterized by widespread intracratonic rifting that mostly followed the Caledonian structure (~N-S trend) (Smelror et al., 2009). The Lower to early upper carboniferous depositional basins were extensional basins, with wide downwarps and narrow

grabens in the ~300km wide rift zone trending N-S with a length of approximately 600km (Faleide et al., 2015). Following the setting of regional extension in the western Barents Sea, sea areas covered most of the shelf and Upper Carboniferous – lower Permian cold water carbonate platform covered much of the area (Faleide et al., 1984, Worsley, 2008, Smelror et al., 2009). In late Paleozoic thick evaporites where deposited locally in large basins that developed in deep seated sutures, whereas sabkhas and warm water carbonates where deposited on the platform areas (Worsley, 2008). From the late Carboniferous the eastern parts of the Barents Sea have been dominated by largely tectonic quiescence and stable platforms, whereas the western Barents Sea area continued to be tectonically active in Mesozoic to Cenozoic times (Gabrielsen et al., 1990).

2.3.2 Mesozoic

In late Permian - early Triassic renewed faulting, uplift and erosion affected the western Barents Sea in a narrow N-S trend (Faleide et al., 2015), with the following mid – late Triassic generally characterized by post rift thermal subsidence (Smelror et al., 2009). Early Triassic is characterized by a regional deep water setting in much of the Barents Sea (Faleide et al., 2015) and lower to middle Triassic deposits consists of transgressive – regressive cycles of marine, deltaic and fluvial clastics (Smelror et al., 2009). In late mid Triassic large parts of the Western Barents Sea was covered by alluvial and coastal settings, probably owing to the uplift of other parts of the Barents Sea area, and the Uralide orogeny in the East (Smelror et al., 2009, Faleide et al., 2015).

At the end of Triassic there was still uplift and erosion to the east and a westward progradation of the coastline, with marine conditions limited to the westernmost parts of the Barents Sea (Smelror et al., 2009). In early to middle Jurassic there was a continental and marine setting (fig.2-5) following a global sea level rise and sandstone deposits dominated, forming what is now the main targeted reservoirs in the SW Barents Sea among them the Stø formation (Smelror et al., 2009).

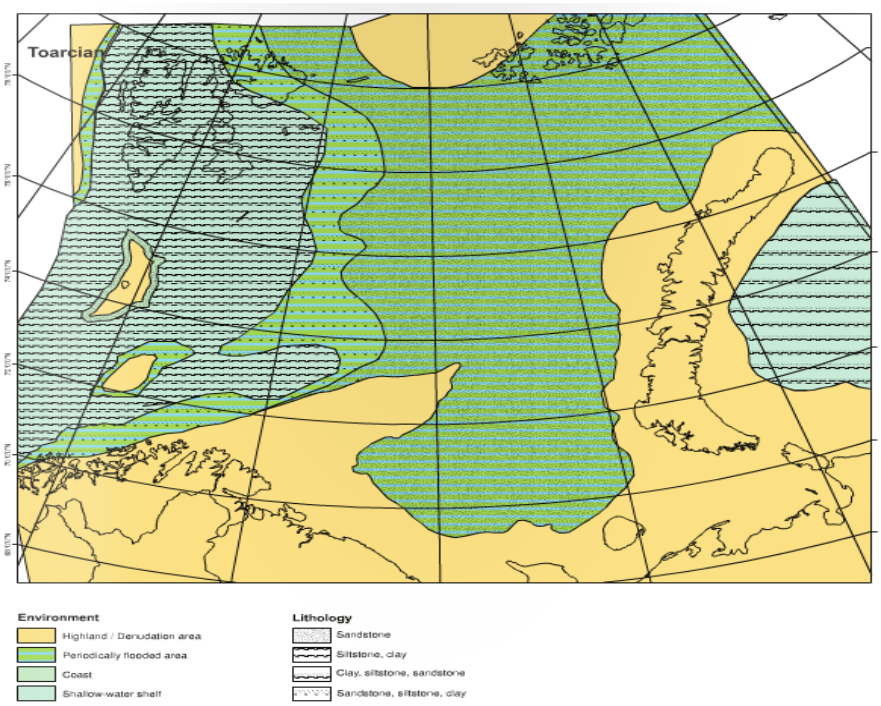

Figure 2-5. The environment of The Barents Sea area in Toarcian (Smelror et al., 2009).

Rifting again commenced in late middle Jurassic and continued into early Cretaceous (Smelror et al., 2009, Faleide et al., 2015) with the top of the shallow marine sandstones of early to middle Jurassic possibly marking the onset of the late Mesozoic rifting (Faleide et al., 2015).

Transgressional events in late to end of Jurassic submerged the entire shelf and shallow to deep marine shelf sedimentation dominated. With the dark organic rich shales of the Hekkingen Fm. Being deposited in late Jurassic (Smelror et al., 2009).

Rifting continued in the Southwestern Barents Sea in the cretaceous forming deep basins such as Harstad, Tromsø, Bjørnøya and Sørvestnaget basins (Smelror et al., 2009).

In the Cretaceous tectonic uplift in Northern Barents Sea areas set up a southwards progradation with large amounts of sediments transported from the uplifted northern areas and southwards into the deep basins in the south-west, eventually setting up large prograding deltas from the north. Sediment origin eventually more from North-East in late lower Cretaceous (Smelror et al., 2009).

2.3.3 Cenozoic

In late Cretaceous the final major rift event in the Western Barents Sea opened the Norwegian-Greenland Sea, with Paleocene-Eocene transition being the time of breakup of the North Atlantic margins (Smelror et al., 2009). The Paleocene-Eocene continental strike-slip system was followed by development of passive shear margin, with break up in early Oligocene, and continuing separation of Barents Sea shelf and Greenland. Eventually in Miocene creating a North Atlantic Marine passage (Smelror et al., 2009).

In the Eocene as a result of the latest rift event and uplift, the major parts of the Barents Shelf were stable uplifted hinterland, and major deposition was only occurring in the deep westernmost basins (Smelror et al., 2009).

The northern hemisphere saw an onset of glaciations in late Pliocene and in late Pliocene-Pleistocene uplift and erosion had a large impact on the Barents Sea shelf area with up 2-3 kilometers of sediments eroded from the northern platforms. There is thus a large unconformity between Mesozoic-Tertiary strata and the overlying glacial deposits (Smelror et al., 2009).

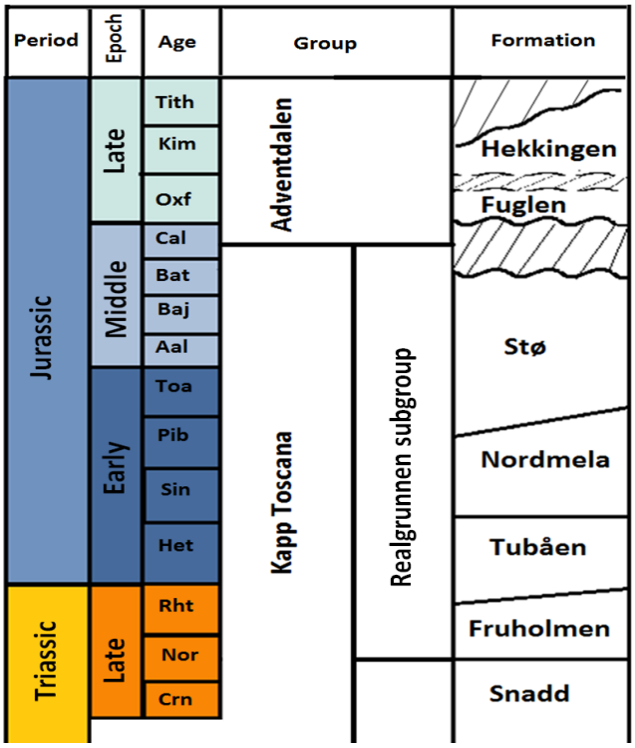

Figure 2-6. Late Triassic - Jurassic stratigraphy in the southwestern Barents Sea. Modified from (Worsley et al., 1988)

2.4 The Stø Formation

The Stø formation is a part of the Realgrunnen subgroup (fig. 2-6), and is of a Pliensbachian to Bajocian age. The sediments of the Stø formation is interpreted to have been deposited in a prograding coastal regime interrupted by several transgressive events marked by thin silt and shalestone layers, and generally consists of very mature sandstones that are moderately to well sorted (Worsley et al., 1988). The sandstones of the Stø formation usually shows a quartz content of 91 to 100% (Bergan & Knarud 1993). The mature sandstones probably reflecting the extensive reworking owing to the shallow marine/coastal depositional environment (Worsley, 2008).

Olaussen et al. (1984) divided the formation into three sections based on appearance in gamma ray logs and core samples; The lowermost unit, overlying the Nordmela formation consists mainly of shallow marine sediments and shows a lateral variation in energy regimes from possibly tidal deposits in the lowermost parts of the formation in the westernmost parts of the basin to shoreface/foreshore and eventually more open marine settings towards the

North-East. The second unit is marked by an increase in gamma ray readings owing to an increasingly more distal setting due to transgression. The unit consists of fine grained argillaceous quartz, fine to medium grained quartz arenites and silt – to mudstones. Mudstone unites are laterally extensive and probably represents intervals of maximum transgression. The third and uppermost unit is marked by the transition to sandstone from the more matrix rich sediments of the upper parts of the underlying unit. This unit is interpreted as shallow marine sediments deposited in a progradational regime. The Stø sandstones in general have good reservoir properties, the major exceptions being areas with a greater burial (before uplift/erosion) as in parts western Hammerfest basin, where the quartz overgrowth can be extensive (Worsley 2008), and in units that have a higher presence of silt – and mudstones, hampering especially the vertical permeability of the rock (Olaussen et al., 1984).

2.5 Early to middle Jurassic depositional system

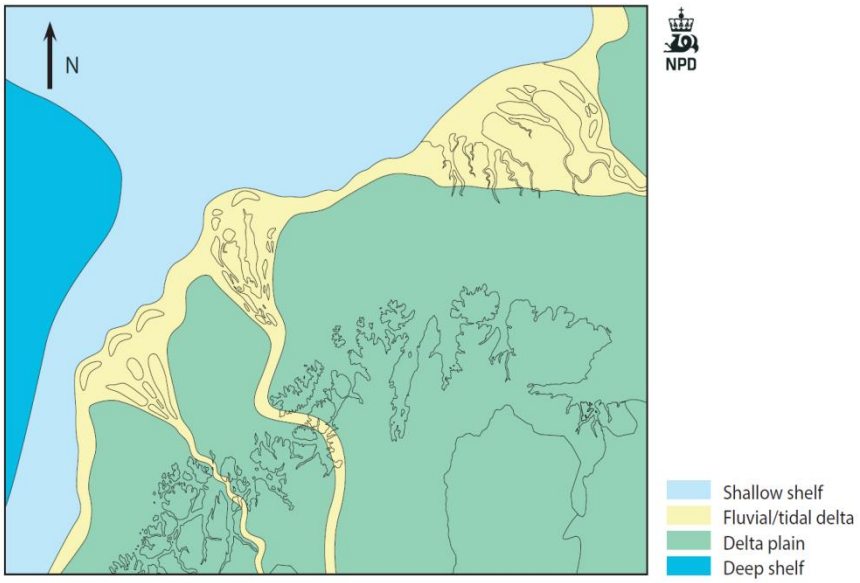

Figure 2-7. Concept of the depositional setting in the early stages of deposition of the Stø formation (Halland et al., 2014).

As mentioned the depositional system in the early to middle Jurassic (fig. 2-5, 2-7 &2-8) were created as a result of the uplift in the eastern parts of the Barents Sea from ca. mid to late Triassic and the subsequent sea level rise in early – mid Jurassic (Smelror et al., 2009). The rising sea level covered large areas of a quite stable platform, owing to the relative tectonic

quiecence in the early to middle Jurassic (Faleide et al., 1984). This also resulted in a fine balance between sediment influx and basin subsidence (Olaussen et al., 1984).

The stable platform meant that the major influence on an overall change in depositional setting were the change in sea level.

The provenance area for the sediments deposited was most likely the uplifted areas to the East and South, and Olaussen et al. (1984) suggested regional Caledonian and Precambrian plutonic and metamorphic rocks and Upper Paleosoic sedimentary rocks as the provence of the sandstones of the stø formation.

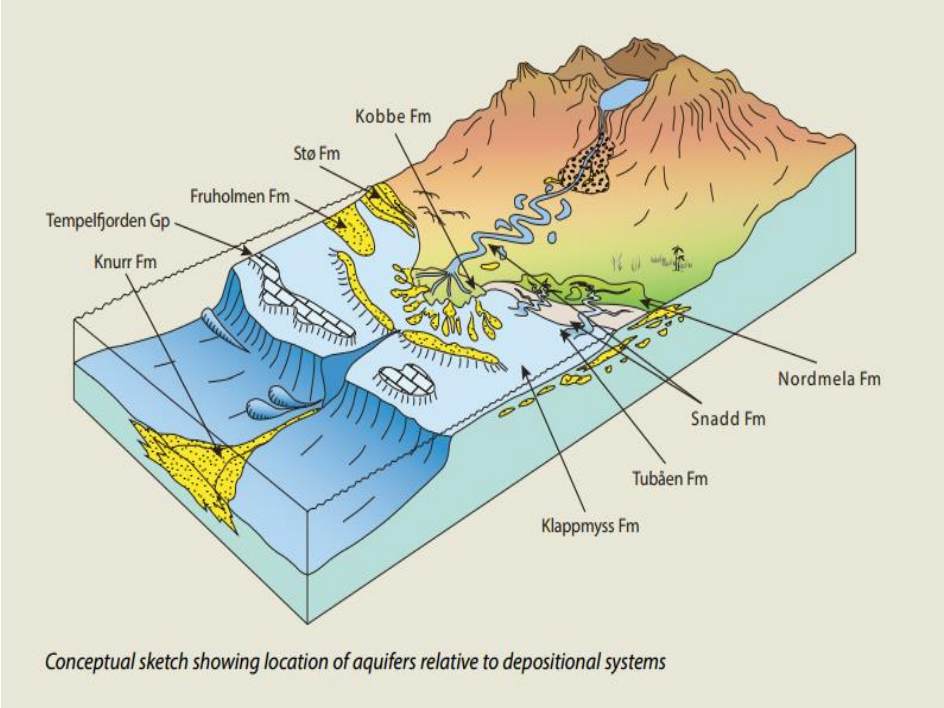

Figure 2-8. Conceptual sketch of depositional systems for certain Southwestern Barents Sea formations (Halland et al., 2014).

2.6 Uplift

The Barents Sea area has been substantially uplifted from a suggested maximum burial possibly as early as Eocene, or Oligocene (Baig et al., 2016) and most uplift is believed to have occurred during the Cenozoic (Dimakis et al., 1998, Cavanagh et al., 2006, Ohm et al., 2008, Baig et al., 2016).

The amount of uplift varies across the Southwestern Barents Sea, generally increasing towards the North-East, with estimates of 800-1400m uplift in the Hammerfest basin and up to 2400m at certain areas of the Bjarmeland platform (Baig et al., 2016).

Three major episodes have been commonly suggested for exhumation in the Barents Sea; Late Paleocene, Oligocene-Miocene and Late Pliocene – Pleistocene(Cavanagh et al., 2006).

Cavanagh et al. (2006) suggested Late Pliocene – Pleistocene exhumation as a result of massive erosion from the ice sheets as the most major factor in uplift, suggesting that the area corresponding to where the Snøhvit field is situated to have been uplifted ~900m over a period of just 1 million years. However Baig et al. (2016) found a large difference in the average erosion estimates in their study to the amount of glacial erosion determined by mass balance, suggesting that there has been a large amount of uplift also occurring before glaciation.

2.7 Petroleum system of the Hammerfest Basin

The Barents Sea contains multiple source rocks, with source rocks being identified at several stratigraphic layers from the carboniferous to cretaceous. With these multiple source rocks and hydrocarbon generation occurring over a large time scale it can be said to represent an overfilled petroleum system (Ohm et al., 2008). The several episodes of uplift and erosion mentioned are responsible for the relatively small amount of hydrocarbons present today (Ohm et al., 2008). Uplift also enabled the possibility for petroleum to be redistributed over large lateral distances (Ohm et al., 2008). The major consequences of the large amount of uplift in the Cenozoic are the possibility for stopped petroleum generation from source rocks, lower relative pressures in reservoirs causing expanding gas to possibly expel oil and fault reactivation that could destroy existing seals (Rodrigues Duran et al., 2013).

A good example of the vast petroleum generation that has occurred is the amount of wells drilled showing traces of hydrocarbons. Of 67 wells drilled by the year 2008 nearly all showed at least traces of hydrocarbon (Ohm et al., 2008).

Most discoveries so far in the Barents Sea have been under filled gas fields with some also showing thin oil legs (Rodrigues Duran et al., 2013).

The petroleum Plays in The Hammerfest basin so far identified are of Triassic and Lower-middle Jurassic age. The Triassic play is in the Hammerfest basin is present in the eastern parts with the depositional settings being Fluvial, shallow marine and deltaic. The reservoirs consists of lower middle and upper Triassic sandstones, with the source rock being Triassic shales, lower Carboniferous coals, upper Permian shales and lower Permian marls (Rodrigues Duran et al., 2013). The lower – middle Jurassic play have a depositional environment of fluvial, deltaic to shallow marine. The reservoirs consists of sandstone of early-middle Jurassic age, and the source rock being upper Jurassic shales, (Hekkingen Fm.) lower Jurassic coals and carbonaceous shales (Rodrigues Duran et al., 2013)

Chapter 3: Theoretical background

3.1 Introduction

For a certain lithology the porosity will unavoidably decrease with increased burial as a result of the increasing pressure and temperature acting upon the sediments, but different lithologies may show different compaction trends (Bjørlykke and Jahren, 2012). The compaction of sediments can broadly be divided into two domains; the mechanical compaction domain, in which the porosity decreases as a result of grain reorganization and crushing under increasing effective pressure, and the mechanical compaction domain where the porosity gets reduced mostly as a function of precipitation of authigenic cement, mainly governed by temperature (Bjørlykke, 1999), and the relative bulk volume reduction caused by the dissolution of detrital grains (Oelkers et al., 2000). As mentioned, even though the pressure and temperatures exerted on various lithological units is the same they may show significantly different compactional trends e.g. (Chuhan et al., 2002, Fawad et al., 2011, Ehrenberg, 1993, Storvoll et al., 2005). The different diagenetic processes is therefore also controlled to various degree by the lithology, and the properties of a sandstone reservoir can be said to be determined by the initial mineralogical and textural composition of the sediments; governed by provenance, climate, transport and the depositional setting, and any subsequent alteration resulting from increasing pressure and temperature during burial e.g. (Bjørlykke et al., 1989). This chapter aims to describe the main processes thought to be dominant in governing the ultimate reservoir quality, from initial deposition and through subsequent burial.

3.2 Sedimentology

3.2.1 Initial composition

The initial composition of the sediments relates to the framework mineralogy, the textural features and type and amount of any matrix present. The initial mineralogical and textural composition of sediments is determined by several factors, from the initial rocks weathered, transport, possibly multiple episodes of intermittent deposition and renewed erosion, and any reworking after deposition. These factors are mostly governed by the climate, paleo geography and the tectonic activity of the area. Clean sandstones i.e. mature quartz rich sands - quarts arenites - generally forms as a result of longer transport and/or several episodes of deposition and erosion removing the easier to remove minerals as clay minerals, carbonates

and then feldspars, and/or extensive reworking after deposition, (Bjørlykke and Jahren, 2015).

Presence of allogenic clay minerals can have a large impact on the reservoir quality, allogenic clays are clay deposited simultaneously as sands, or introduced immediately after burial (Wilson and Pittman, 1977). The distribution and minerology of allogenic clays is an important parameter that influences subsequent diagenesis e.g. during mechanical compaction where lithologies with a higher content of more ductile grains such as clays may compact more readily (Fawad et al., 2011). Clay minerals present may also vastly impact the reservoir quality by enabling reactions as e.g. illite-chlorite, smectite-chlorite, smectite-illite, and as catalysts for quartz dissolution at stylolites and interfaces with quartz grains (Bjørkum et al., 1998). So clays can facilitate reactions that can be detrimental to the porosity and permeability of a reservoir, but also preserve porosity by acting as grain coats or precursor for grain coats. The individual processes are explained later in this chapter.

Allogenic clay in sandstones may occur in several manners as illustrated by (Wilson and Pittman, 1977) (fig.3-1)

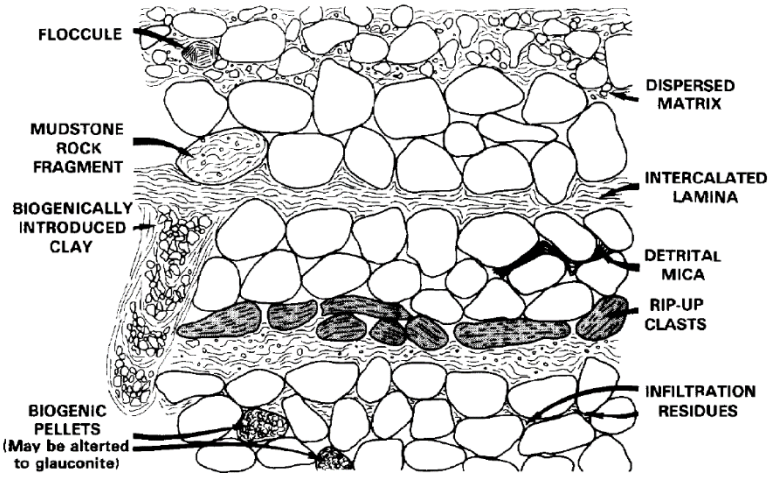

Figure 3-1. Modes of occurrence of allogenic clay in sandstones (Wilson and Pittman, 1977)

3.2.2 Relative importance of the initial composition of sediments during subsequent diagenetic alteration

The extent to which the depositional setting and initial composition of sandstones influences the alteration occurring during burial should be determined by examining what factors control the processes affecting a sediment with increasing temperature and pressure.

Fawad et al. (2011) performed experimental compaction of sands of different lithologies and textural composition to investigate the importance of the initial composition of sediments during mechanical compaction and found large variations in the compaction trends for varying textural and mineralogical compositions.

At the onset of chemical compaction and precipitation of quartz cement, discussed further in section 3.5.1, the relevance of the primary composition of the sediments relates primarily to whether the alteration and precipitation of minerals especially quartz cement occur in a mostly closed system where the components are sourced locally, or whether these can be transported over any significant distances.

Bjørlykke (1994) argued that for any significant quartz to be precipitated as a result of quartz being introduced from larger distances the flux of porewater would need to be larger than what is feasible under normal circumstances. Furthermore, he argued that if quartz cement where to originate in this manner the amount of cement precipitated would be a function of the flux of water, the more permeable layers would then be more heavily cemented. Bjørlykke and Egeberg (1993) showed that for 1% of quartz cement to be precipitated by advective flow it would require a flux of $10^8 cm^3/cm^2$ an unnaturally high flux in most cases.

Any major change in bulk composition of the sediments or formation of any significant secondary porosity can then only occur at shallow depths, either from reactions with sea water near the seafloor or from any eventual high porewater flux of meteoric water (Bjørlykke and Jahren, 2012). At depth beyond the reach of any significant pore water flow the reactions can then be seen as occurring in a closed system, and the relative significance of the initial provenance and facies of the sediments are therefore large especially for non isochemical reactions. (Bjørlykke and Jahren, 2012)

Accepting the relation of primary facies and provenance to the subsequent alteration during burial, a better estimation of reservoir quality can then be performed based on estimation of these initial parameters, something that for instance can be attempted by trying to reconstruct facies distribution from mapping the distribution and shape of lithological units in seismic profiles.

3.3 Diagenetic processes in sandstone

As mentioned the compaction of a rock unit is broadly divided into two domains based on the processes acting upon the rock; mechanical and chemical compaction. Several diagenetic processes act upon sandstones and different processes occur at different depths corresponding to various pressures and temperatures. The following sections have therefore been divided by defining three intervals of burial; shallow, intermediate and deep. Shallow burial is defined as immediately after deposition and down to a depth of 2-2.5 km, assumed to correspond to temperatures around ~80 °C where quartz cementation becomes noticeable (Bjørlykke and Egeberg, 1993). Intermediate burial is defined as being the interval from 2-2.5 km and down the transition to deep burial defined as where the reservoir quality is assumed to be severely reduced due to extensive quartz cementation, if not hampered by any porosity preserving mechanisms, and the illitization of kaolinite and K-feldspar if present assumed to correspond to temperatures of around 130 ºC (Bjørlykke et al., 1989).

3.3.1 Shallow burial

Immediately after deposition the sediments have the highest potential to change its bulk composition and can be said to exist in an open system where processes such as mineral dissolution, transportation of dissolved components and influx of groundwater under-saturated with respect to the minerals present occur (Bjørlykke, 2014). This potential to change the bulk composition gradually decreases with burial depth until the porewater flux diminishes to the point where it can be seen as a closed system. The flux of porewater is then too low such that any potential to transport minerals and ions in solution is low and the porewater reaches an equilibrium with minerals present as a response to the higher solubility of minerals with increasing temperatures (Bjørlykke, 1994).

3.3.1.1 Meteoric water flushing

The flow of meteoric water is mostly controlled by the geography of an area and the continuity and geometry of permeable rock bodies (Bjørlykke et al., 1989). Rainwater is initially under saturated with respect to minerals present in the sediments and is slightly acidic from reactions with CO_2 and SO_2 in the atmosphere forming carbonic acid; H_2CO_3 and sulphuric acid; H_2SO_4 (Bjørlykke and Jahren, 2015). The minerals that are most readily dissolved by meteoric water are carbonates for which the pore water will quickly reach equilibrium, and then feldspar and mica. Meteoric water flow is an important factor in shallow burial diagenesis as it facilitates reactions that are not isochemical, meaning that ions need to be supplied/and or removed in solution for the reaction to take place. One such reaction is the dissolution of feldspar and/or mica, and precipitation of kaolinite which requires a supply of water under saturated with respect to feldspar and mica, and a constant removal of the reaction products Na^+, K^+ and silica. The amount of dissolution of feldspar and mica, and amount of kaolinite precipitated are therefore a function of the flux of meteoric water (Bjørlykke et al., 1989). The reactions can be written as:

$$\underset{Feldspar}{2K(Na)AlSi_3O_8} + 2H^+ + 9H_2O = \underset{Kaolinite}{Al_2Si_2O_5(OH)_4} + \underset{Dissolved\ silica}{4H_4SiO_4} + 2K^+(2Na^+)$$

$$\underset{Mica}{2KAl_3Si_3O_{10}(OH)_2} + 2H^+ + 3H_2O = \underset{Kaolinite}{3Al_2Si_2O_5(OH)_4} + 2K^+$$

From (Bjørlykke and Jahren, 2015)

The leaching, especially of feldspar, will cause formation of secondary porosity, but as kaolinite will precipitate in the pores there is little net porosity gain, and some loss of permeability. The precipitation of kaolinite can also have further consequences for the reservoir quality at greater burial depths as kaolinite and K-feldspar becomes unstable at greater temperatures and will lead to precipitation of illite at temperatures above ~120-140 ºC e.g. (Chuhan et al., 2000).

3.3.1.2 Biogenic activity

Biogenic activity affects the sediments in several ways; they can cause textural alteration of the sediments by means of burrowing organisms that have the possibility to mix clay and sand layers reducing the porosity and permeability, or if the burrowing organisms destroy intercalated clay laminae the porosity may be reduced, but the vertical permeability can be improved. Calcareous organisms present will cause the formation of carbonate fragments and calcite cement, siliceous organisms are a source for silica (Opal A), which later can alter to Opal CT and in turn quartz, presence of organic silica can cause the formation of grain coating micro quartz at depth, preserving porosity e.g. (Ramm et al., 1997)

3.3.1.3 Carbonate Cementation

Carbonate cement forms at shallow burial depths mainly from biogenic carbonate present, and is very much linked to the depositional environment. (Saigal et al., 1987) The carbonate cement forms mainly due to the dissolution of organic carbonates and precipitates as calcite cement in the pore space or replaces the original biogenic carbonate containing fossils and then be recognized either as concretions or calcite layers. (Bjørlykke and Jahren, 2015)

3.3.1.4 Mechanical compaction

After sediments are deposited the weight of any subsequent overburden will increase the effective pressure exerted on the sediments. During burial the sediments loses porosity and hence bulk volume, at depth typically less than 2 – 2,5 kilometers which corresponds to temperatures below 70-90°C in basins with a geothermal gradient of 35°C/Km, this loss of porosity and bulk volume is mainly caused by mechanical compaction. Mechanical compaction alters the bulk volume and decreases the intergranular volume mainly by the rearranging of grain and as effective pressure increases grain crushing, mostly at grain contacts. The initial composition and texture of the sediments affects this process to a large degree and under experimental compaction of different sands Fawad et al. (2011) found large variations in porosity decrease and sonic velocity increase with depth. Their results showed that poorly sorted sands shows lower initial porosity than well sorted sands. Well sorted coarse sands compact more readily and show a larger increase in sonic velocity than fine sands of comparable lithology. Furthermore, quartz rich sands having more than 55% quartz,

shows a lower increase in sonic velocities with depth than less quartz rich sands, a result they postulated could be from the sintering and increased grain rearrangement in more ductile grains. The reason for the increasing loss of porosity in coarser grained sands is probably due to the lower relative surface area of grain contacts increasing the effective stress, less sorted sands also compact more readily as smaller grains can fill the void between larger grains (Chuhan et al., 2002)

The intergranular volume (IGV) of the sediments will mainly be determined by the amount of mechanical compaction as the formation of quartz cement prevents further mechanical compaction and the IGV will then remain fairly constant albeit the composition of it will change with more of the IGV being authigenic cement (Paxton et al., 2002).

3.4 Intermediate burial

Intermediate burial defined as the onset of chemical compaction marks an important transition in the evolution of the reservoir quality. The change from mechanical compaction domain to that of chemical compaction is quite abrupt as only a 2-4 percent of quartz cement will stiffen the rock sufficiently to resist any further compaction from the effective pressure caused by the weight of the overburden (Bjørlykke and Jahren, 2015).

3.4.1 Quartz cementation

In the chemical compaction domain, the precipitation of quartz cement is the single most important process responsible for the reduction of porosity in sandstones (Bjørlykke et al., 1989).

Cementation is generally caused by dissolution of unstable mineral phases and precipitation of more stable phases as the reactions are governed by thermodynamics and will be driven to more stable phases as temperature and pressure increases. The temperatures under diagenesis is however relatively low and relatively unstable phases may persist for a long period of time. Quartz cement seem to precipitate only at temperatures above 70-80°C and most forming at temperatures above 90-100°C (Bjørlykke and Egeberg, 1993). A question has long been to identify the source of quartz cement in basins. Assuming that the system is mostly behaving as a closed system, the sources needs to either be present in the porewater, as more unstable

phases as opal A, and opal CT, sourced from dissolution of quartz or as product of other mineral reactions. As the solubility of detrital quartz grains is probably the same as quartz cement assuming unbroken grains, there needs to be factors than enables the quartz to dissolve, pressure solution was believed to be the main way for this to occur; increasing solubility at grain contacts or at stylolites (Bjørlykke and Egeberg, 1993) but Bjørkum (1996) found that dissolution of quartz could occur at lower pressure than the overburden load, indicating that much of what was thought to be pressure solution may result from processes induced by the contact with mica and/or illite at stylolite interfaces, the illite/mica induced dissolution of quartz is also thoroughly discussed in the paper by Oelkers et al. (2000). Based on this precipitation of quartz cementation is quite independent of the pressure and are mainly dependent on temperature and the surface area available for precipitation (Oelkers et al., 2000). Walderhaug (1994) found the typical precipitation rates at 80 ºC to be ~ $1 * 10^{-20}$ moles/cm^2 to ~$5 * 10^{-19}$ moles/cm^2 at temperatures of 140 ºC.

The dissolution of quartz at stylolite or at least in the presence of mica and/or illite will then diffuse over some distance and precipitate on quartz grains (fig. 3-2) (Bjørkum et al., 1998). The distance of diffusion is another important factor and when Walderhaug and Bjørkum (2003) looked at the effect of stylolite spacing on quartz cement and found quartz cement to be much less common at distances more than 20cm from nearest stylolite, a situation relevant for instance in the lower Stø formation. The lower content of cement only 20cm from stylolites is another indication that there is little or no influx of silica brought in from larger

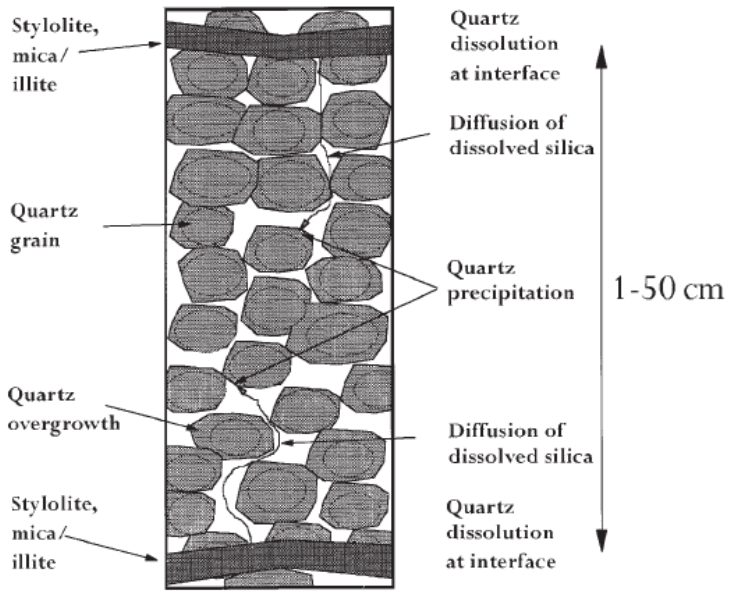

Figure 3-2. Clay induced dissolution at stylolite interfaces due to interaction of quartz and mica (Bjørkum et al., 1998).

distances and that in cases where stylolite spacing is large the precipitation rate for quartz will in these cases be controlled by transport.

3.4.2 Albitization

The albitization of K-feldspar grains can occur during shallow burial, and can commence at temperatures around 65 °C, and proceeds as shown by the reaction below (Saigal et al., 1988). Saigal et al. (1988) also suggested that the source of sodium needed to facilitate the reaction could be derived from the smectite to illite reaction occurring in interbedded shales in sandstones.

$$KAlSi_3O_8 + Na^+ = NaAlSi_3O_8 + K^+$$

K-Feldspar + Sodium ions = Albite + Potassium ions (after Saigal et al. (1988)

3.4.3 Authigenic clay

Authigenic clays are formed after the sediments have been deposited and occur as pseudomorphus replacement of grains, or precipitated as pore filling, fracture filling or grain lining clay (Wilson and Pittman, 1977) (fig.3-3)

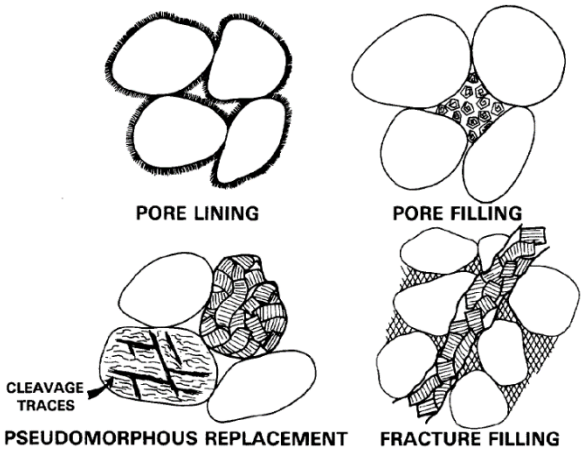

Figure 3-3. The various ways of which authigenic clay occur in sandstones (Wilson and Pittman, 1977).

Pseudomorphus replacement will have little direct effect on the reservoir quality of the rock, whereas pore – and fracture filling clay can reduce the primary porosity and permeability of the rock.

Grain lining, or coating, clays can help preserve primary porosity by reducing the surface area available for quartz cementation.

3.4.4 Smectite to illite and/or chlorite

The reaction below shows the formation of illite from K-feldspar and smectite (Abercrombie et al., 1994)

$$KAlSi_3O_8 + 2K_{0.3}Al_{1.9}Si_4O_{10}(OH)_2 = 2K_{0.8}Al_{1.9}(Al_{0.5}Si_{3.5})O_{10}(OH)_2 + 4SiO_2$$

K-feldspar + smectite = illite + silica

The smectite to illite reaction commences as the silica supersaturation in the pore space drops as a result from the opal CT to quartz formation at temperatures around 65 °C and may reach completion at temperatures as low as ~90 °C assuming slow burial rates (Abercrombie et al., 1994).

The silica released from the smectite to illite reaction may precipitated locally as micro quartz grains typically smaller than 3µm in size in shales (Thyberg et al., 2010). And this could also occur shale rich areas of sandstones where it locally behaves more like a shale.

Chlorite in nearshore marine settings are believed to form from iron rich clays possibly sourced from the influx of iron rich river discharge (Ehrenberg, 1993). It is believed to form from Fe-rich precursor clays at temperatures around 80-100 °C (Aagaard et al., 2000).

Grain coating chlorite were extensive have been seen to preserve porosities up to 10-15% higher than expected in deeply buried sediments (Ehrenberg, 1993).

3.5 Deep burial

During deep burial at temperatures of 120-130 °C and above, precipitation of quartz cement continues at ever increasing rates unless hindered by grain coats, the rate of quartz cement is as mentioned highly dependent on temperature and at temperatures of 140 °C it can be up to several orders higher than what it is at temperatures around 80 °C (Walderhaug, 1994)

3.5.1 Illite from Kaolinite and K-feldspar

Authigenic illite requires a source of aluminum and forms mainly at the expense of smectite (section 3.6.1) or kaolinite and K-feldspar (Bjørlykke et al., 1995).

Authigenic illite is often fibrous in appearance and precipitation of authigenic illite can greatly reduce the permeability in a deeply buried sandstone. The illitization of kaolin is mostly found to take place at temperatures of 130-140°C and above and is linked to the source of potassium from K-feldspar, Chuhan et al. (2000) found that the Potassium was sourced from K-feldspar locally and thus the initial amount of K-feldspar in the sediment will greatly determine the ability for illitization to occur in sediments buried to depths greater than that corresponding to a temperature of 130-140°C and above.

The formation of illite from kaolinite and K-feldspar proceed according to the reaction shown below.

$$KAlSi_3O_8 + Al_2Si_2O_5(OH)_4 = KAl_3Si_3O_{10}(OH)_2 + 2SiO_2 + H_2O$$

K-feldspar + Kaolonite = Illite + Silica (Bjørlykke and Jahren, 2015)

3.6 Porosity Preserving mechanisms

3.6.1 Introduction

This chapter has up until now discussed the various ways in which the reservoir quality of sandstones deteriorates as pressure and temperature increases. However, several factors can act as antagonists to these processes and if they preserve a porosity higher than what is

statistically expected from a certain lithology and burial history they are classified as having an anomalously high porosity (Bloch et al., 2002).

Factors that can preserve a higher than expected porosity by reducing the amount of quartz cement precipitated are important to understand when targeting deeper reservoirs as precipitation of quartz cement is the major factor responsible for porosity reduction in deeply buried sandstone reservoirs (Bjørlykke and Egeberg, 1993).

3.6.2 Overpressure

In the mechanical compaction domain, the primary way to preserve porosity for a given lithology is the development of overpressure; the higher pore pressure will reduce the effective pressure exerted on grain contacts and pose a hindrance to mechanical compaction.

3.6.3 Grain coating

As mentioned time, temperature and available surface area governs the precipitation rates for quartz cement, and the amount of cement will if unhindered be detrimental to the reservoir quality. Formation of micro quartz coating on detrital quartz can reduce the amount of quartz cement formed later by reducing the surface area available for precipitation. An important source of this may be siliceous organisms composed of opal which can dissolve creating a high concentration of silica and may precipitate at relatively low temperatures (~60-65 °C) microquartz coating is mainly seen in relation to siliceous sponge spicules common from upper Jurassic and younger (Hendry and Trewin, 1995) and is not expected to be largely relevant for the Stø formation.

Chlorite, which in marine settings is most often appearing to have formed from Fe-rich precursor clays as smectites, can act as grain coating on detrital quartz grain and preserve high porosities to large depths acting in the same manor – hindering the precipitation of quartz by reducing the available surface area (Ehrenberg, 1993).

Storvoll et al. (2002) found that grain coating illite also could act against quartz cementation, for this to occur the illite coating would need to be present at lower temperatures than that

seen in formation of illite from kaolinite, and would therefor need to be sourced from smectite in a similar manor as that of illite, and they also found mixed illite/chlorite grain coats.

If the quartz grain has an efficient grain coating, sandstones have been seen to remain uncemented to a depth of 4-5km, experiencing extensive grain crushing (Chuhan et al., 2002).

3.6.4 Early oil emplacement

Even after oil is introduced in a reservoir sandstones cementation can be seen to continue e.g. (Walderhaug, 1990) This is probably due to pore water still being in contact with grain surfaces if the system is water wet, if the oils in place are asphaltic or there is bitumen that can form effective coating, precipitation of quartz cement could be prevented.

Chapter 4: Methods and data

4.1 introduction

The characterization and evaluation of the reservoir quality of the Stø formation were conducted by means of petrographical and petrophysical analyses. The data available consisted of 20 thin section samples used in the petrographical analysis, and geophysical well logs used for the petrophysical analysis. All depth measurements are measured drillers depth (MD) from seafloor (MBSF) unless otherwise stated. The depths for well tops from NPD and depth of samples were given in measured depth from kelly bushing and these were converted to MBSF by the information on height of kelly bushing and water depth available from NPD. The difference between true vertical depth and measured depth were low for both wells (table A3 appendix A) and assumed to be well within the bounds of uncertainty relevant for this study.

4.2 Well database

The data – thin section samples from cores, and the geophysical well logs – are taken from the two wells; 7120/2-3S and 7120/12-2. A summary of the well database can be found in appendix B. The samples used for each petrographical investigation are presented in table C1& C2 in appendix C The geophysical well logs available for each well are presented in table B1 in appendix B

4.3 Petrographical

The petrographical investigation was conducted by use of optical microscopy and a scanning electron microscope with cathode luminescence abilities.

4.3.1 Optical microscopy

The samples investigated were taken from cored intervals from the two wells at various depths (table C1 appendix C), all in the Stø formation. The samples were prepared as thin sections; 30µm thick sections of rock fixed with epoxy on glass plates. The thin sections were studied using a Nikon microscope with polarized light, and a point counting machine. 400

points in each sample were analyzed with respect to bulk composition. 100 points for each sample were analyzed with respect to grain size and shape, sorting and grain contacts.

4.3.1.1 Mineralogical composition

Point counting where used to determine the relative amount - and type - of framework minerals, authigenic minerals, cement, matrix and intergranular pore space. The mineral identification was done visually with the aid from the "Atlas of sedimentary rocks" by Adams et al. (1984) an XRD analysis would further help in improving these result but this was unfortunately not available. Quartz grains were recognized by their extinction angles. Feldspars where recognized by twinning, Plagioclase feldspars showing parallel twinning, microcline crossed. Quartz cement was identified by the existence of a dust rim separating it from the detrital quartz grain and/or the characteristic euhedral shape of the authigenic cement. After determining the relative amount of grain framework minerals the rocks could be classified using Dotts sandstone categorization scheme (fig. 4-1) (Dott, 1964)

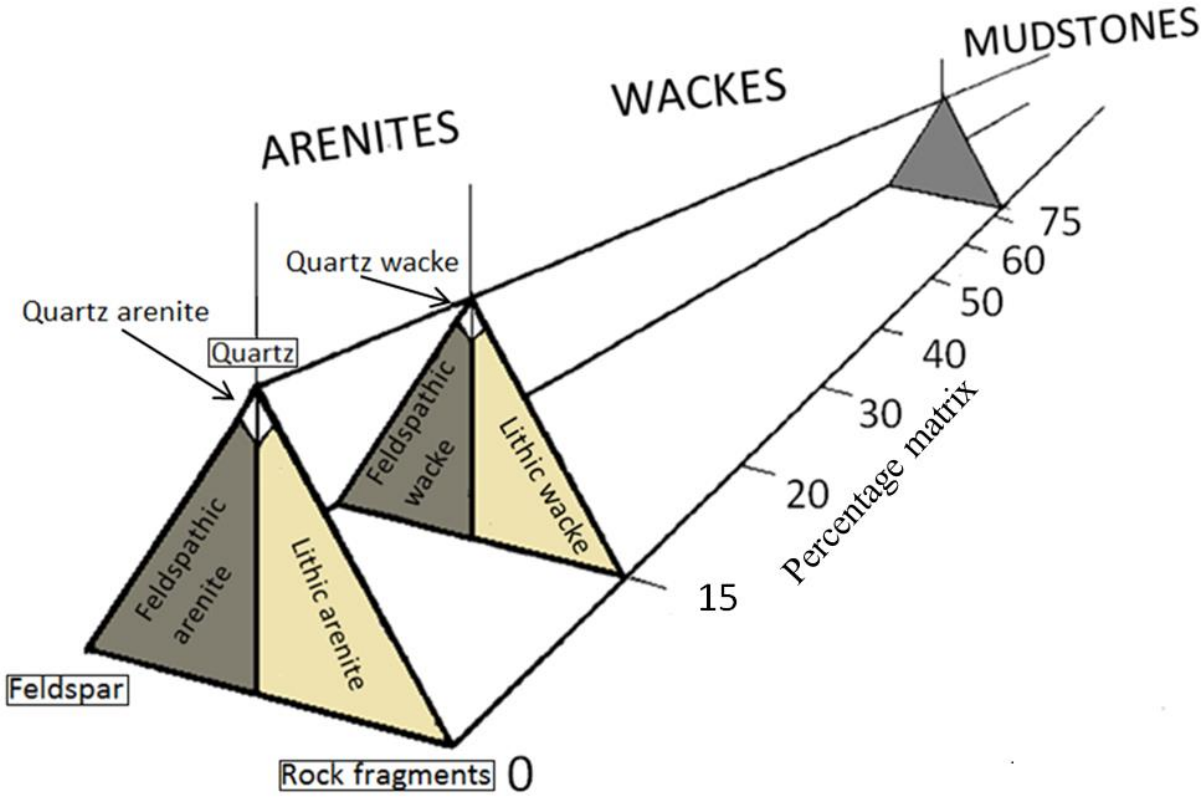

Figure 4-1. Dotts categorization scheme for sandstones. Redrawn after (Dott, 1964).

The type of matrix present was at times hard to positively identify using the optical microscope and not having performed an XRD analysis, but a distinction, especially between authigenic and allogenic clay were mostly done by the appearance in regards to the framework grains as described by (Wilson and Pittman, 1977).

4.3.1.2 Textural analysis

The average grain size, sorting, roundness, type of grain contacts and the preservation especially of feldspar grains were investigated. Porosity and intergranular volume was also determined.

4.3.1.3 Grain size and sorting

For each sample grain size measurements were performed on 100 grains. Length was measured on the longest axis on each grain. Measurements were taken by imaging sections of the samples under a certain magnification, the number of pixels contained in the axis of a grain could then be converted to millimeters by comparing with a given value of pixels per millimeter, determined by measuring the number of pixels per millimeter with the aid of a simple ruler.

Measurements were then converted to phi scale by utilizing the Wentworth grain size scale (eq. 4-1).

Equation 4-1 $$\varphi = -log_2 d$$

Sorting was determined by using standard deviation values given by (Folk and Ward, 1957) (eq.4-2)

Equation 4-2 $$SD(\Phi) = \frac{\varphi_{84}-\varphi_{16}}{4} + \frac{\varphi_{95}-\varphi_{5}}{6{,}6}$$

Resulting standard deviation values and corresponding verbal terms after (Folk, 1974) are displayed in table 4-1.

Table 4-1 - Standard deviation values and the corresponding verbal term after (Folk, 1974)

Standard deviation (Φ)	Verbal term (Folk, 1974)
>0,35	Very well sorted
0,35-0,50	Well sorted
0,50-0,71	Moderately well sorted
0,71-1,0	Moderately sorted
1,0-2,0	Poorly sorted
2,0-4,0	Very poorly sorted
<4,0	Extremely poorly sorted

4.3.1.4 Grain shape

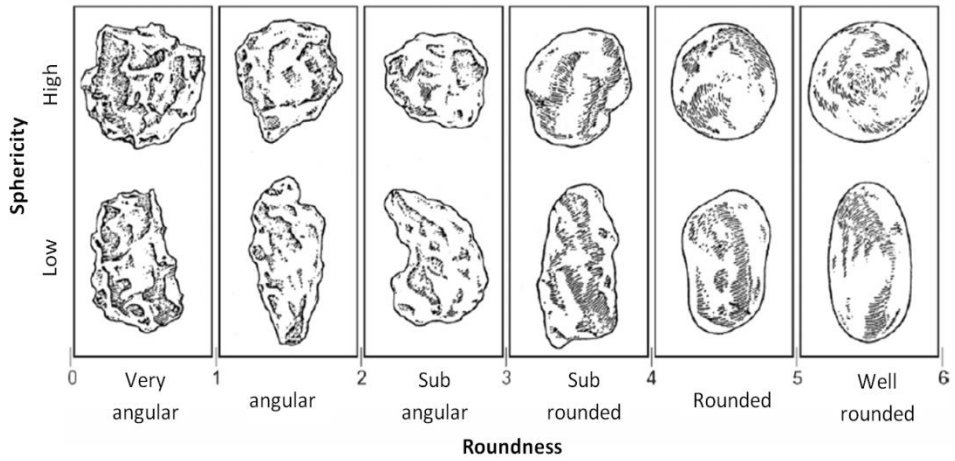

Figure 4-2. Visual comparison of grains with varying degree of roundness and sphericity after (Powers, 1953).

The particle shape for 100 grains in each sample where determined based on their appearance compared to those in (Powers, 1953) (fig 4-2). The validity of these results may differ between sample as a varying degree of quartz cement, and dust rims not always apparent makes the exact shape of the original grain harder to determine. The grain shape is an important parameter as ideally if only the original detrital grains are measured, the grain shape can indicate the amount of weathering, during transport and immediately after deposition.

4.3.1.5 Quartz cement

Amount of quartz cement in each sample were also determined by point counting. For some of the samples these results might not be accurate as the grains were visually "smeared" especially in the most clay rich sample probably as an effect of clay minerals both authigenic and allogenic, quartz cementation without a visually noticeable dust rim and perhaps effects of sample preparation meant the cement might not be readily visible in the microscope.

4.3.1.6 Grain contacts

Grain contacts for 100 grains were determined for each sample, Grain contacts generally change with increasing mechanical compaction and the type of grain contacts were determined to aid in the estimation of the degree of mechanical compaction. The grain contacts were determined by comparing with figure 4-3 (Santin et al., 2009).

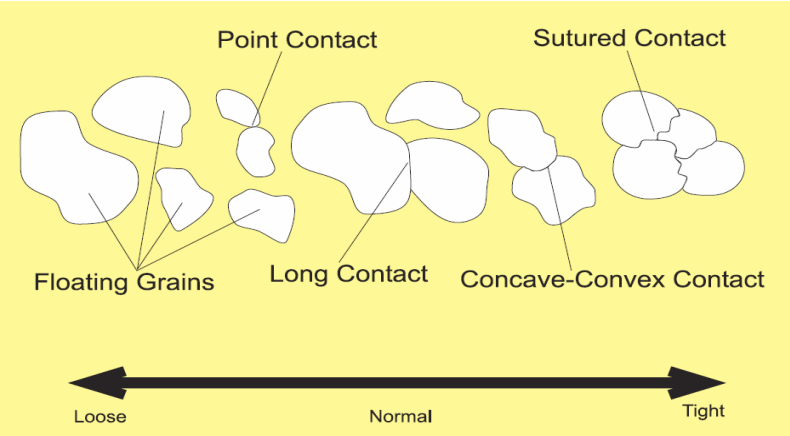

Figure 4-3. Types of grain contacts and indication of rock packing (Santin et al., 2009)

4.3.1.7 Intergranular volume

IGV consists of intergranular pore space, authigenic cement and depositional matrix (Paxton et al., 2002)

During mechanical compaction the intergranular volume diminishes with depth as the sediments undergo mechanical compaction. At time of deposition the IGV in clean sandstones will typically be around 40-42% and decrease with burial as a function of the effective pressure, and the textural and mineralogical composition of sediments. IGV reduction can be halted by any overpressure if present. At the onset of cementation any further mechanical compaction will seize and the IGV will remain fairly constant and can therefor give a good indication for the amount of mechanical compaction exerted on the rock even when measuring samples that have been more or less cemented. During chemical compaction the IGV will incorporate a varying relative amount of intergranular pore space, matrix and authigenic cement.

4.3.1.8 Uncertainties

Experience of the interpreter is important when analyzing thin sections, Clay minerals can be hard to differentiate and identify, and altered grains may not be correctly identified. Quartz cement may not always be counted if a dust rim or a clear euhedral shape is present. Furthermore, an assumption is made that the 400 points counted makes up a statistically sound representation of the entire sample.

4.3.2 Scanning electron microscope

A selection of samples was carbon coated and imaged using a scanning electron microscope (SEM). The high resolution of a scanning electron microscope enables it to resolve even the smallest minerals and textural features in a sample. Simply put a scanning electron microscopes works by using a focused beam of electrons directed at the sample in a near vacuum. Electrons will interact with the sample ejecting X-rays, primary backscattered electrons and secondary electrons, this can be detected by specific detectors and can then be processed into an image. For this analysis the detection of backscattered electrons (BSE) where utilized, this process penetrate deeper than the method using secondary electrons(SE),

resulting in a somewhat lower resolution, but has the ability to analyze the elements present as the signal correlates well with the atomic number of the elements hit, and this together with the x-ray characteristic can be used to determine the elements present in the sample which was done by comparing the spectrum peaks with those given in the SEM Petrology Atlas (Welton, 1984)

Cathode luminescence was used as a mean to distinguish the authigenic quartz cement from the detrital quartz grains. Cathode luminescence works by the emission of light (photons) as the result of the high energy electrons exiting the atoms and then returns to its ground state. Ideally any authigenic quartz will appear darker than the detrital grains.

4.3.2.1 Uncertainties

Uncertainties in the scanning electron microscopy are the possibility of the samples to be contaminated during preparation, either by foreign artefacts hampering the elemental analysis, or the physical appearance of objects in the samples. Another source of error is the possible misjudgment of the elemental analysis, especially if the measured mineral is exceedingly small and in close contact with other mineral components.

4.4 Petrophysical

The petrophysical analysis was mainly performed to estimate the amount of compaction and uplift. For the Stø formation the shaliness of the formation as well as an estimate of the porosity was performed.

The logs that were available for each well are presented in table C1 in appendix C. The logs that were utilized were the gamma ray log, sonic velocity log (P-wave), neutron and density log, all of which were available for the entire Stø formation in both wells.

4.4.1 Gamma ray log

The gamma ray logging tool measures naturally occurring radiation emitted from the sediments, a result of any potassium (K^{40}), and uranium and thorium present. Shale will generally show a high gamma ray log reading due to the contents of potassium. (Ellis and

Singer, 2008). Gamma ray logging can therefore be used as a lithology indicator in the way that it will ideally reflect the shaliness of a formation. From the gamma ray log an estimate of the shale content (Vshale) for the Stø formation was produced by first calculating the IGR (eq.4-3) The IGR is calculated by estimating a minimum and maximum API value from the log, with the minimum value generally being the lowest good reading of the log thought to correspond to clean sand, and the maximum value being the highest log reading excluding the very high readings that for example might belong to organic rich shales. IGR calculations are thus highly dependent on the experience of the interpreter. IGR calculations gives a linear relation with the gamma ray log and for a more realistic result a correction should be applied, in this case the Larionov (1969) equation for older rocks were used (Eq.4-4).

Equation 4-3 $$IGR = \frac{GRlog - GRmin}{GRmax - GRmin}$$

Equation 4-4 $$Vsh = 0.83(23.7 * IGR - 1)$$ (Larionov, 1969)

GRlog is the values from the gamma ray log, GRmax is the defined highest gamma ray reading and GRmin is the minimum reading.

4.4.2 Density log

The density log shows the measurements of bulk density of the rocks as measured by the density tool. Density logging tools estimates the bulk thickness of the sediments by emitting gamma radiation and measuring the response, formations with higher bulk densities attenuates the radiation to a larger degree than less dense formations. The density log can in the same way as the sonic log discussed below show the compaction trend of the rock as compaction reduces porosity and increases the density of the rock. The increasing density is a function of depth and lithology. Factors that will cause a lower than expected density are; overpressure in the mechanical compaction domain and grain coating reducing quartz cementation in the chemical compaction domain. Early formation of carbonate cement can cause higher than expected density values.)

The density log is in this thesis primarily used to estimate porosity. By applying equation 4-7 the porosity can be estimated with knowledge or an estimate of the matrix and pore fluid

present. The bulk density of a rock will comprise of the sum of the density of the matrix and the fluid in the pore space, and the relative amount of each thus giving equation 4-5

Equation 4-5 $$\rho = (\rho matrix * (1 - \varphi) + (\rho fluid * \varphi)$$

Where the density of the rock: ρ is a function of the density of the matrix (ρmatrix) which amounts to all that is not porosity (1-φ) and the density of the pore filling fluid(s) (ρfluid) the amount of which is corresponding to the porosity (φ).

The porosity estimation is described in section 4.3.5.

4.4.3 Sonic log

The sonic log is derived from a logging tool that measures how fast sound travel through a rock, the values, often called interval transit time, or Δt gives the time it takes for the sound to travel through a certain distance of the rock (μs/ft), To get the velocity (m/s) equation 4-6 is used

Equation 4-6 $$Vp = \frac{1}{\Delta t} * 304800$$

The sonic log will in general show the same trend as density, as the sonic velocities for a lithology will increase as it gets more compacted. From this a compaction trend can be established by plotting the velocity versus depth. At onset of cementation the velocities will quickly increase substantially as the cement stiffens the rock fabric. The compaction trend can be used to compare with published compaction trends to see if there has been any uplift. If the sediments have been uplifted it is assumed that not much "decompaction" will occur even though the effective pressure is reduced, and the rocks are said to be over compacted (Mondol, 2015). The compaction trends of uplifted sediments will therefor show higher sonic velocities than the experimental compaction trends. The uplift is estimated by seeing at what depth the sediments must have been to yield the values observed in the log.

Identifying the depth where the change to chemical compaction domain occurs as seen by the increase in sonic velocities (and density logs) can also be compared to the estimated depth where this should occur given by the geothermal gradient of the area to estimate uplift.

4.4.4 Neutron porosity log

The neutron log is acquired by a tool that emits a neutron source into the sediments; the neutrons are absorbed by the formation mainly as a function of the amount of hydrogen present. Pore space is most often occupied by water, with water most commonly the major contributor towards the hydrogen content in the sediments and therefor the response will ideally reflect the porosity of the rock. However, hydrogen is also present in clay minerals, especially smectite and kaolinite and for shales the neutron porosity will give then give higher values. Oil will normally give similar response as to water, whereas gas will give to low values as there are fewer hydrogen atoms per volume in the less dense gas compared to water and oil (Mondol, 2015).

4.4.5 Porosity estimation

Although the Stø formation is mostly consisting of clean quartz arenites there is also varying shale content. Another factor is the existence of a varying content of gas occupying the pore space. As these two factors can both interfere with the direct measurements by neutron porosity the procedures described below were used to procure a more accurate estimation.

Porosity from density

To calculate the porosities using the density log a value for the density of the rock matrix and the pore fluid needs to be estimated, the Stø formation is sandstone dominated and for the rock matrix a density value of that corresponding to quartz (2.65g/cm^3) was used, the density logging tool normally measures in the flushed zone of the formation (Asquith and Krygowski, 2004) and the actual value of the pore fluid would therefore not give the best result, however using the exact value of the drilling fluid, which were for the depth of the Stø formation; 1.31g/cm^3 in well 7120/12-2 and 1.21g/cm^3 in well 7120/3-3S (www.npd.no), will not be correct either as the heavier elements of this probably do not penetrate into the invaded zone. The pore fluid value was therefor set to an estimate of 1.12(g/cm^3). The porosity was calculated with these values using the equation below.

Equation 4-7 $$\Phi d = \frac{\rho\ matrix - \rho\ log}{\rho\ matrix - \rho\ fluid}$$

$_p$matrix is the density of only the matrix present, $_p$log is the value from the bulk density log and ρ fluid is the density of only the fluid(s).

Porosity from density - and neutron porosity average

Several effects can thwart the porosity estimates from density and the measured neutron porosity. For the density porosity the most important ones are the shale content if it has a density different from that of quartz and any gas present in the flushed zone, the effects of shale and gas in the neutron porosity were addressed above.

These issues can to a certain extent be mitigated especially if the error in readings and measurements is caused by the presence of gas as this will give a to low neutron porosity reading and to high values in the density porosity estimate. The porosity is then acquired by averaging of the two logs or equation 4-8 believed to work especially well when there is gas present (Mondol, 2015).

Equation 4-8 $$\Phi nd = \sqrt{\frac{\Phi d^2 + \Phi n^2}{2}}$$

Here φ_d is porosity as calculated by equation 4-7 and φ_n being the measured neutron porosity

4.4.6 Cement calculated from P-wave

As mentioned the onset of cement has a large effect on the P-wave velocities. The P-wave were used to estimate the amount of cement in the Stø formation in the two wells by using the findings of Marcussen et al. (2010) from the Etive formation, a somewhat comparable lithology of clean shallow marine sands. The strong correlation of increasing sonic velocities with an increasing amount of cement forms the basis for the estimation. Fluid replacement modeling were performed on the sonic velocities for comparison with the results from Marcussen et al. (2010), the estimated average values used for the formation interval where that of 80% gas saturation, and 15% shale. The estimated output velocity being that of 100% water saturation.

4.4.7 Geothermal gradient

Sediments buried to depths corresponding to temperatures above ~70°C enables the quartz cement to precipitate and increasing temperatures will accelerate this process, the depth corresponding to these temperatures varies as a result of the geothermal gradient of the area often presented as the temperature change per kilometer (Δ°C/1km). An estimate of this geothermal gradient is therefore important in trying to relate the degree of quartz cementation with the time temperature integral of the sediments. The geothermal gradient (G) is calculated by using equation 4-9 Utilizing the measured bottom hole temperature acquired from the well and the surface temperature estimated to be 4° at sea floor in this case. The measured geothermal gradient may not be accurate as the bottom hole temperature may not be the actual temperature of the surroundings at that depth. The time between end of drilling and measuring of the BHT will increase the chances of this temperature being more correct. No such information was available.

Equation 4-9 $$G = \frac{BHT - Ts}{Db - (Ds + KB)}$$

BHT is the measured bottom hole temperature, Ts is the seafloor temperature, Db is the total vertical depth(TVD), Ds is the water depth and KB is Kelly bushing

4.4.8 Uplift estimation

To estimate the amount of uplift for the two wells an estimated compaction trend from Storvoll et al. 2005 where used to compare with readings from the well. The compaction trend from Storvoll et al. 2005 is an average from several wells from the northern North Sea, Haltenbanken and the Barents Sea. The Sonic velocity from the wells were plotted against depth and any values corresponding to a gamma ray value below 60 API were removed. The compaction trend where then plotted and compared as to see how much compensation in depth would need to be applied to match the published compaction trend.

Since the experimental compaction curves are only valid for mechanical compaction only the uppermost parts of the well logs where used for comparison as they could be assumed to not have extensive cementation as the estimated uplift of the corresponding area is, as discussed in chapter 2, around 1000-1500 meter

Chapter 5: Petrophysical analysis

5.1 Introduction

All depths given are measured depth below seafloor (MBSF) unless otherwise stated.

The depth of formation intervals was acquired from the NPD fact pages for both wells (factpages.npd.no).

The primary objective of the petrophysical analysis is to examine the compaction, and to what temperatures the sediments may have been exposed to by estimating the maximum burial of the sediments prior to any uplift. During burial, as the sediments compact, several physical parameters changes, the mechanical compaction crushes and reorganizes grains thus reducing pore space and reducing the bulk volume of the sediments, and increasing the density. As the temperatures reaches ~70ºC and quartz cement can start to precipitate, as only 2-4% of cement is needed to halt further mechanical compaction it is assumed to quickly seize, any further compaction will then be governed by time and temperature e.g. (Bjørkum et al., 1998, Walderhaug, 1996, Oelkers et al., 2000). These changes in the rock can directly or indirectly be measured by various well logs. With increasing compaction, the general trend is an increase in density, sonic velocity and a reduction in porosity.

5.2 Gamma ray log

The gamma ray log was used to indicate the shaliness of the formation and to identify depositional changes by the trend of the gamma ray response.

The gamma ray log for the Stø formation is markedly different in the two wells (fig. 5-1); in well 7120/2-3S it can easily be divided into two distinct units with quite an abrupt change between the two, the uppermost part showing higher readings and a slightly more serrated pattern with two clear spikes in gamma ray readings. The lower unit consists of ca.100m of continuous low gamma readings (~30API). The boundary between both the underlying Nordmela Fm. and the overlying Fuglen Fm. is marked by a sharp increase in gamma ray readings (fig. 5-2) In well 7120/12-2 (fig. 5-1) the gamma ray log response shows a more serrated pattern throughout the formation. Overall the readings show two series of upwards coarsening trends with a sharp increase in gamma ray readings separating the two at a depth of 1755m, and three “spikes” of higher readings at the interval; 1733-1745m. Boundary

between the overlying Fuglen formation is marked by an abrupt increase in gamma ray values, there is no clear break between Stø and the underlying Nordmela formation (fig. 5-2).

The shale volume for the Stø formation was calculated for both wells (fig. 5-3) using IGR and corrected by Larionov equation for older rocks (Larionov, 1969). The maximum gamma ray value was set to the highest gamma ray log reading in the nearby formations, excluding the abnormally high values at certain places in what is probably organic rich shales. The minimum gamma ray value was set to the lowest reading in the Stø formation (fig. 5-2)

The shale volume calculation is solely based on the gamma ray log and shows the same trend as the gamma ray log with the two markedly different intervals in well 7120/2-3S, the lower interval appearing to contain an exceedingly small amount of shale whereas the upper interval has a more bell shaped appearance with two spikes of significantly higher readings, and then quite a sharp break towards higher values in the absolute uppermost parts of the formation. In well 7120/12-2, the overall trend is two intervals of upwards coarsening sections, with a sharp increase in readings separating the two; in addition, there are four clear spikes of higher readings.

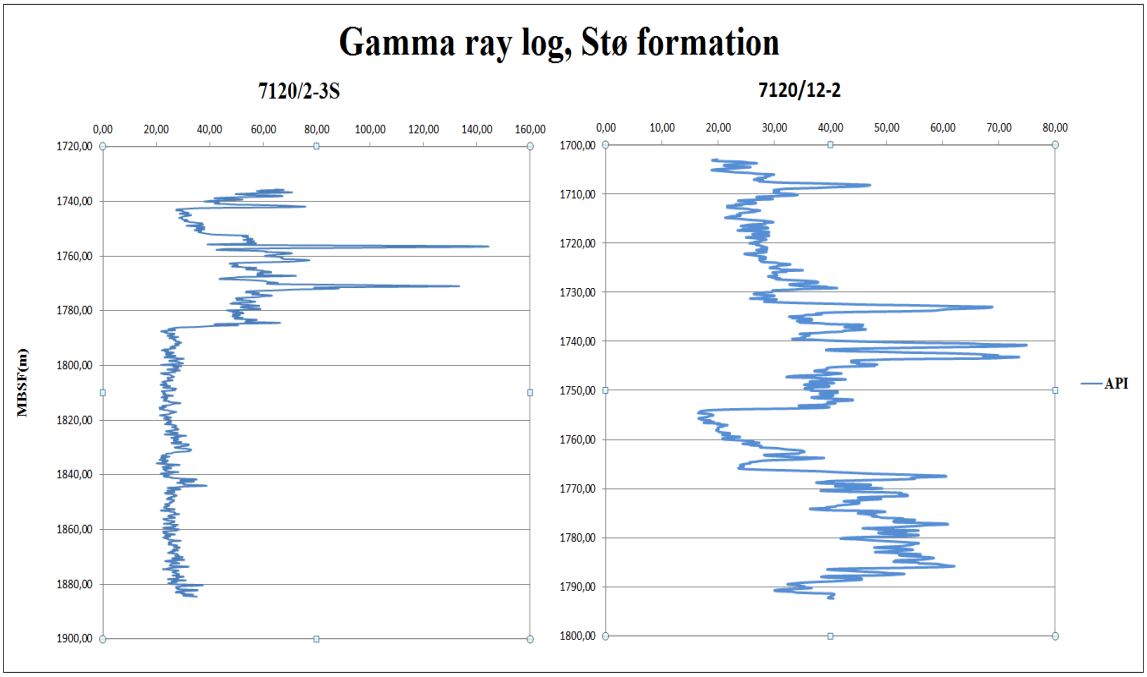

Figure 5-1. The gamma ray log for Stø formation in well 7120/2-3S and 7120/12-2.

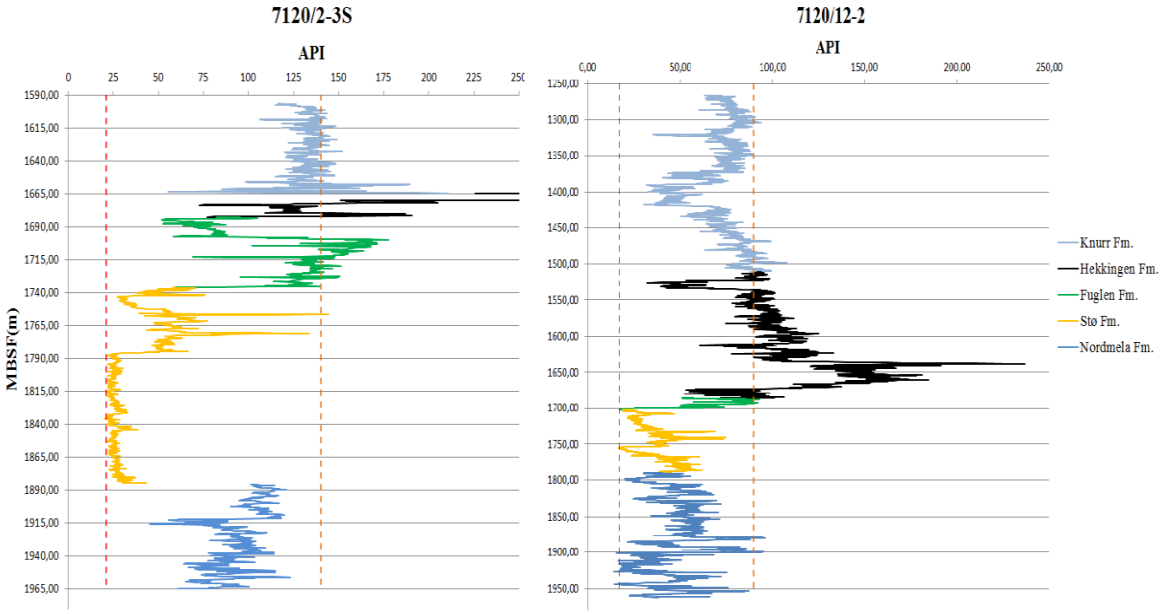

Figure 5-2. The gamma ray log for Stø and surrounding formations, the dotted lines marks the API values selected as the maximum and minimum values used for calculating IGR.

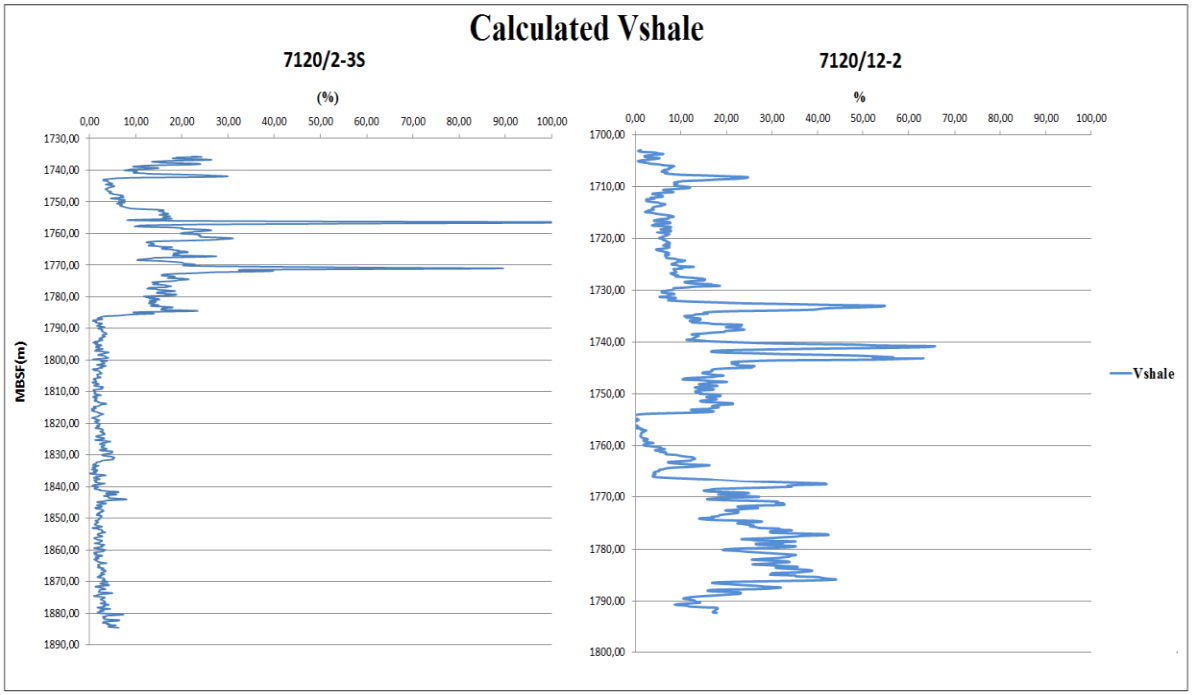

Figure 5-3. Calculated vshale for the Stø formation in both wells.

5.3 Compaction trends

Both the mechanical and chemical compaction has the ultimate effect of reducing the porosity and increasing the density of the sediments, but the processes behind is different and the factors influencing the way the sediments respond in the two domains are different as mentioned in chapter 3. The amount of mechanical compaction is expected to determine the intergranular volume of the sediments and that this will remain fairly constant from onset of cementation Assuming a general trend in increasing pressure from the overburden and little or no overpressure, the IGV variation at a certain depth is mainly governed by the mineralogical and textural features of the rock as determined at deposition or immediate burial; features investigated in the petrographical analysis. The chemical compaction is highly dependent on the temperature and estimating the maximum temperatures that the sediments have been exposed to can then be used to estimate an expected amount of cementation and compare that with the results from the petrographical analysis to try and isolate factors that acts against or in favor of precipitation of quartz cement.

5.3.1 Uplift estimation

The measured sonic velocity (P-wave) was plotted against depth for both wells (fig. 5-4 & 5-5). In general, the sonic velocities will increase in a mostly linear fashion for a specific lithology as the sediments compact, with the major exceptions being lower than expected velocities due to overpressure reducing mechanical compaction or a relative large and abrupt increase in velocities due to the onset of chemical compaction. There are two main ways that the sonic log can be used to estimate the amount of uplift: One is the identification of the depth of the transition zone between the mechanical- and chemical compaction domain and comparing that two where it is expected to occur based on the geothermal gradient of the area, the other one is to compare the sonic log to an experimentally derived compaction trend that is comparable to the area, the sediment is expected to not decompact significantly as a result of any uplift and instead remain over compacted (Mondol, 2015) therefor enabling the comparison to compaction trends. In this thesis the latter method was used as there was no unambiguously clear cut candidate for being the transition zone, and furthermore this would also be based on the estimated geothermal gradient derived from the measured bottom holes temperature from the wells, which may have a varying degree of uncertainty, and furthermore the current geothermal gradient may not be representative to what it was prior to uplift since a

major part of the uplift is believed to have taken place in relative recent times e.g. (Baig et al., 2016) and (Cavanagh et al., 2006) mentions that certain parts of the Hammerfest basin currently shows temperatures at depth being ~20°C above expected.

The compaction trend from Storvoll et al. (2005) was plotted with the sonic log from the two wells (fig. 5-4 & 5-5) and both wells clearly show a large discrepancy between the measured log and the experimental compaction trend, with both logs having significantly higher sonic velocities compared to the experimental trend. The upper parts of the log assumed to be unaffected by quartz cement were used to estimate the amount of uplift, from this the uplift is estimated to be ~1250m in well 7120/2-3S and ~900m in well 7120/12-2.

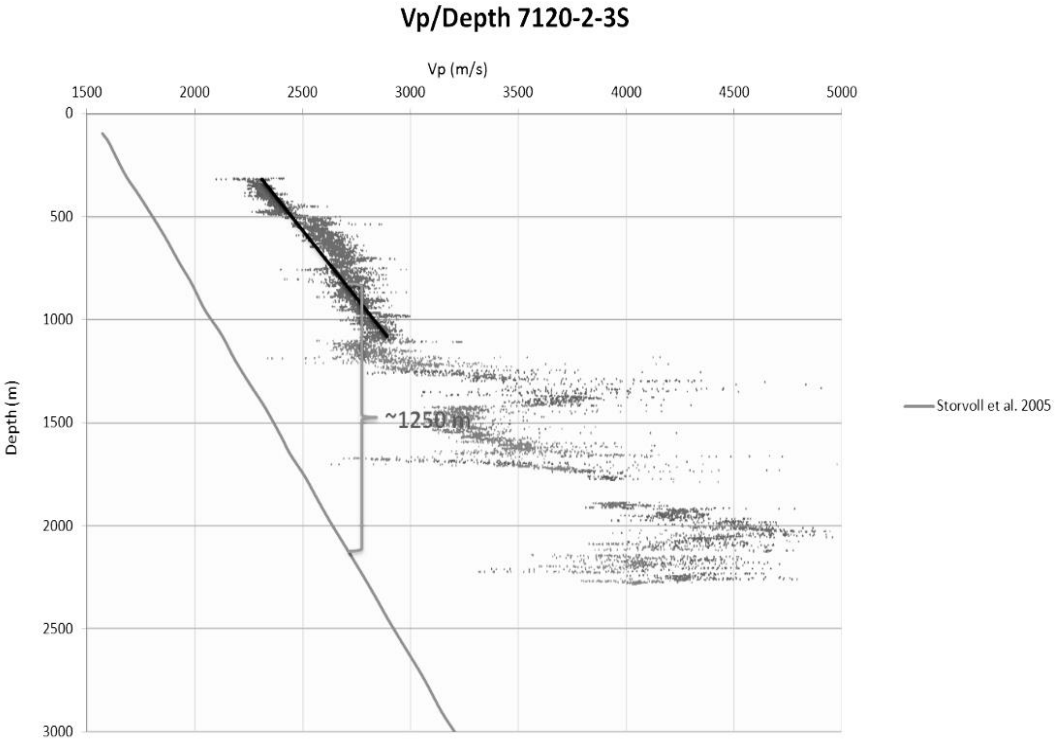

Figure 5-4. Sonic velocity plotted as a function of depth for well 7120/2-3, compared to the experimental compaction trend from (Storvoll et al., 2005). The sonic velocities are seen to be significantly higher than the experimental compaction curve and for the upper parts of the

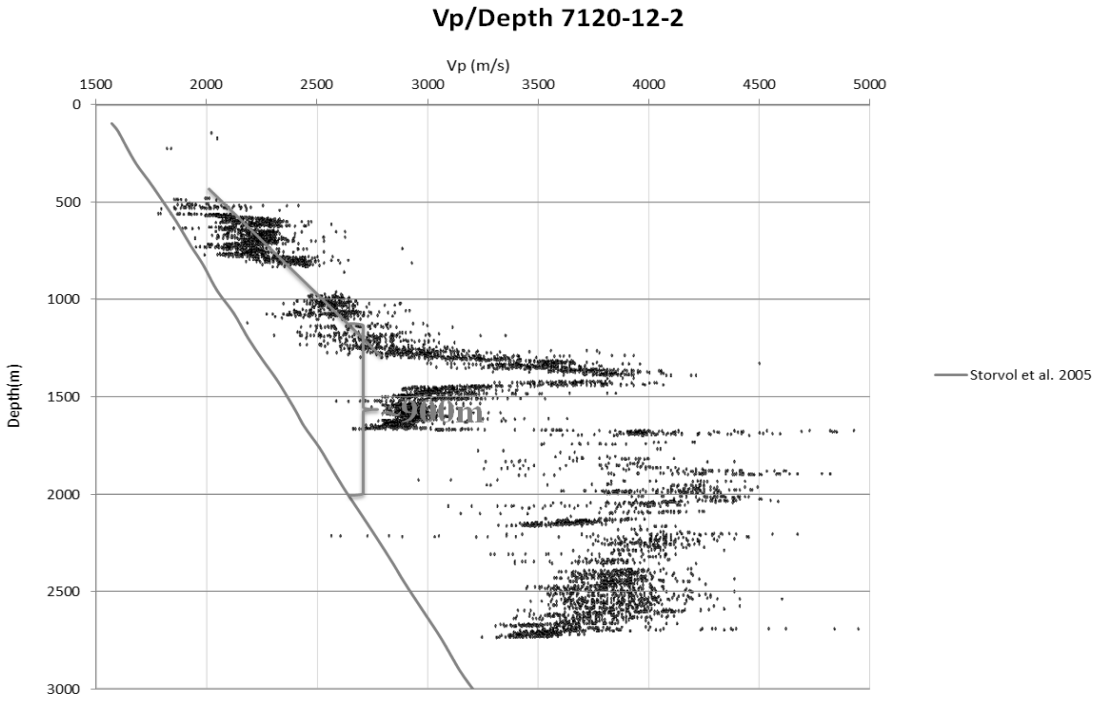

Figure 5-5. Sonic velocity plotted as a function of depth for well 7120/12-2, compared to the experimental compaction trend from (Storvoll et al., 2005).

Table 5-1. Present day depth and estimated maximum burial depth for the Stø formation based on the estimated uplift, the temperature at present depth and before uplift is based on the geothermal gradient calculated from the bottom hole temperature acquired from the NPD (table A3, appendix A), the temperatures for well 7120/12-2 has been marked with a question mark due to the untypically low bottom hole temperature for this well.

Well	Present depth of the Stø Fm. (MBSF)	Present temperature at current burial depth (ºC)	Estimated maximum burial depth of the Stø Fm. (MBSF)	Temperature at maximum burial depth (ºC)
7120/2-3S	**1735.5 – 1885.5**	**67.7 – 73.5345**	**2985.5-3135.5**	**116.4-122.3**
7120/12-2	**1703 - 1789**	**42.2 – 44.4 (?)**	**2603 – 2689**	**64.6 – 66.7 (?)**

The calculated uplift and the geothermal gradients are presented in table 5-1. The current geothermal gradients were calculated from the bottom-hole temperature available from the NPD factpages (factpages.npd.no) shown in table A3 in appendix A. The calculated uplift and

geothermal gradient were used to estimate the maximum burial depth and correspondingly the maximum temperature that the sediments of the Stø formation had been subjected to. The bottom hole temperature provided for well 7120/12-2 corresponds to a geothermal gradient of 24,8 ºC/km a seemingly low value, in (Smelror et al., 2009) the estimated average geothermal gradients of the Southwestern Barents Sea is ~31-38 ºC and most likely more towards 38 ºC since bottom hole temperatures are biased towards lower temperatures. Furthermore, no information of when the measurements were taken relative to last circulation of drilling fluid is available either, making it difficult to estimate the validity of the measurement.

The present day temperatures in the Stø formation is for the well 7120/12-3S; 67,7 – 73,5 ºC and for well 7120/12-2; 42,2 – 44,4 ºC (?). At the estimated maximum burial depth, the sediments in the Stø formation have been subjected to temperatures of 116,4 – 122,3 ºC in well 7120/2-3S and 64,6 – 66,7 ºC (?) in well 7120/12-2.

5.3.2 Porosity estimation

The porosity was calculated from the well logs as described in chapter 4, the porosity calculations were done for the interval corresponding to that of the Stø formation. For the calculation of porosity from the density log a density of quartz (2,65g/cm^3) was used for the matrix and for the pore fluid an estimated density of the mud filtrate (1.12g/cm^3) was used. The resulting porosity is plotted against depth (fig. 5-6 & 5-7) as well as the distribution of porosity values (fig. 5-8 & 5-9)

The porosity distribution in a sandstone reservoir, over a relatively small interval, will often trend towards a normal distribution when the lithology is similar, deviations from this and a more bimodal appearance with larger porosities prevailing may then indicate that porosity preserving mechanisms have been present (Bloch et al., 2002). The porosity distribution in the Stø formation in well 7120/2-3S is approaching a normal distribution with low positive skewness and low standard deviation, and has a largely similar mean and median porosity around 14% (fig. 5-8). The porosity distribution in the Stø formation in well 7120/12-2 is more bimodal in appearance having a larger skewness, negative in this case, and a much higher average porosity of around 21% (fig. 5-9).

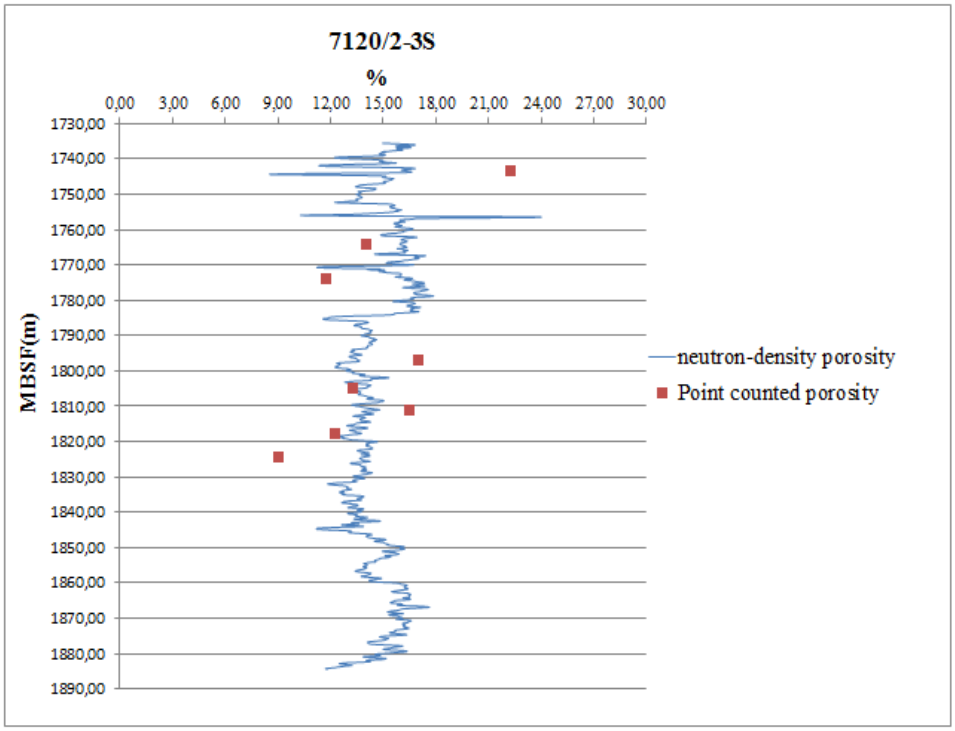

Figure 5-6. Porosity as calculated from neutron porosity and density porosity, plotted against depth for the Stø formation along with the porosity determined from point counting in well 7120/2-3S.

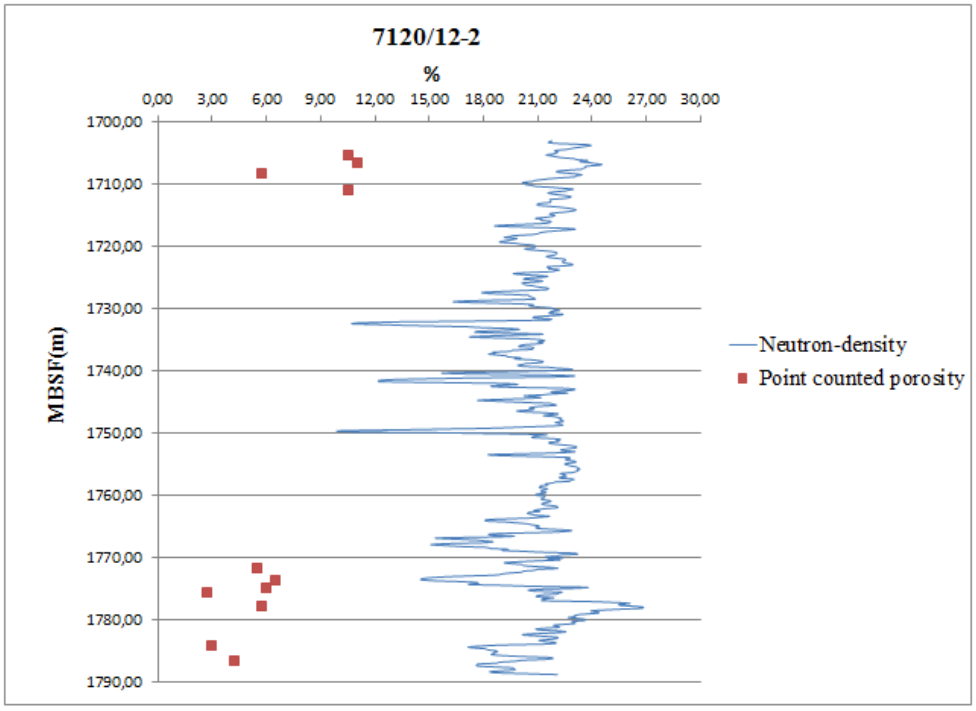

Figure 5-7. Porosity as calculated from neutron porosity and density porosity, plotted against depth for the Stø formation in well 7120/12-2. Also shown are the results from point counting.

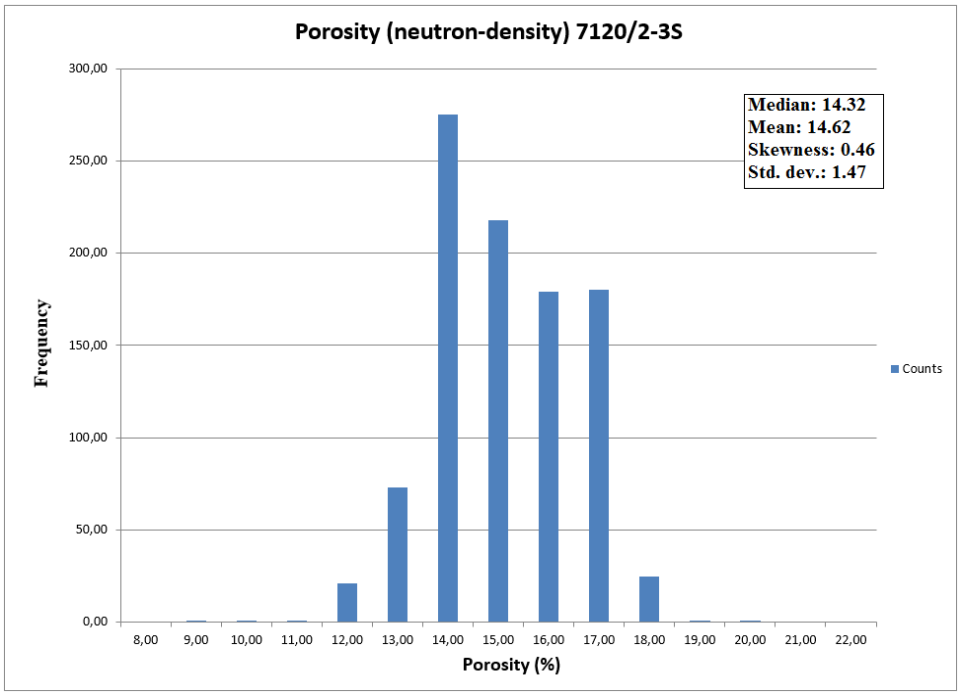

Figure 5-8. The porosity distribution for the Stø formation in well 7120/2-3. The distribution is approaching normal to somewhat uniform with only a slight positive skewness and a relatively low standard deviation.

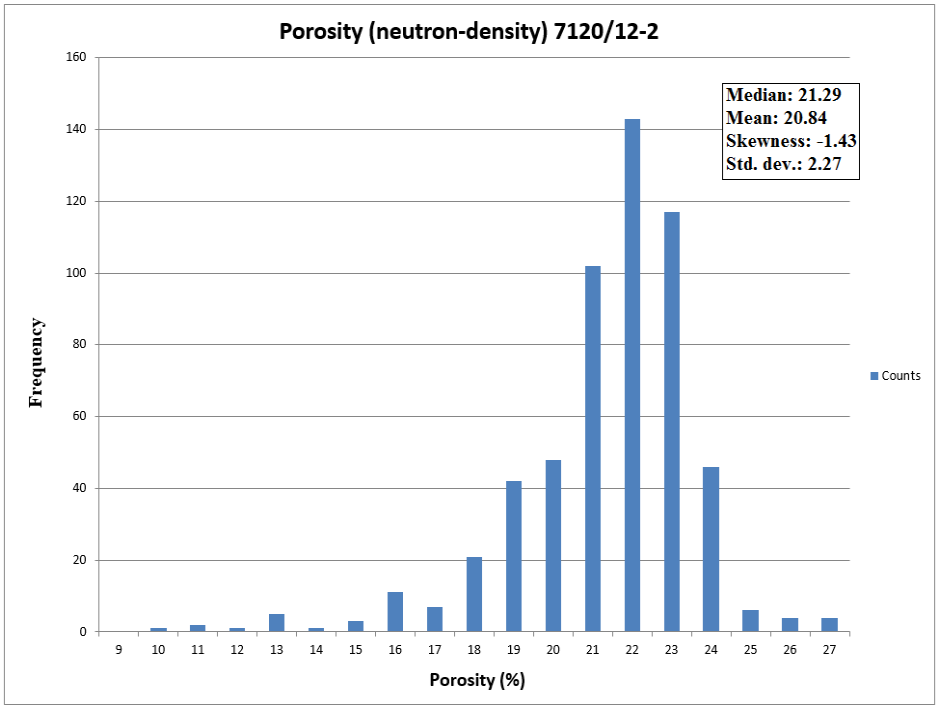

Figure 5-9. Porosity distribution for the Stø formation in well 7120/12-2. The distribution is slightly more bimodal than that in well 7120-2-3S and shows a negative skewness and somewhat larger standard deviation. the average porosity is also significantly higher.

5.4 Quartz cement from sonic log

Figure 5-10 shows the estimated volume of quartz cement in the Stø formation for the two wells. The calculation assumes a linear correlation between P-wave velocity and the amount of quartz cement, based on the results of Marcussen et al. (2010) from the Etive Fm.

The overall trend is a higher content of cement in well 7120/2-3S than in well 7120/12-2. Excluding the anomalously high readings in well 7120/12-2 the quartz content here appears to remain more constant throughout the formation, where as in well 7120/2-3 there is difference mainly between the upper and lower section of the formation.

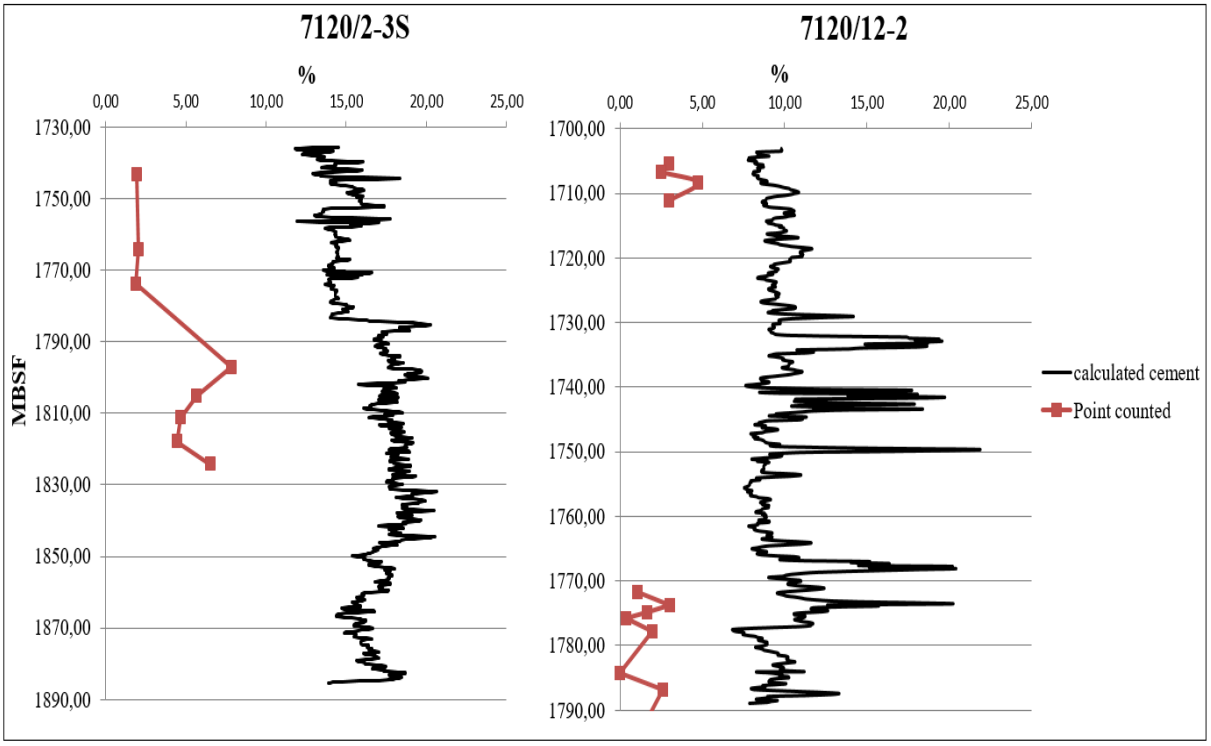

Figure 5-10. The cement volume for the Stø formation in each well as calculated from the sonic velocity (P-wave) by employing the relationship between P-wave velocity and amount of cement from (Marcussen et al., 2010).

Chapter 6: Petrographical analysis

6.1 Introduction

20 thin section samples – 8 from well 7120/2-3S and 12 from well 7120/12-2 - were analyzed by means of optical microscopy, with 5 thin section samples being further analyzed in a scanning electron microscope, to identify the mineralogical and textural composition of the Stø formation. The main objective was to try and correlate the amount and distribution of quartz cement, possible areas of dissolution, interaction with detrital quartz grains and clay minerals with the initial composition of the sediments as a result of varying depositional settings.

Mineralogical investigations were performed to identify and quantify the composition of the samples, the textural investigations were focused on the size, shape, and sorting of particles, grain contacts and intergranular volume.

The samples were grouped into five units based on depth, the trend of the gamma ray log response and corresponding Vshale calculations, and by the mineralogical composition – mainly matrix and mica content – as determined by point counting. The division of samples is shown in (table C1 Appendix C)

6.2 Mineralogical analysis – optical microscopy

The Stø formation generally consists of clean mature sandstone, and all but one unit shows an abundance of quartz grains (>95%) and a matrix content below 15% (fig. 6-2) plotting as quartz arenites when plotted against the sandstone classification from (Dott, 1964) (fig.6-1). One unit – 2B - has a matrix content above 15% (fig. 6-2 & 6-3) and plots overall as an arkosic wacke. The content of feldspars and lithic fragment is overall low, but varies between different intervals (fig.6-2). The intergranular volume consists of open pore space, various clay matrix and authigenic cement.

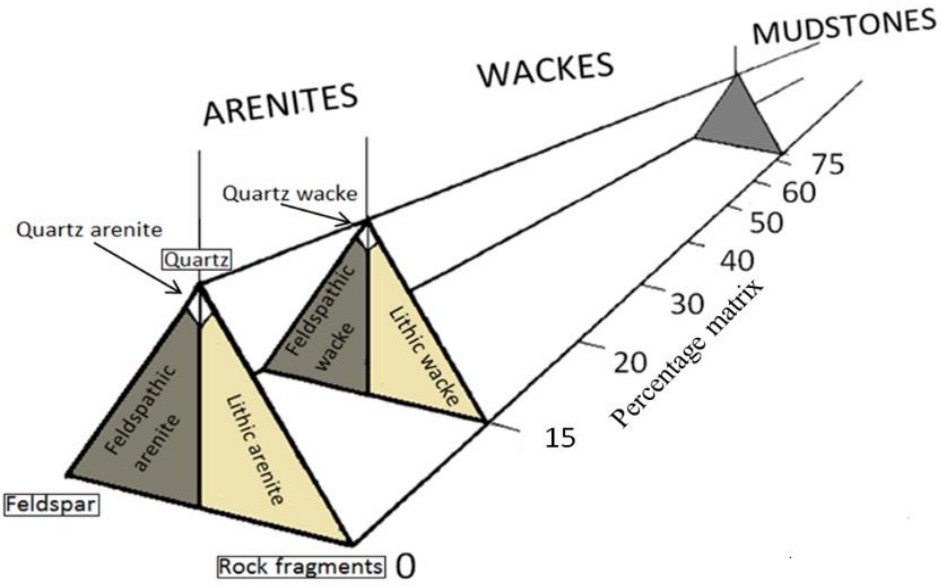

Figure 6-1. Sandstone Classification, modified from (Dott, 1964)

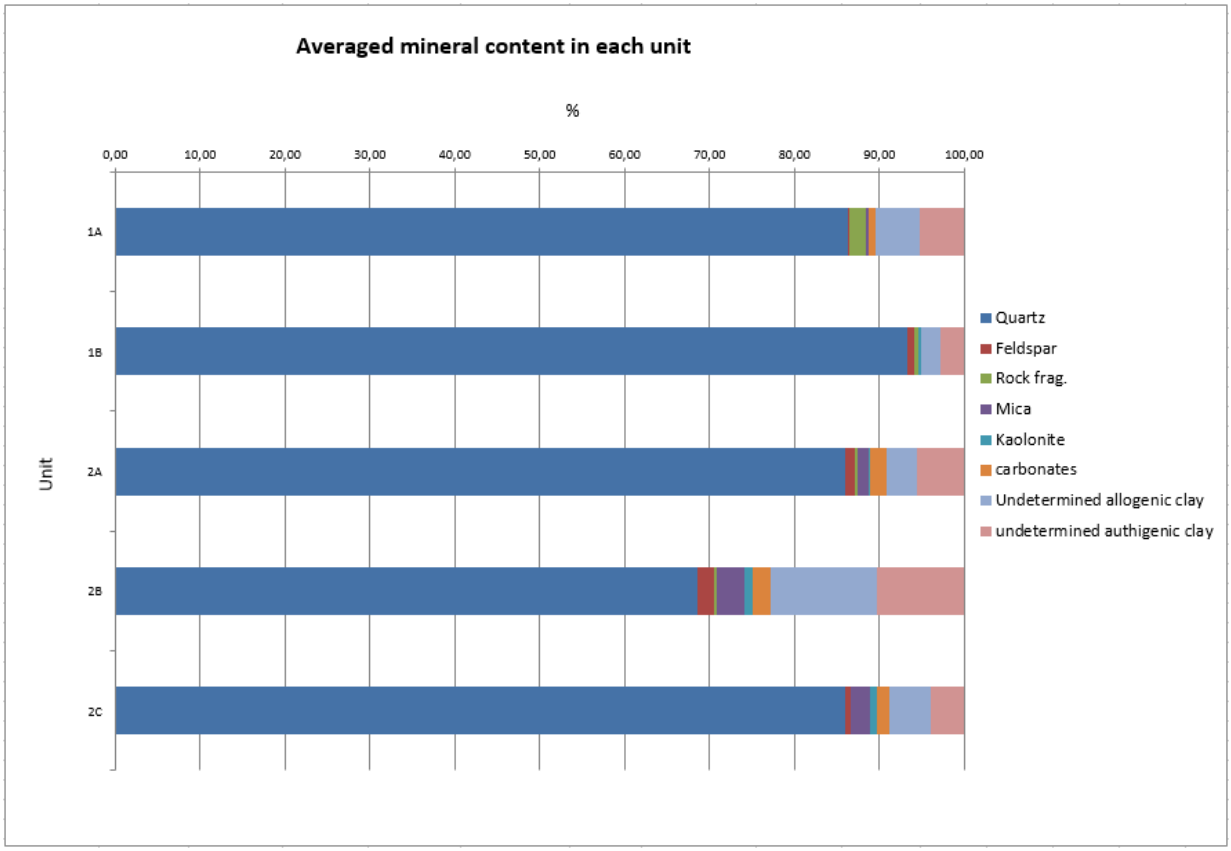

Figure 6-2. Average mineral content in each unit determined by point counting, the undetermined clay minerals was classified based on coexistence with other grains and in pore space, see also figure 6-15. Much of the undetermined clays were later identified in SEM but no complete correlation could be made.

In the two units corresponding to well 7120/2-3S (1A & 1B) The framework mineralogy as determined from point counting is almost exclusively consisting of quartz grains, unit 1A showed almost no feldspar (<1%), there was a slightly higher content of lithic fragments (<3%). unit 1B had a slightly higher content of feldspar than the overlying unit, but still only a small amount (<2%) of the bulk volume of the sample. Only a few lithic fragments were observed. The matrix content is slightly higher in unit 1A compared to 1B, for both units it appeared to be an even distribution between allogenic and authigenic clay minerals (fig.6-2). The matrix content was 8% in unit 1A versus 5% in unit 1B (fig.6-4). Unit 1A contained some carbonate fragments ~1%, whereas no carbonate where observed in unit 1B. There was some mica observed in unit 1A, most of which seemed to be muscovite. From the SEM analysis much of the pore filling clay was seen to be kaolinite and the kaolinite content determined from point counting is too low. This is most likely the case for all samples containing matrix of pore filling and grain replacing appearances (fig.6-15). The framework mineralogy was mostly the same in the units corresponding to well 7120/12-2. The matrix content for the upper and lower unit (2A & 2C) were similar at 8% and 9% respectively, unit 2B showed as mentioned the highest matrix content of all the samples and with 23% it was significantly higher than the other units. Carbonate fragments and some carbonate cement were observed in all three units (1-3%). Mica was found in all units with unit 2B having the highest content (4%), whereas unit 2C had a mica content of 3%, and 2% in unit 2A. Figure 6-6 shows a selection of images taken during optical microscopy showing the appearance of some of the samples under the microscope.

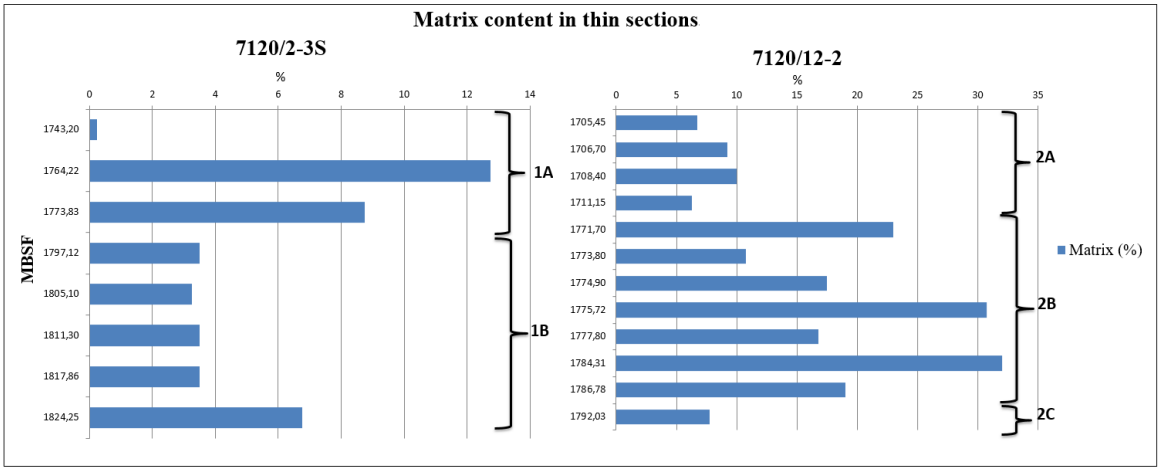

Figure 6-3. The total amount of matrix in each thin section sample relative to bulk volume

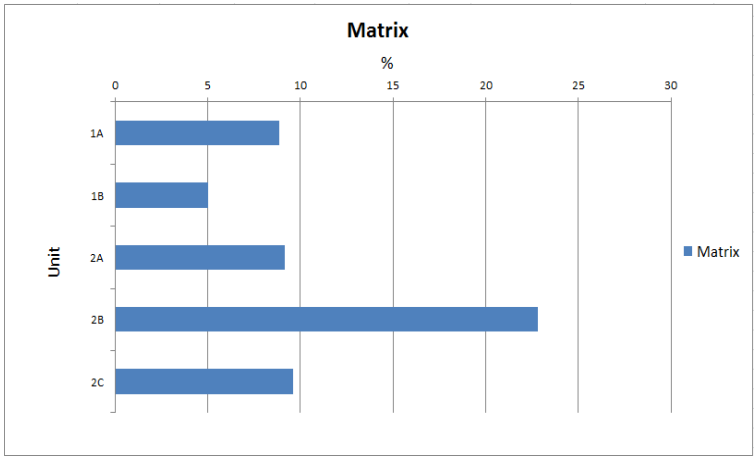

Figure 6-4. The average amount of matrix relative to bulk volume in each unit.

6.2.1 Quartz

The total quartz content relative to the bulk volume of the sediments ranges from 68% to 93% in the extreme cases corresponding to unit 2B and 1B respectively, the average quartz content for all units excluding 2B is 88%. Quartz, excluding authigenic quartz was almost exclusively found as monocrystalline and some polycrystalline fragments, and a minor amount in rock fragments.

6.2.2 Feldspar

Feldspar contents were overall low 1-4%. The feldspars present were predominently K-feldspars and some albite, the feldspars showed various stages of weathering but were predominently seen to have been significantly affected by weathering, see section 6.3.4.

6.2.3 Clay minerals

The clay minerals where in most cases to minuscule to be able to positively identify individual minerals using optical microscopy, and where mostly classified by the overall visual appearance in the sample using the scheme of (Wilson and Pittman, 1977) for

appearance of various clays in sandstones (fig.3-1 & 3). Clay minerals were more easily observed in the SEM presented in section 6.4.2.

6.2.4 Quartz cement estimated from point counting

The amount of quartz cement was determined visually during point counting and is shown as a percentage of the entire selection of points counted (fig.6-5). The amount of visible quartz cement varies greatly between the two units in well 7120/2-3; in unit 1A there was only 1.5% quartz cement visible, where unit 1B showed a content of 5.5% quartz cement. The units in well 7120/12-2 show a somewhat higher amount of quartz cement in the uppermost unit (2A) averaging 3%, and only just over ~1% in units 2B&C.

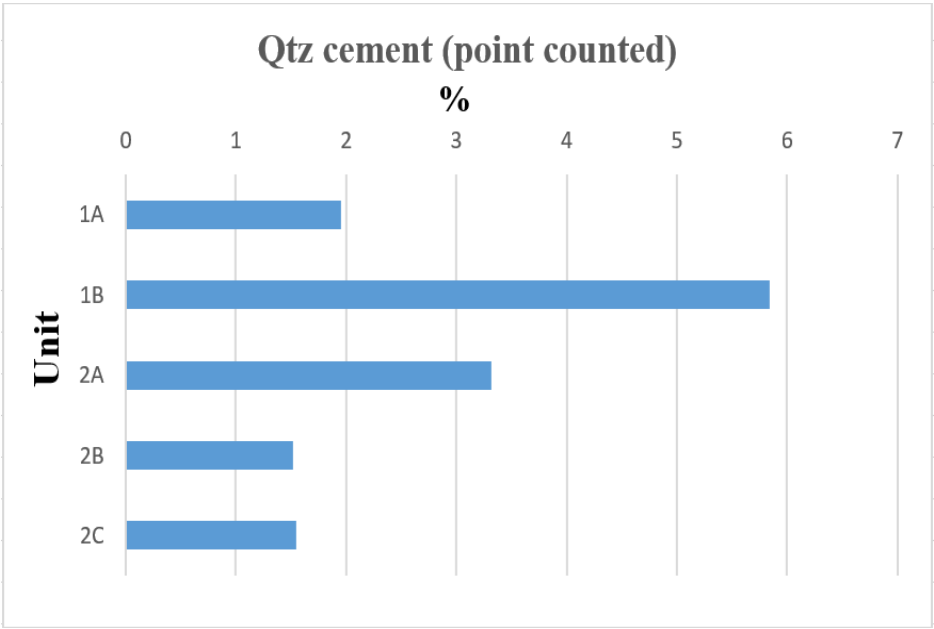

Figure 6.5. Percentage of quartz cement averaged for each unit

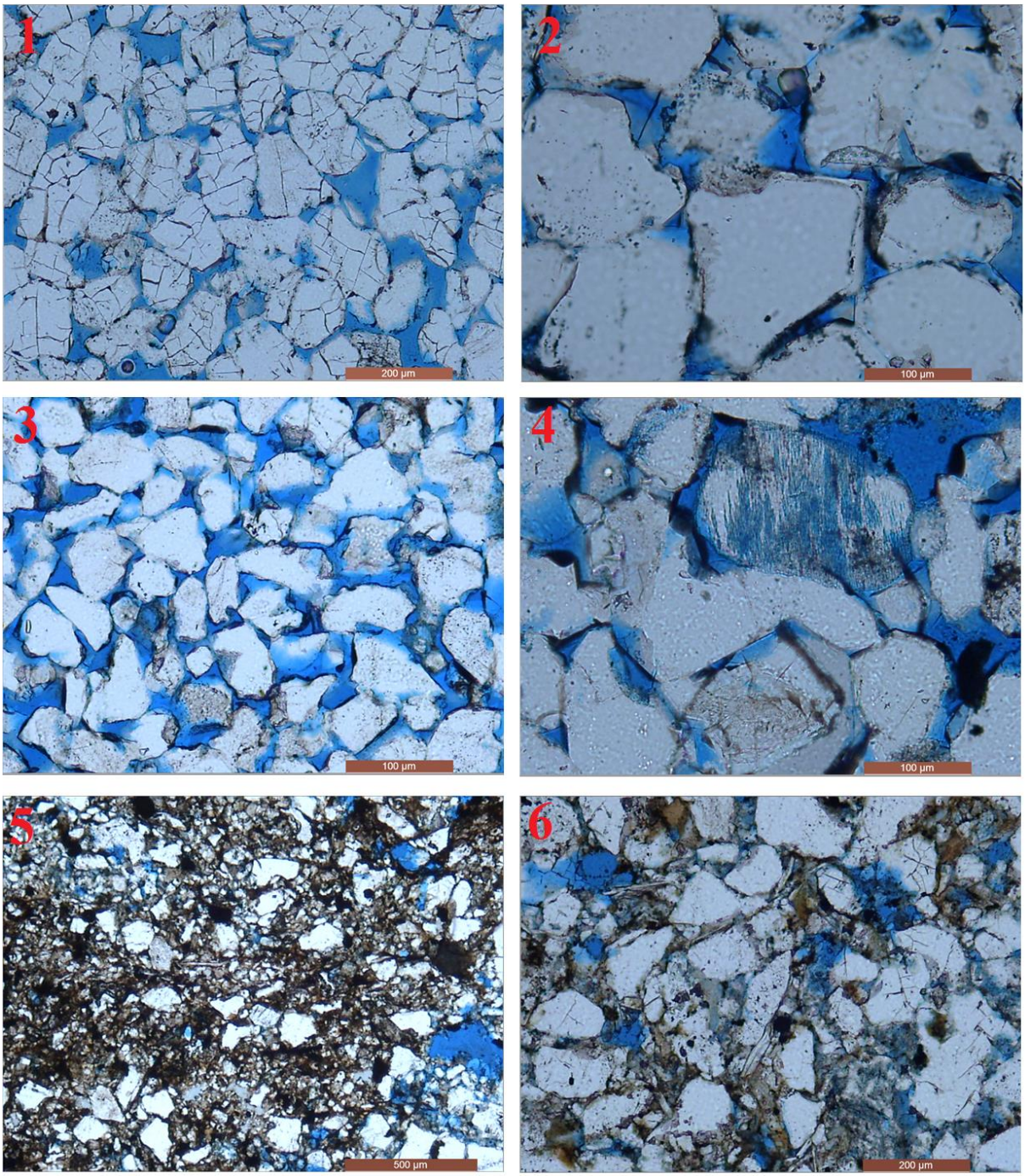

Figure 6-6. Optical microscopy of thin sections. (1) Well: 7120-2-3S, depth: 1743.70 (m), unit: 1A. Clean sample consisting of mainly only quartz and some quartz cement. (2) Well: 7120/2-3S, depth: 1824.25 (m), unit: 1B. Detrital quartz grains with quartz cement overgrowth showing typical euhedral shapes. (3) Well: 7120/12-2, depth: 1711.15 (m), unit: 2A. quartz grains with little quartz cement. (4) Well: 7120/12-2, depth: 1773.80 (m), unit 2B. Highly weathered feldspar grain. (5) & (6) Well: 7120/12-2, depth: 1784,31 (m), unit: 2B. Significant amount of clay minerals occurring as clay drapes (left). Detrital mica grains in-between and shaped around detrital quartz grains, pore filing clay (right).6

6.3 Textural analysis

Textural analysis was performed on 100 grains per sample, each sample where analyzed, then the values for samples corresponding to the same unit where averaged. In addition, the weathering of grains was determined qualitatively by appearance in optical microscope and SEM.

6.3.1 Grain-size, shape and sorting

6.3.1.1 Grain size

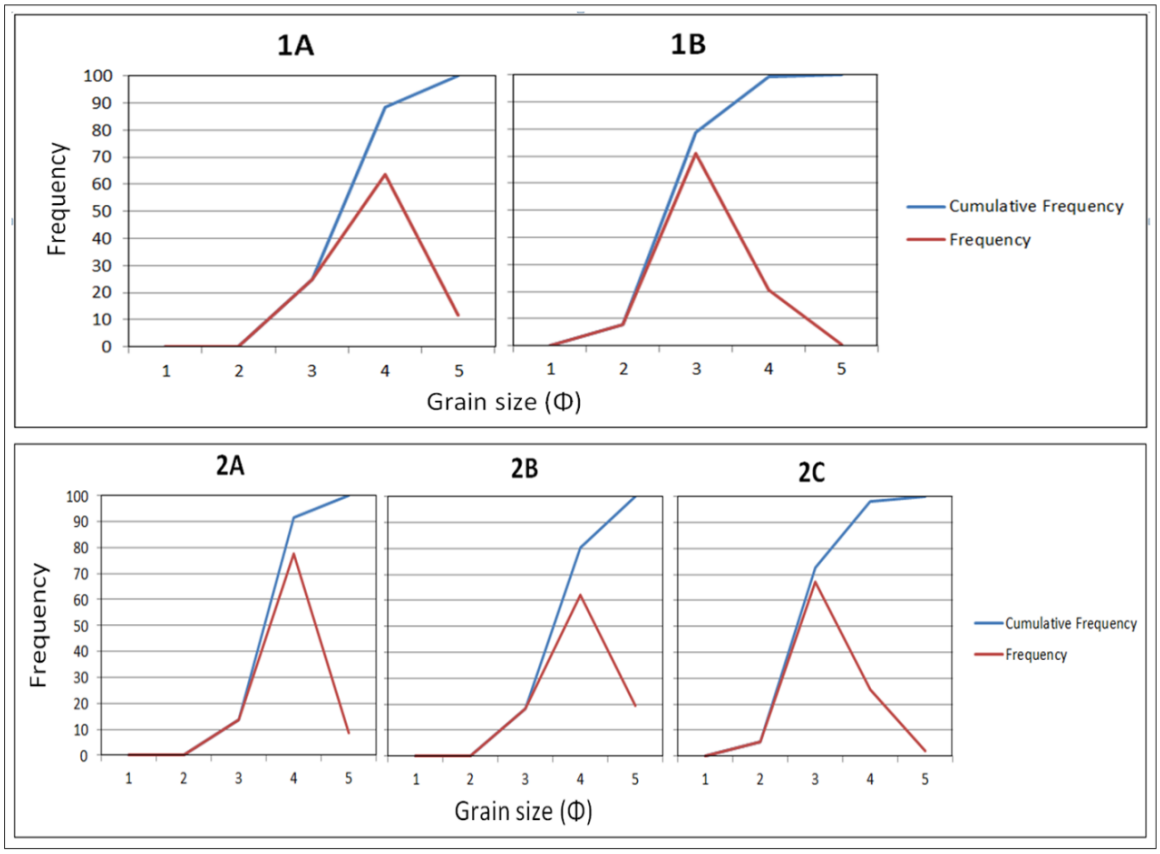

Figure 6-7. Grain size distribution showing both cumulative and non-cumulative plots for all units.

The sandstones in all units contain mostly fine to very fine sized particles (fig. 6-7)

Unit 1A show a negative skewness of grain size with the most prominent grain size being very fine sand with even some silt sized particles.

Unit 1B shows a near normal distribution of grain sizes with the median grain size being fine sand.

Unit 2A shows a majority of grain sizes being that of very fine sand with an abrupt increase in frequency both between fine to very fine and very fine to silt,

Unit 2B shows a similar distribution of grain sizes as that seen in unit 1A with a negative skewness and the majority of grain sizes corresponding to that of very fine sand.

Unit 2C is very similar to unit 1B with a near normal distribution of grain sizes, the median grain size being that of fine sand.

6.3.1.2 Sorting

The sorting is seen to be fairly equal in all units, ranging from well to moderately well sorted (table 6-1). Unit 1B and 2A are both well sorted, whereas units 1A, 2B and 2C are moderately well sorted. There was no significant correlation between sorting and average grain size (fig. 6-8)

Table 6-1. Grain-size sorting in each unit

Unit	Standard Deviation	Verbal Term
1A	0,56	Moderately well sorted
1B	0,47	Well sorted
2A	0,41	Well sorted
2B	0,64	Moderately well sorted
2C	0,52	Moderately well sorted

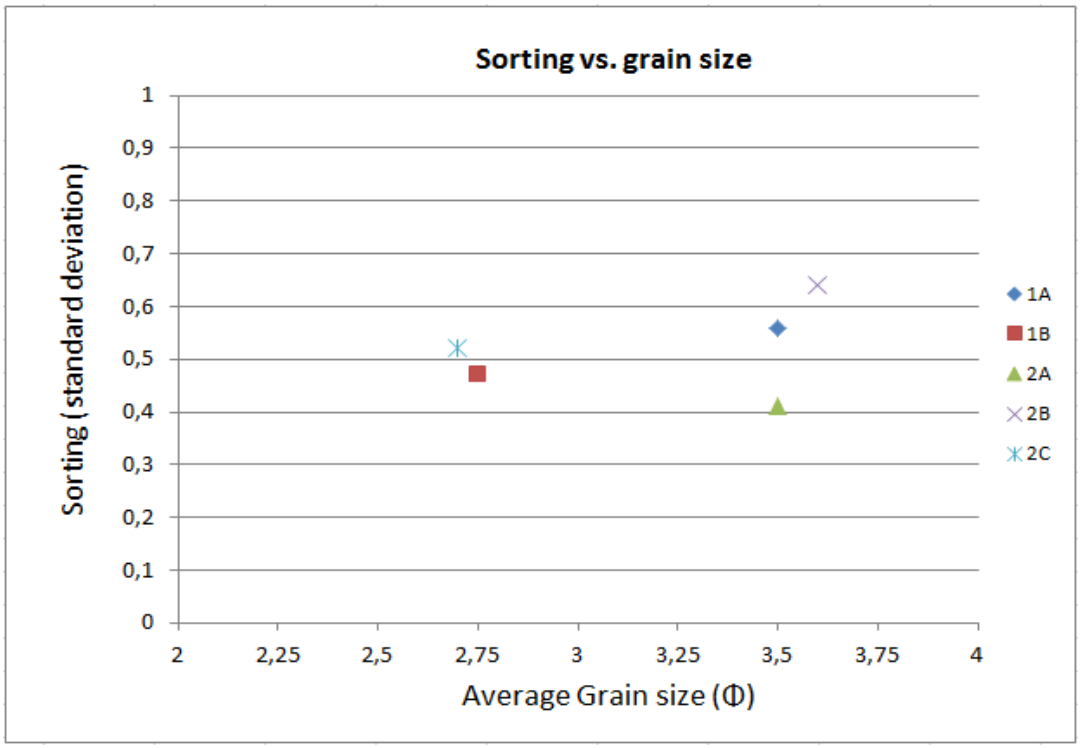

Figure 6-8. Sorting versus grain size for all units

6.3.1.3 Grain shape

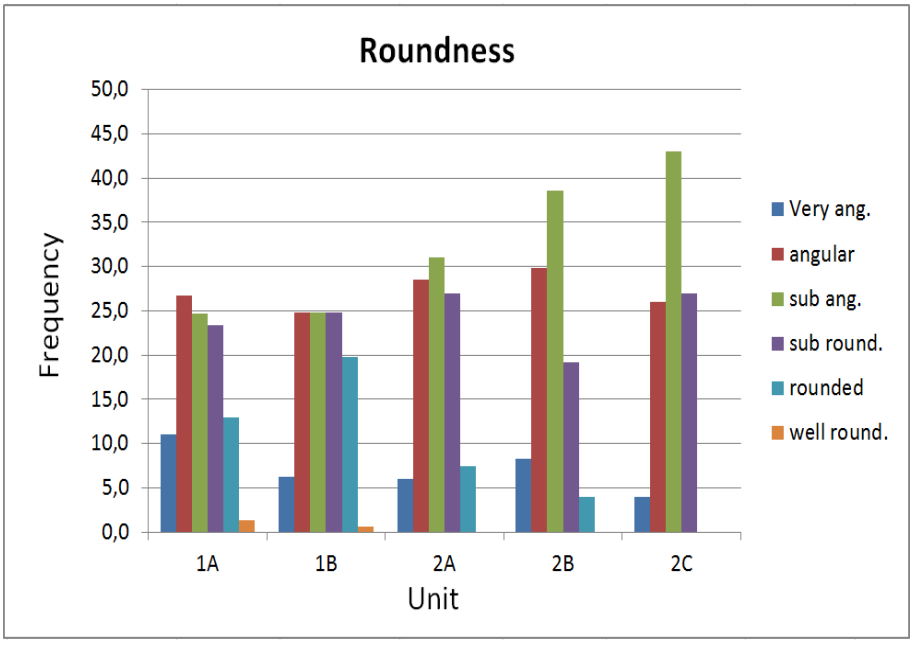

Figure 6-9. Distribution of grain shapes

The distribution of grain shapes is shown in figure 6-9, The vast majority of grains seems to be angular, sub angular and sub-rounded. Units 1A &B has a higher content rounded grains than the remaining units. It is worth noting that if the not the original grain is interpreted these results would be skewed towards higher angularity.

6.3.2 Grain contacts

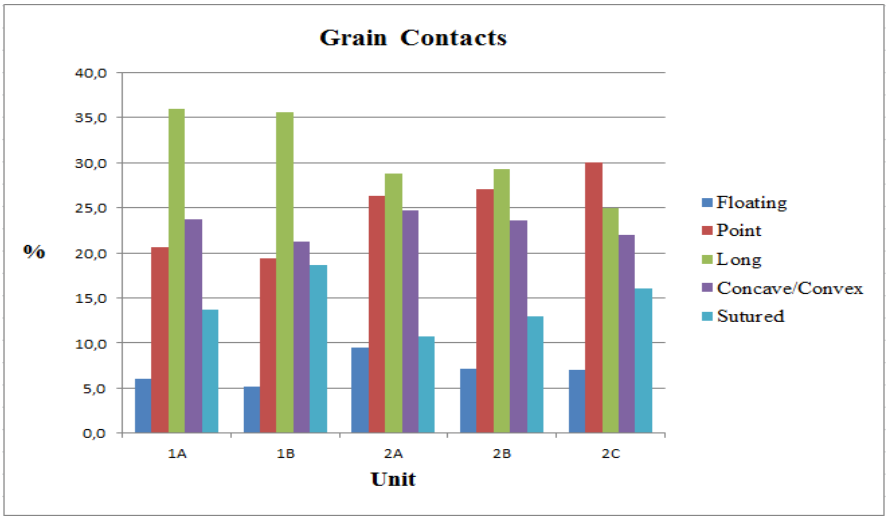

Figure 6-10. Types of grain contacts averaged for each unit.

Figure 6-10 shows the distribution of grain contacts for each unit, the vast majority of grain contacts overall are point-, long- and concave/convex contacts. In unit A&B the most prominent type of grain contact is long, with and almost evenly amount of point and concave/convex contacts. The biggest difference between unit 1 A&B is the increasing amount of sutured contacts in unit B. Units 2 A, B&C are quite similar in their distribution of grain contacts with a slight increase in the amount of sutured contacts with depth.

6.3.3 IGV

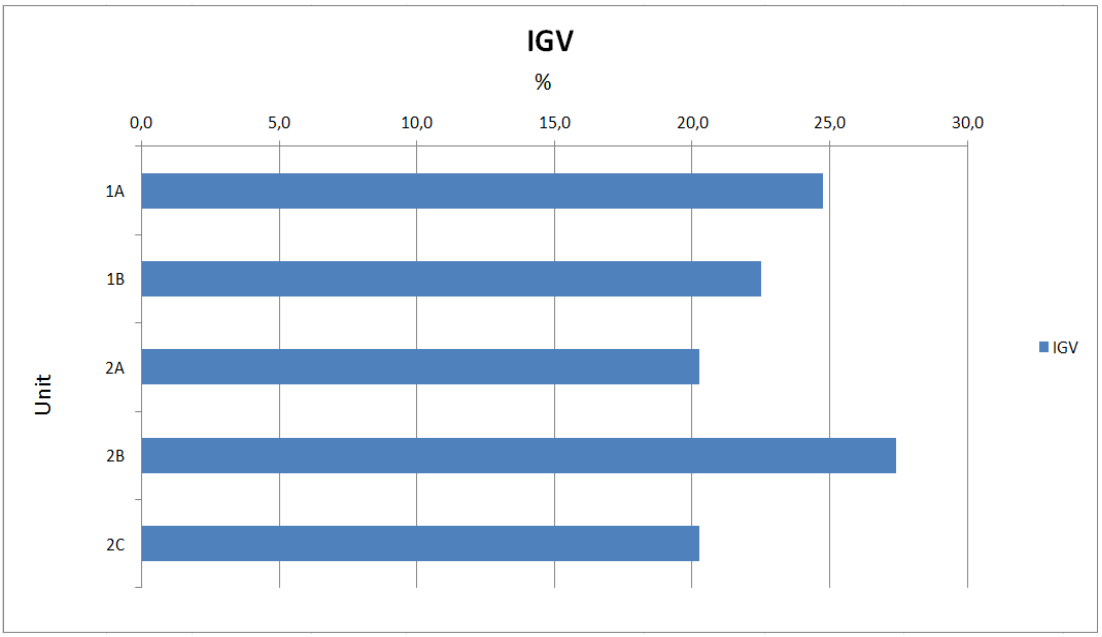

Figure 6-11. Distribution of intergranular volume in all units

The intergranular volume (IGV) is fairly similar for all samples ranging from a high of 27.5% in unit 2B to 20.5% in units 2A & C (fig. 6-11).

Unit 1A has an IGV of 24.5% and this declines to 22.5 % in unit 1B.

Unit 2B has a significantly higher IGV than the two other units from well 7120/12-2. Unit 2B is also the unit with significantly higher content of matrix.

When comparing the IGV with the average grain size for each unit there seems to a correlation between finer grain sizes and a higher IGV (fig. 6-12). Compared with the grain sorting a higher IGV seems to correspond to a higher standard deviation, bearing in mind that the sorting was fairly similar in all units (fig. 6-13). The matrix content versus IGV shows a bit more uncertain correlation, but excluding the significantly different unit 2B, there seems to be a slight trend of higher IGV with lower matrix contents (fig. 6-14).

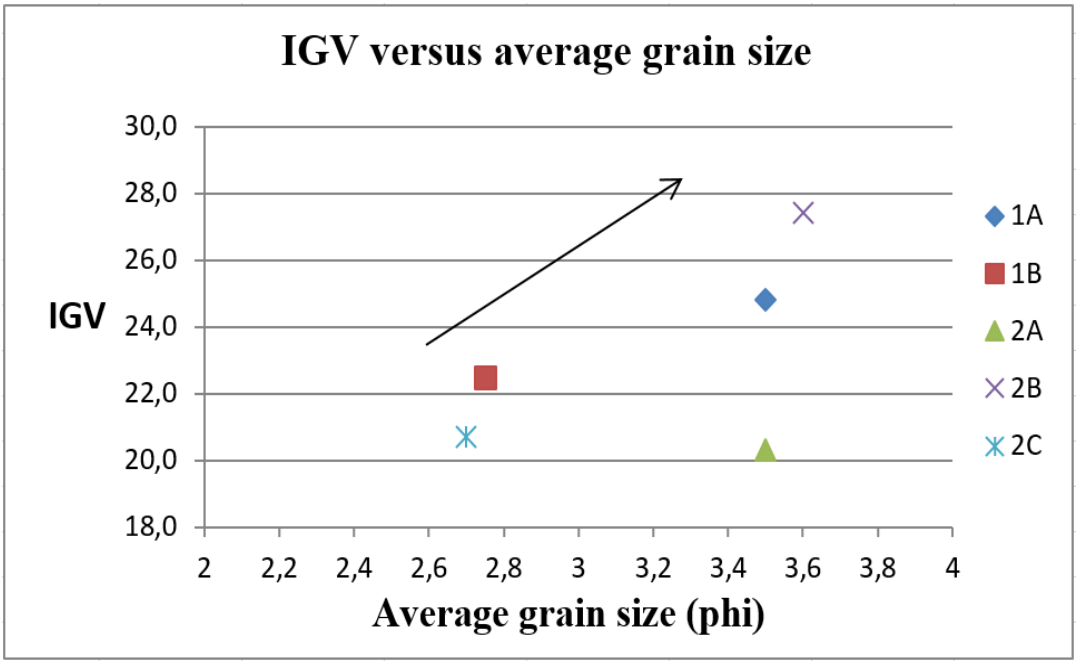

Figure 6-12. Intergranular volume plotted versus the average grain size, there seem to be a correlation between higher Intergranular volume and finer grain sizes.

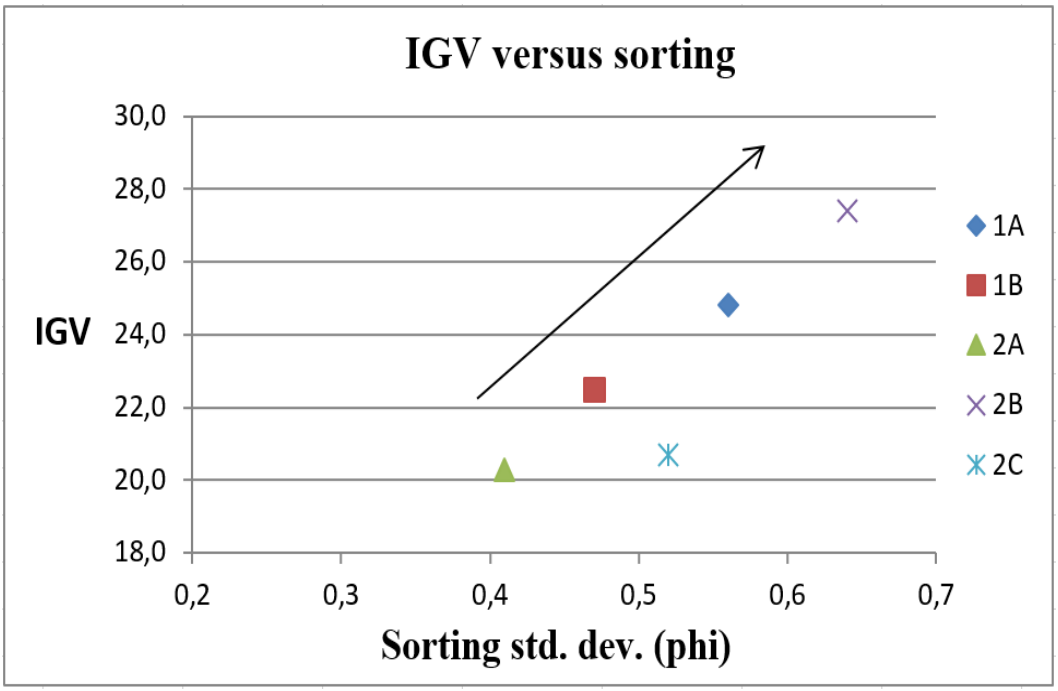

Figure 6-13. Intergranular volume versus sorting, there seem to be a correlation between higher standard deviation values and higher intergranular volume.

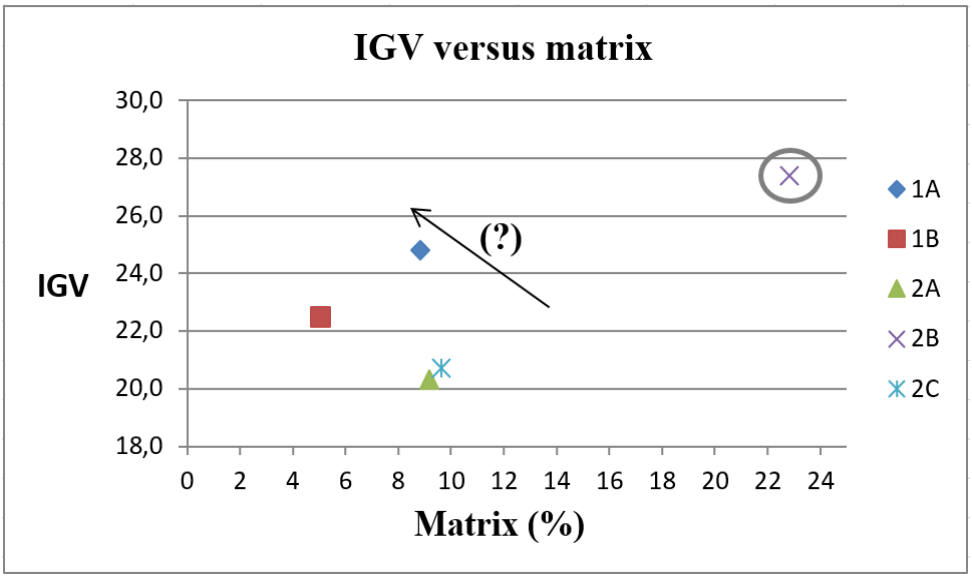

Figure 6-14. Intergranular volume versus matrix content, excluding the outlier belonging to unit 2B, there seem to be a trend of higher intergranular volume with lower matrix contents.

6.3.4 Leaching/dissolution of grains

Grain leaching was most prominently seen in detrital K-feldspar grains.

The overall feldspar content was as mentioned low, the feldspar that were present were mostly K-feldspar and minor amounts of albite. The K-feldspar present were almost exclusively showing a various degree of leaching and/or dissolution, trending towards severely leached e.g. image 4 in figure 6-6 and figure 6-24. There were not enough appearances of feldspar in the point counting to sufficiently quantify the degree of leaching but seeing as all but a minor amount was highly to severely altered that was determined to be the overall trend for the Stø formation in these two wells.

6.3.5 Appearance of clay minerals

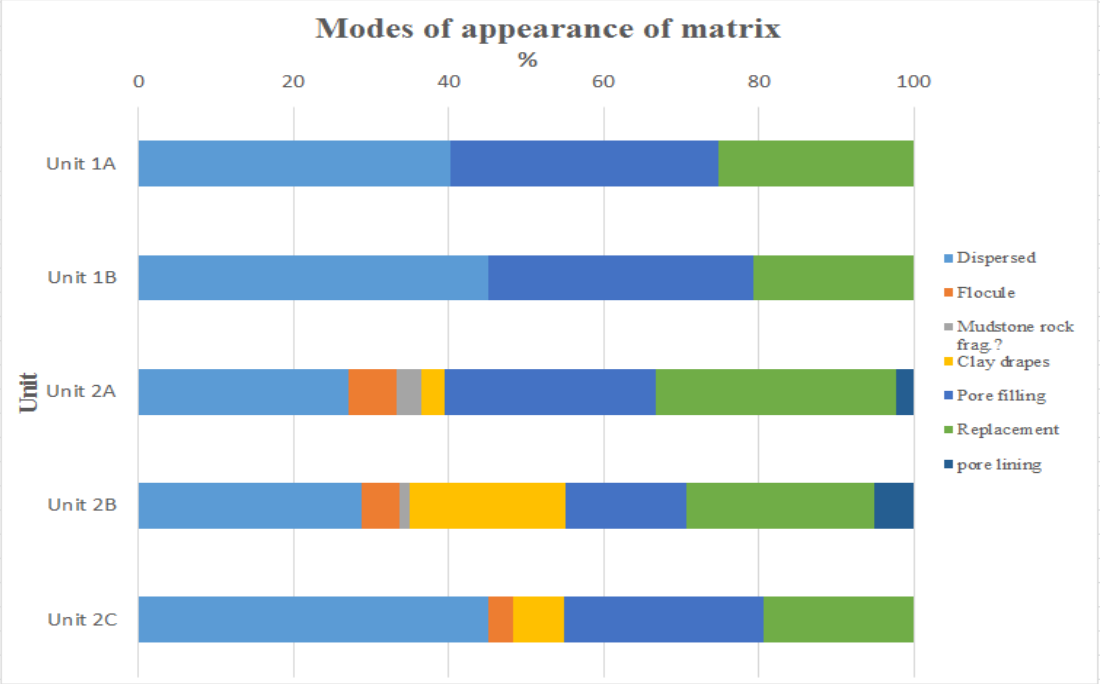

Figure 6-15. The visually determined modes of appearance of clay minerals averaged for each unit. Note that the clay drapes have been counted along with the matrix, the clay drapes does not act as matrix in a grain-supported setting and will not count towards the total amount of matrix.

Figure 6-15 shows the appearance of clay minerals in the thin sections as determined from point counting done with an optical microscope, the classification is highly qualitative and is strictly based on the relation of the clay minerals to the framework grains in each sample as compared with the illustrations of (Wilson and Pittman, 1977). The features of pore lining minerals can in cases have been far too small to have been noticed in the optical microscopy analysis. The most striking visual difference between the Stø formation in the two wells is the amount of matrix, although it also varies between samples from the different intervals in each well. In the samples from well 7120/2-3S the clay matrix had the appearance of dispersed clay, pore filling or “replacement” clay, the clay was determined to be replacing a previous grain most likely a precompacted clay clast when an initial grain shape could be recognized but it was found to be mostly containing a composition of slightly dispersed clay minerals.

The clay assembly was overall quite different in the samples from well 7120/12-2, especially in unit 2B, here the clay was more concentrated in certain areas as clay laminae or even clay

drapes as seen in image 5 in figure 6-6. In units 2B there was also some pore lining clay visible, no classification of type could be determined by the use of optical microscope.

The clay minerals could much easier be identified in the SEM analysis; the dispersed clay was mostly smaller kaolinite, illite and larger mica grains. Pore filling clay minerals were mostly kaolinite and illite.

The clay minerals seen to be remnants of- or precipitated from what is likely a previously somewhat compacted clay clast was often that of illite, kaolinite and sometimes authigenic microquartz, with some K-feldspar. Pore lining clay was seen less frequently than expected in SEM, those that were seen were mostly consisting of illite, kaolinite and minor amount of chlorite, although only a minor amount could be said to in fact be acting as grain-coating.

6.4 Scanning electron microscope (SEM) and cathode luminescence (CL)

6.4.1 Quartz cement

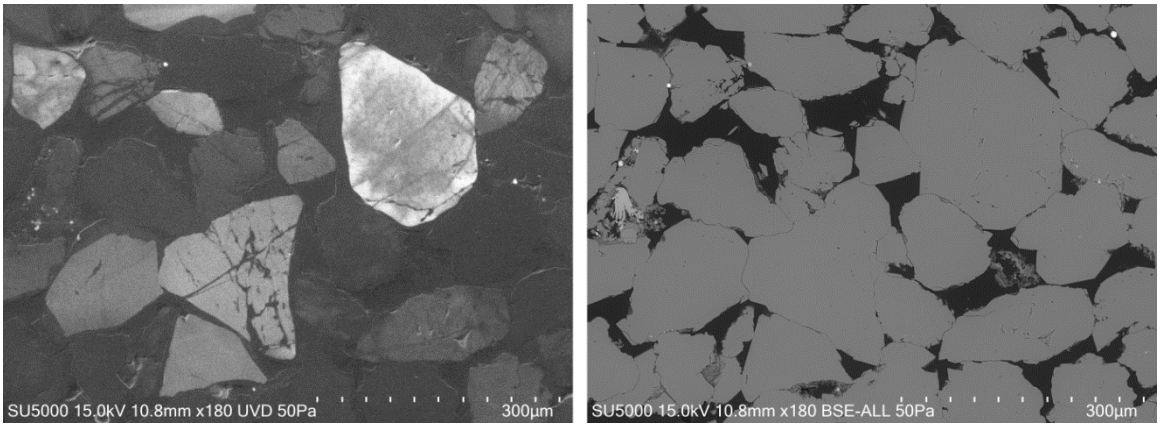

Figure 6-16. CL image (left) and backscatter electron image (right) The CL image clearly shows the authigenic cement overgrowth on several quartz grains as well as filling fractures in the detrital quartz grains. Well: 7120/2-3S, depth: 1743.20 (m).

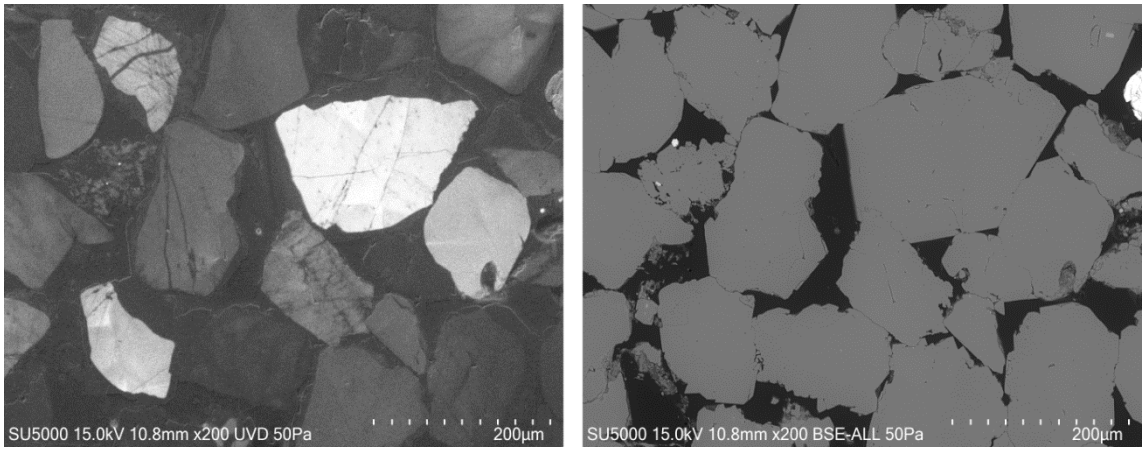

Figure 6-17. CL image (left) and backscatter electron image (right) The CL image clearly shows the authigenic cement overgrowth on several quartz grains as well as fracture filling. Well: 7120/2-3S, depth:1743.20 (m).

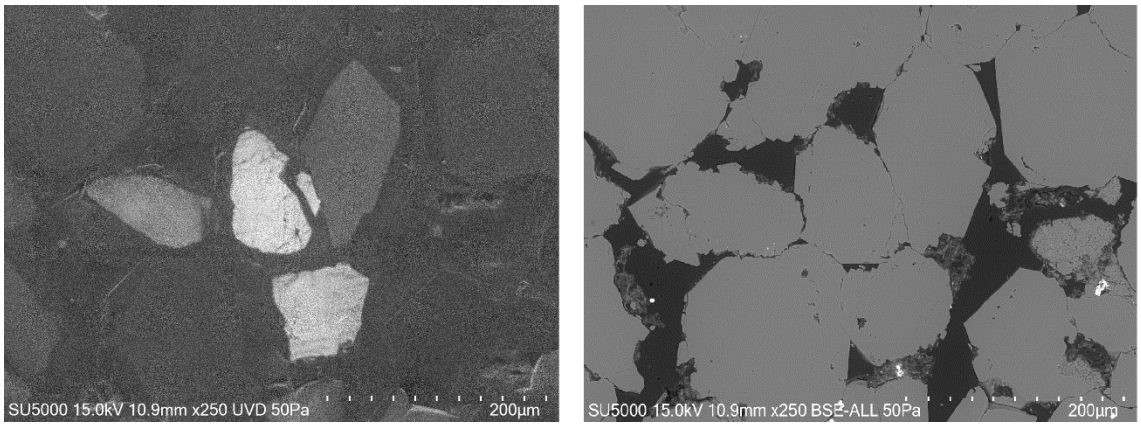

Figure 6-18. CL image (left) and backscatter electron image (right) The CL image clearly shows that all the quartz grains are covered by a significant amount of quartz cement. Well: 7120/2-3S, depth: 1824.25 (m).

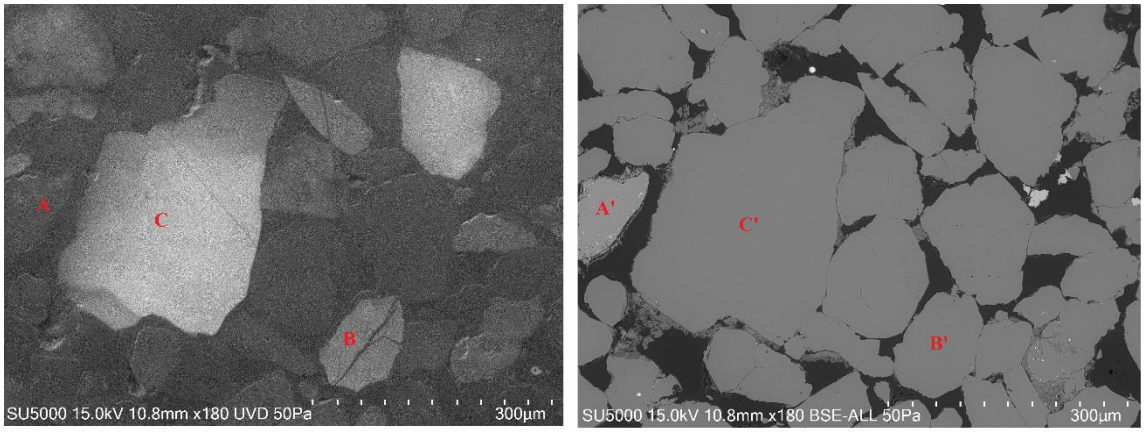

Figure 6-19. CL image (left) and backscatter electron image (right). The grain marked with (B) in the CL image clearly show the authigenic quartz cement covering the grain as well as filling the fractures. In the BSE image (B') it can be seen to have no visible grain coating. Grains A and C show little or no quartz cement in the CL image and can in the BSE image (A' and C') be coated by illite/chlorite. Seen especially well in A' where there is continuous coverage. Well: 7120/12-2 depth: 1711.15 (m).

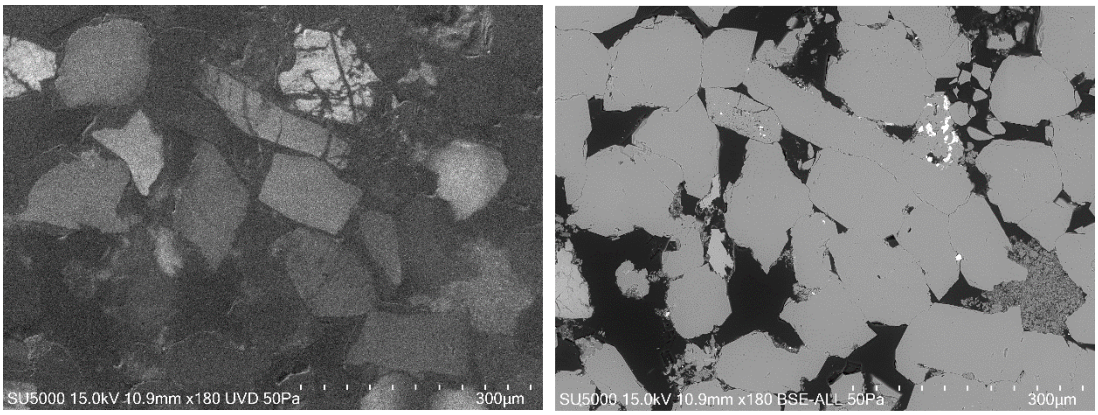

Figure 6-20. CL image (left) and backscatter electron image (right) The CL image clearly shows the authigenic cement overgrowth on several quartz grains as well as filling fractures in the detrital quartz grains note also the presence of pore filling kaolonite. Well: 7120/12-2, depth: 1773.80 (m).

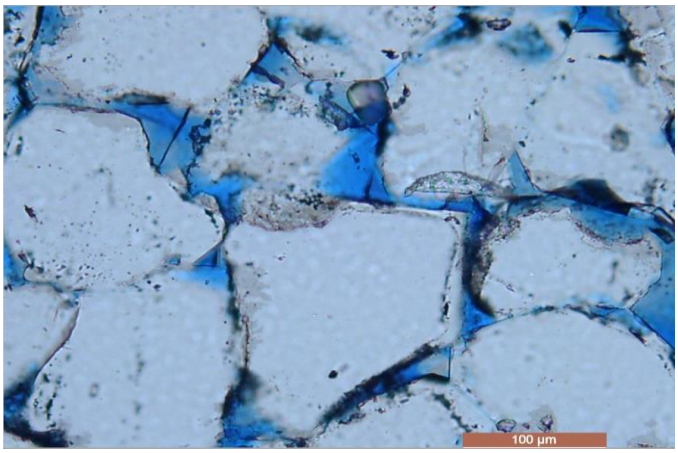

Figure 6-21. Example of quartz cement as seen in the optical microscope, with the characteristic euhedral shape and a dust rim separating the cement from the detrital grain. Well: 7120/2-3S, Depth: 1824.25 (m).

Figures 6-16 to 6-20 shows backscattered electron images and cathode luminescence images of the thin sections. Figure 6-21 is shown as an example of the appearance of quartz cement growth in the optical microscope. The authigenic quartz will ideally be recognized in the CL images as being darker than the detrital grains enabling a good visualization of the relative amount of quartz cement, the BSE images are also shown to further visualize the difference in appearance of the grains where there is a significant amount of quartz cement present. Quartz cement are overall more prevailing in the samples from well 7120/2-3S (fig, 6-16,6-17 & 6-18) compared to those from well 7120/12-2 (fig. 6-19 & 6-20). Several grains are clearly seen to have striking euhedral edges, and when seen in the CL images the quartz cement become evident. All samples investigated in the SEM from well 7120/2-3S showed at least some quartz cement, and most grains were covered by a significant amount. In the samples from well 7120/12-2 the amount of quartz cement varied to a much larger degree, but where present at least in some amount in all samples investigated in SEM. The overall appearance was also that the quartz grains in the samples from well 7120/2-3S had more often long to concave/convex and sutured grain contacts the difference is seen clearly in figure 6-26.

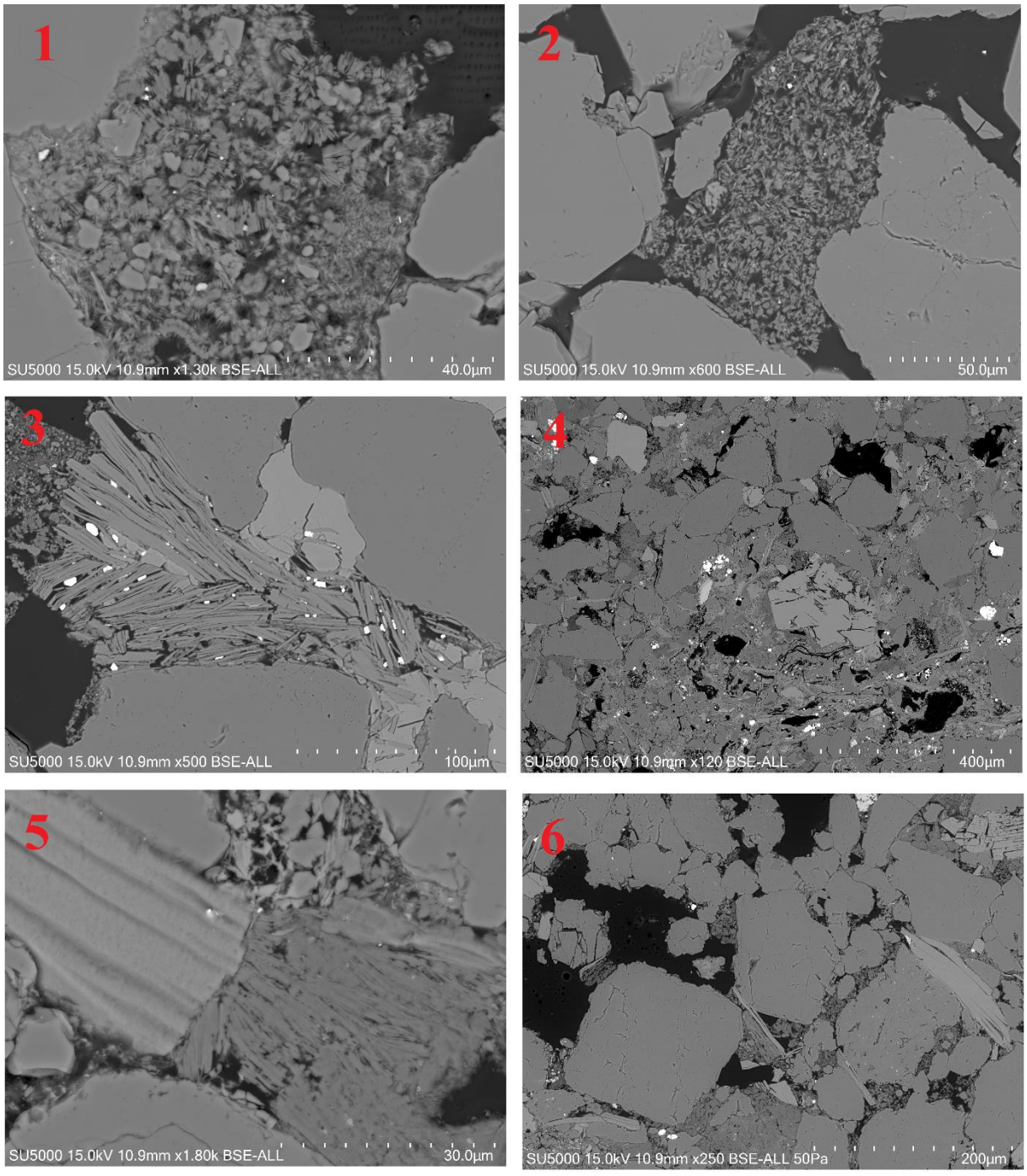

Figure 6-22. 1: Well: 7120/2-3S, depth: 1743.20 (m) Kaolinite, illite and microquartz filling the pore space between detrital quartz grains. 2: Well: 7120/12-2, depth: 1773,80 (m) Kalonite and illite shown to have replaced a previous grain, most likely a slightly compacted mud clast. 3: Well 7120/12-2, depth: 1784.31. Chlorite from possible biotite precursor in between quartz grains (darker) and ankerite (lighter), some kaolinite on the left hand side. 4: Well: 7120/12-2, depth: 1784.31 (m). Quartz, mica, pyrite and intermediately weathered K-feldspar grain with kaolinite. Pore space between detrital grains are almost completely filled with kaolonite, illite and allogenic clays. 5: Well 7120/12-2 , depth: 1784.31 (m). Mica (muscovite) and kaolinite. 6: Well: 7120/12-2, depth: 1784.31. Quartz kaolinite and muscovite. Note the appearances of quartz grains with rough surfaces.

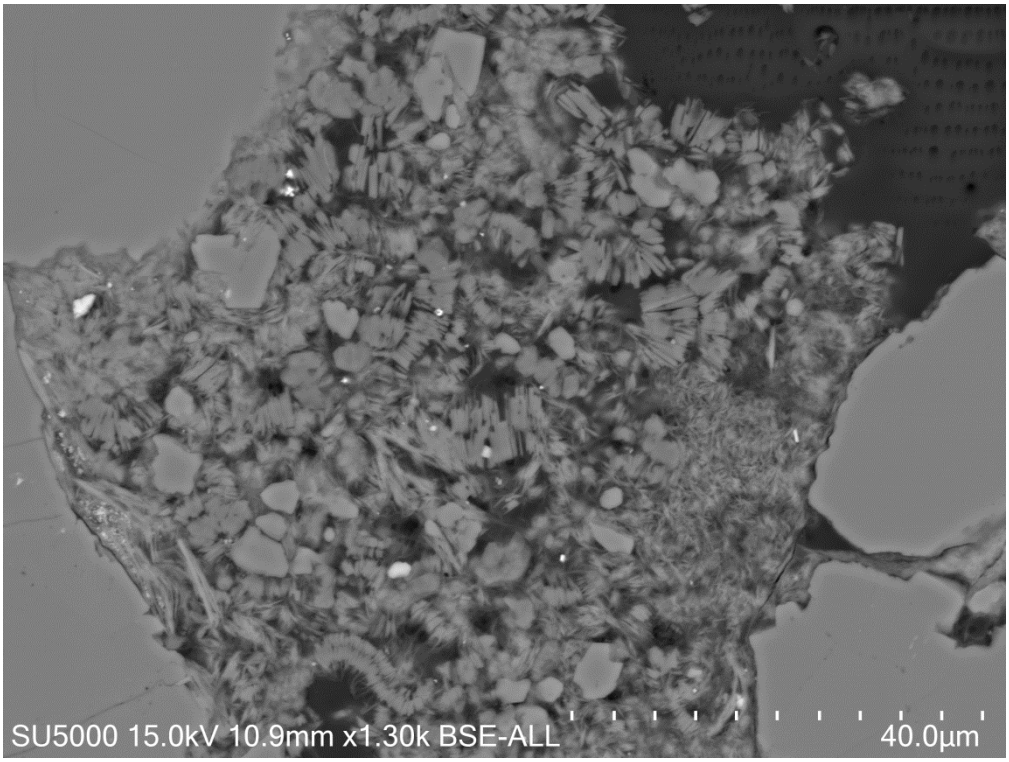

Figure 6-23. enlarged view of image 1 in figure 6-22.

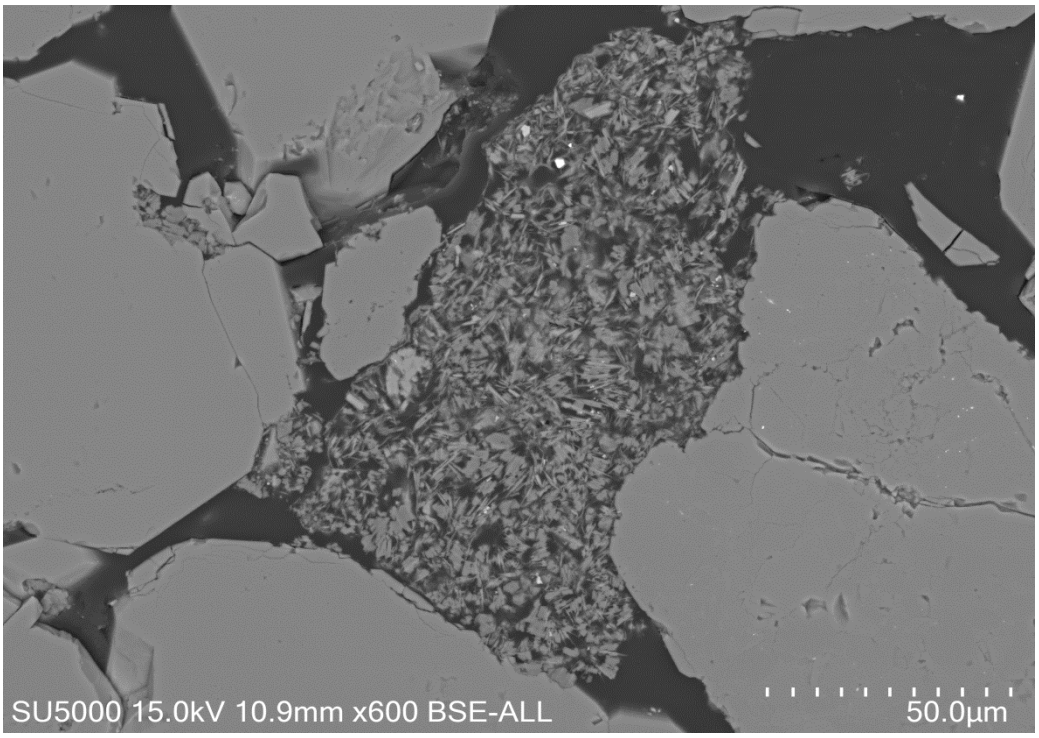

Figure 6-24. Enlarged view of image 2 in figure 6-22.

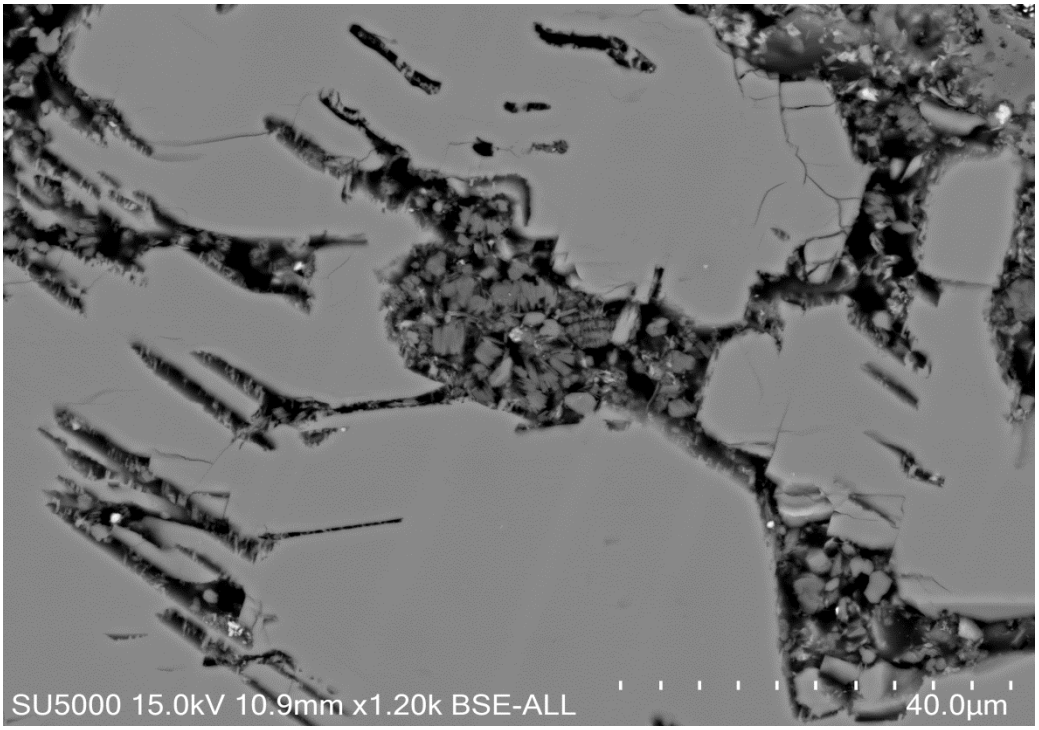

Figure 6-25. Well: 7120-12-2, depth: 1784.31 (m). Kaolinite filling secondary porosity in leached K-feldspar grain.

6.4.2 Authigenic clay, grain dissolution-leaching and mineral transformations

The most common authigenic clay mineral encountered was pore filling kaolinite and illite (fig. 6- 22, 23, 24 & 25) often related to the occurrence of highly leached K-feldspar grains. Chlorite was in some cases seen in relation with illite as seen in figure 6-19 and 6-27, but were also seen as pseudomorphus replacement between quartz grains as seen in image 3 in figure 6-22. From the elemental analysis the chlorite was seen to contain a significantly higher content of iron in relation to magnesium except for the chlorite found in relation with ankerite (fig. 6-22) which showed higher magnesium content and lower iron content.

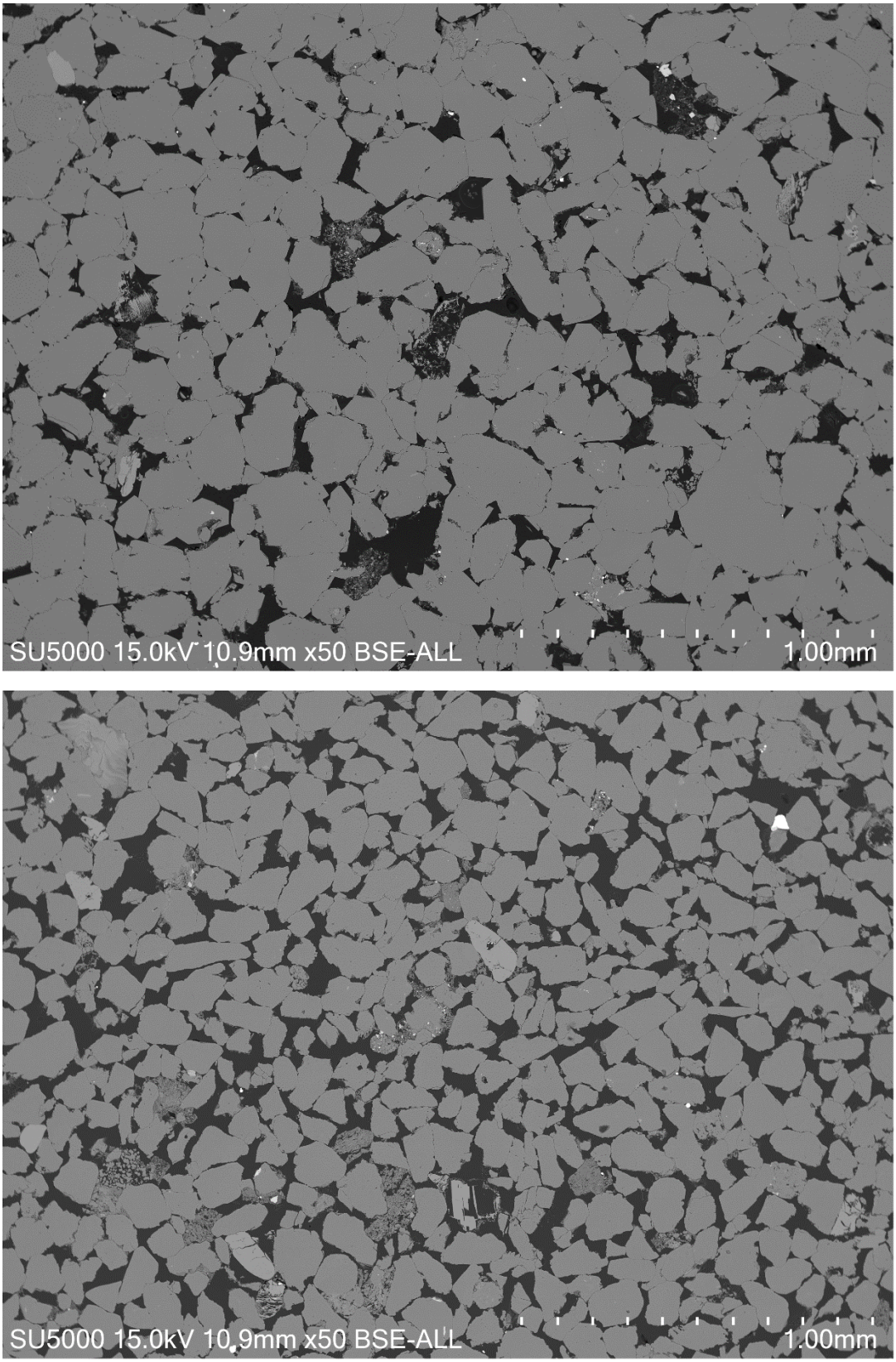

Figure 6-26. Top: Well: 7120-2-3S, depth: 1824.25 (m). Bottom: Well: 7120-12-2, depth: 1711.15 (m). The top picture show quartz grains covered with a significant amount of quartz cement, severely weathered feldspar grain and some pore filling kaolinite. The picture at the bottom shows quartz grains with little quartz cement, weathered Feldspar grain and some pore filling kaolinite.

Micro quartz grains (>4µm) was often seen in association with kaolinite and illite possibly stemming from precompacted mud clasts (fig. 6-23).

Some albite was present mainly in the samples from well 7120/12-2 and could be seen filling the fractures of K-feldspar grains and as pure albite grains (fig. 6-28).

A small amount of carbonates was seen in the samples, and most were ankerite, with a minor amount of dolomite. The ankerite was seen to completely fill out the pore space between quartz grains when present (fig. 6-22).

The K-feldspar grains were all showing at least some signs of leaching and/or dissolution with the majority being strongly leached, in some cases only the outline of the existing grain could be seen with some small remnants of K-feldspar and kaolinite and in some cases also illite in the pore space, as seen in figure 6-22. The degree K-feldspar leaching fluctuated in each sample, but it appeared to overall be more severely weathered grains in the samples from well 7120/2-3S.

In some areas of the samples from well 7120/12-2 corresponding to unit 2B there were a substantial amount of clay minerals almost completely filling the pore space between the framework grains (fig. 6-22) these areas also had a large amount of mica, mostly muscovite, present and the mica could be seen to lie in close contact with the quartz grains and even appearing to be “fused” with the quartz. The quartz grains in these areas also had a noticeable different appearance than what was commonly encountered in that the edges were usually appearing “weathered” or broken up giving what can be described as a rough appearance.

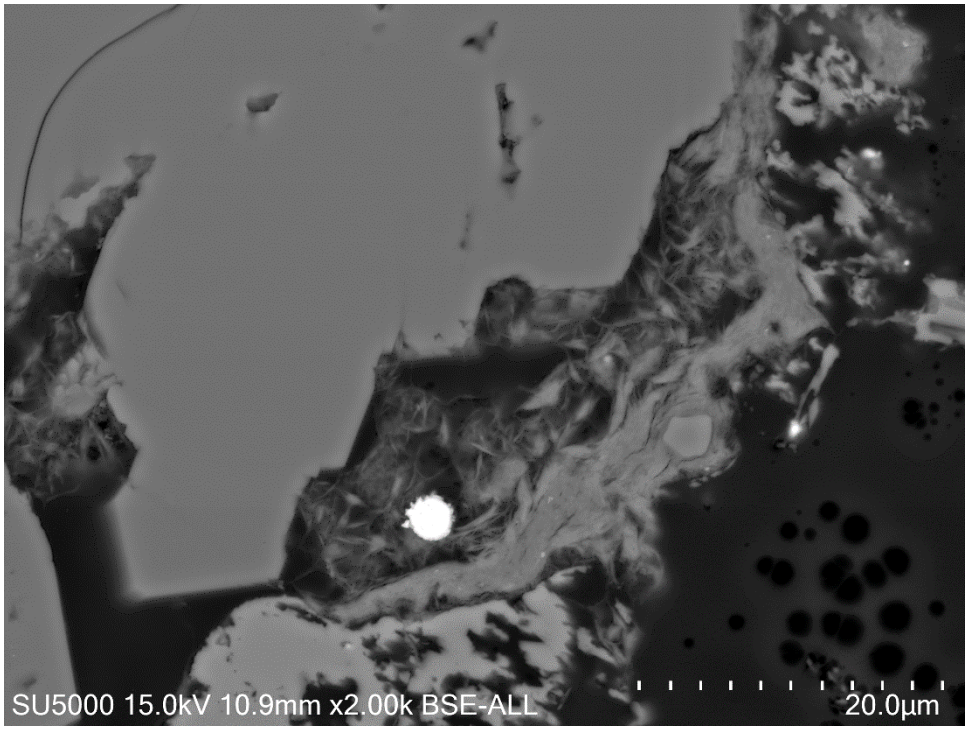

Figur 6-27. Illite and chlorite adjacent to quartz grain with quartz cement (above to the left) and weathered feldspar grain (below) the bright spot is pyrite. Well: 7120/2-3S, Depth:1824.25 (m).

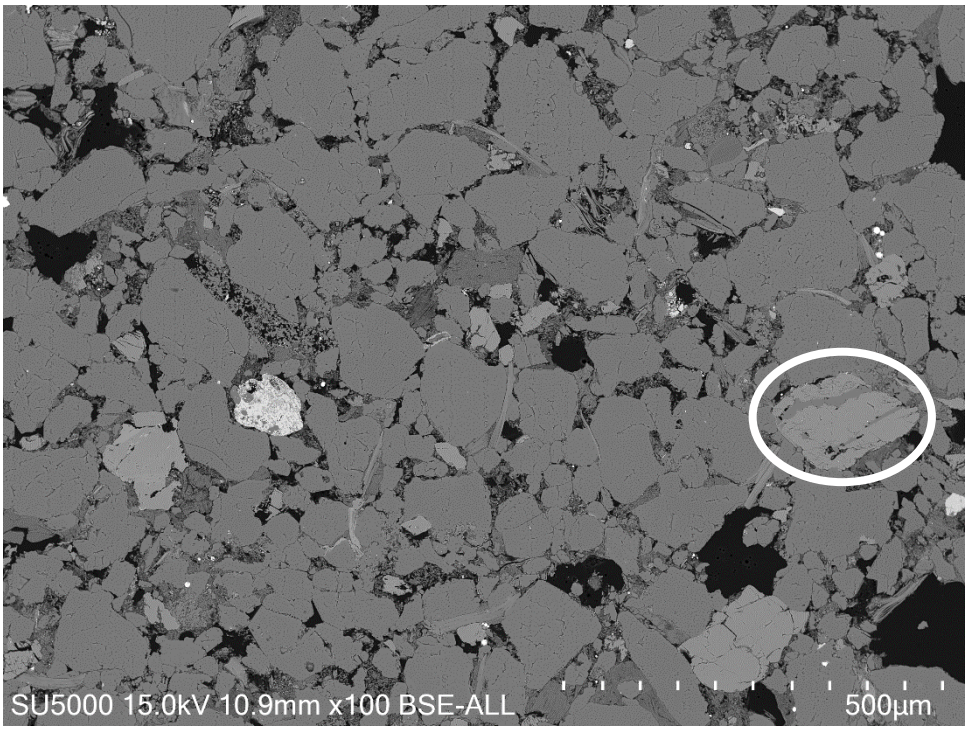

Figure 6-28. Well 7120/12-2, depth: 1784.31 (m). Note especially the albite in relation to the K-feldspar grain, and the appearance of mica in relation to quartz grains.

6.4.3 Grain coats

In the samples from well 7120/2-3 little grain coats where observed and most authigenic clay was seen to exist as pore filling, most being kaolinite and/or illite. A few grains contained some illite to chlorite/illite coating but the once that did never appeared to be completely covered and still showed at least some amount of quartz cement. In several cases grain lining illite was found on the authigenic quartz cement appearing to have formed after the authigenic quartz. Well 7120/12-2 showed somewhat more cases of grain coats appearing to have hindered quartz cementation as seen in figure 6-19 where the grains not having coating being covered by quartz cement whereas the coated grains have little or no cement. However even in the samples from this well there where not an extensive amount of grain coats. With quartz cement also here being quite prevalent although not nearly as extensive as that seen in the samples from well 7120/2-3S. One big difference between the samples from the two wells were the areas in the samples from unit 2B showing a large amount of clay minerals. (fig. 6-22) This consisted of mostly authigenic kaolonite and illite as well as allogenic clay, and in these areas there were close to no quartz cement but the porosity was nevertheless exceedingly small with almost all pores filled with clay.

6.4.4 Other minerals

Of the less common minerals encountered Pyrite was the most common, followed by rutile and zircon, all of which were seen in varying amount in all samples. Pyrite was most abundant in the samples corresponding to unit 2B which was seen in the petrophysical analysis to have a higher content of shale and higher matrix content as determined from point counting.

Chapter 7: Discussion

7.1 Introduction

A better understanding of the reservoir quality of a sandstone and how it relates to the initial composition of the sediments facilitates better estimates of the reservoir quality prior to drilling. The reservoir quality of the Stø formation and how it varies between the two wells and between different intervals in the same well forms the basis for the attempt at correlating the presently observed reservoir quality with the initial composition of the sediments.

Variations in reservoir quality observed over small intervals in the same well can be correlated with the different responses to diagenetic processes from different lithologies under the following assumptions, also presented more thoroughly in chapter 3; (1) The initial composition of sediments are determined at deposition, governed by facies, provenance and climate, and to a varying extent by leaching and precipitation in the near subsurface when the flux of porewater is high enough to transport solids in solution in to, and out of a sediment body. (2) Below the reach of a high enough porewater flux or if there is no significant meteoric water flushing present, the bulk composition is assumed to remain constant and any subsequent alteration of textural or mineralogical features will be governed by pressure, time and temperature, meaning that it behaves as a closed system where there is little or no transportation of solids in solution over any significant distances, the findings of Walderhaug and Bjørkum (2003) that the amount of quartz cement diminishes quickly after distances of only 20cm and more from nearest stylolite is a good indication that this is in fact the case.

Under these assumptions it means that any variations in the reservoir quality of sandstones subjected to the same burial history will relate to the differences in the initial lithological composition and assuming that the initial and final composition is correctly estimated a correlation can be made.

The following discussion will therefor mainly be divided into two parts; first a discussion about the main differences between the two wells and internally over the formation in each well, in regards to the depositional setting and initial composition, and burial history. Then the observations of the present parameters relating to the composition of the Stø formation will be presented, these results can then be compared to try and see how the varying initial composition and burial history relates to the ultimate reservoir quality at depth.

The estimates of the initial composition and depositional setting is based mainly on the makeup of the detrital framework grains, the amount of matrix and the petrophysical gamma ray log and shale volume calculations. In addition the amount of shallow burial alterations has been inferred from leaching of detrital grains, mainly K-feldspar and precipitation of kaolinite. No core logging was performed for this thesis, but pictures of the cored intervals of well 7120/12-2 were available from NPD.

7.2 Depositional setting and provenance

The Stø formation consists primarily of mature sandstones with the framework mineralogy in both wells consisting predominantly of quartz with only a minor amount of feldspathic and lithic grains.

The main difference between the various units were the amount of clay minerals present, predominantly as matrix in grain supported sandstones but also as clay drapes in certain areas, ranging from exceedingly clean samples as some of the samples in unit 1B from the lower parts of the formation in well 7120/2-3S, to the high content of matrix and clay drapes seen in the samples from unit 2B from the lower parts of the formation in well 7120/12-2.

The shaliness of the formation as calculated from the gamma ray log is seen to fluctuate within the formation and the most striking difference between the two wells are the consistently clean interval in the lower parts of the formation in well 7120/2-3S (fig.7-1). At two instances in well 7120/2-3S and one in well 7120/12-2 the Vshale can be seen to show an abrupt increase. The rapid increase in shaliness has been interpreted as being caused by transgression events. The higher gamma ray readings, and thus Vshale calculations, indicate a depositional setting preserving more clay minerals in the sediments. As the potential for the fine grained clay fraction to be preserved in the sediments greatly relates to the hydro dynamical state of the water at the sediment-water interface (Peters and Loss, 2012) these sediments are determined to have been deposited in a more distal setting with less energy and less reworking of the sediments.

The funnel shape of the upwards coarsening intervals in the gamma ray log are indicative of barrier bars, beaches, and delta marine fringe settings (Mondol, 2015). The funnel shape response of the gamma ray seen to repeat in well 7120/12-2 is consistent with the interpretation of overall rhythmic intervals of barrier bar and coastal environments during deposition of the Stø formation (Worsley, 2008). The lower parts of the formation in well 7120/2-3S corresponding to unit 1B is interpreted as being deposited in an upper to lower shore face high energy setting possibly as bar complexes to beach settings, and the long interval of clean readings are probably due to the fine balance between influx of sediments and rate of subsidence, maintaining the position of the coastline (Olaussen et al., 1984). The upper parts of the formation in this well, corresponding to unit 1A are divided from the lower unit by the interpreted transgression event, and contain more clay matrix. This interval shows an overall upwards coarsening trend indicating a progradation of the coastline and gradually more proximal settings with higher energy depositional environments.

The same facies as that seen in unit 1B is not recognized in the Stø formation in well 7120/12-2. Instead the appearance in the gamma ray log shows two repetitions of a somewhat similar trend as that in the upper parts of the formation in well 7120/2-3S, with an upwards coarsening trend interpreted as being two intervals of development from more distal marine settings (fig.7-2) with an intermediate content of clay, to more proximal barrier bar/beach depositional settings with less clay preserved in the sediments (fig. 7-3).

Based on the petrophysical and petrographical results the following characteristics summarize the composition of the varying units.

Unit 1A: Very fine to fine grained, moderately well sorted quartz arenite with a moderate content of clay matrix, averaging around 10 %.

Unit 1B: fine grained, well sorted clean sandstone with a low content of matrix averaging around 5 %.

Unit 2A: very fine, well sorted sandstone with an average of 10 % matrix, with the majority of the clay matrix is found in the lower parts of the unit.

Unit 2B: very fine to fine grained, moderately well sorted and in places argillaceous sandstone with an overall high content of matrix averaging around 20 %. Several shale laminated horizons, certain intervals nearly classified as mudstone. Increasingly micaceous with depth, with an average of 4 %.

Unit 2C: fine grained, moderately well sorted sandstone, 10 % matrix, relatively high mica content (3%)

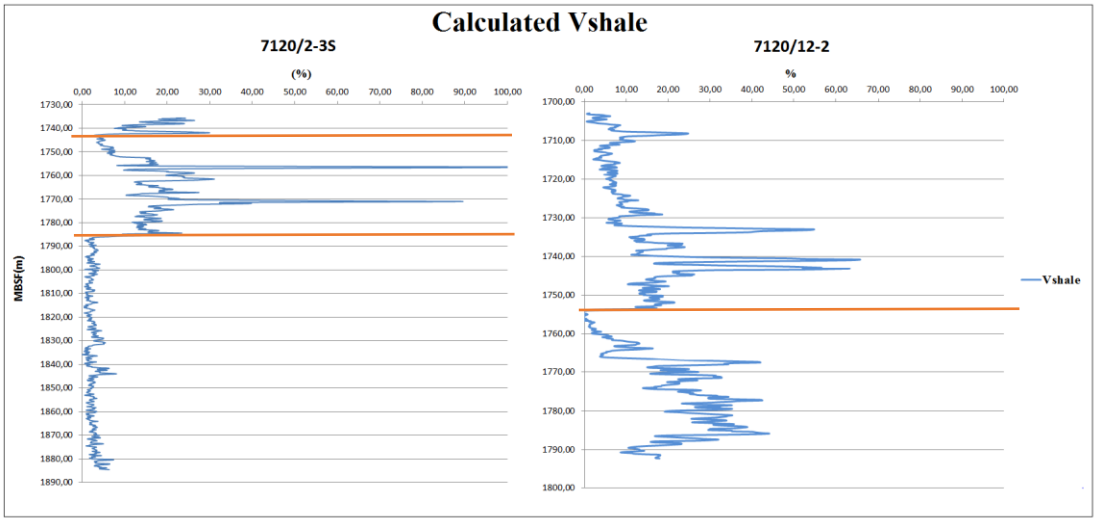

Figure 7-1. Calculated vshale for the Stø formation with red lines indicating possible transgression events.

Figure 7-2. Argillaceous sandstone with frequent shale laminations in the interval of Stø formation in well 7120/12-2, corresponding to unit 2B. Depth: 1783-1786 MBSF. From NPD factpages (factpages.npd.no)

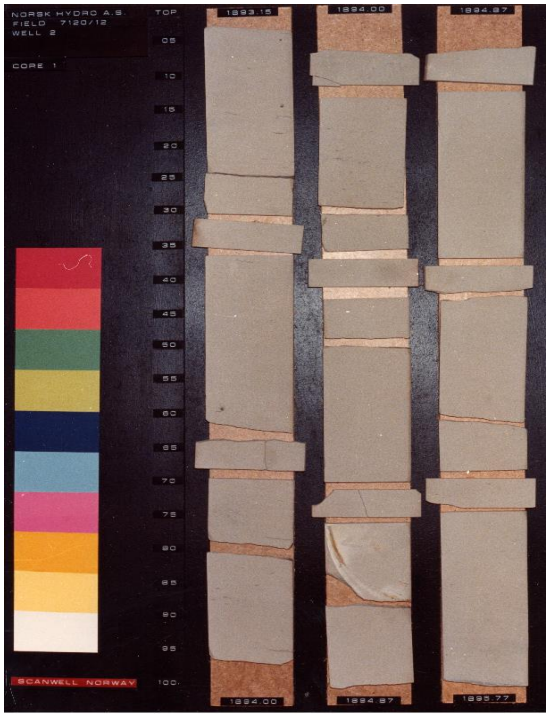

Figure 7-3. Clean homogenous sandstone from the upper part of the Stø formation in well 7120/12-2. Depth: 1704-1706 MBSF. From NPD factpages (factpages.npd.no)

At time of deposition in the early to middle Jurassic the area was influenced by low subsidence rates (Bergan and Knarud, 1993), and more stable platforms (Faleide et al., 1984). The stable platform setting can cause longer transport time for the sediments with repeated deposition and erosion of the sediments before finally reaching the position of final deposition gradually increasing the textural and mineralogical maturity of the sediments (Bjørlykke and Jahren, 2015). Furthermore, high energy shallow marine depositional settings as that predominant for the Stø formation e.g. (Olaussen et al., 1984, Worsley et al., 1988, Bergan and Knarud, 1993) also favors the formation of more mature sandstones due to higher level of reworking of the sediments.

The stable platform conditions meant that the major influence on depositional setting was the progradation of sediments and sea level change. The variations, predominantly in matrix content, must therefore be seen mainly as a response to the relative energy of the depositional environment.

Provenance

At time of deposition of the Stø formation there was probably a reduction in the sediment influx from the easterly provenance area of the Uralian mountains. The denudation of the Caledonian mountains may have facilitated the erosion of un-metamorphosed quartzites of the late Proterozoic (Bergan and Knarud, 1993).

Olaussen et al. (1984) suggested two major and one minor possible source for the sediments in the Stø formation; regional metamorphic rock of possible Caledonian to Precambrian basement, low grade or un-metamorphosed pre-Mesozoic sedimentary rocks and plutonic rocks. The types of rocks weathered will greatly influence the initial composition of the sediments, and the possible quartzitic late Proterozoic source rock will further facilitate the mature sandstones observed. However as there is likely several provenance areas for the sediments of the Stø formation as suggested by Olaussen et al. (1984) and as can be inferred from the interpreted paleogeography also shown in figure 2-5 (Smelror et al., 2009). There was likely also a higher content of e.g. clay minerals as mica, and feldspathic grains initially deposited. The higher content of these minerals in the more clay rich samples compared to the cleaner samples indicates that reworking and shallow burial alteration is important in the preservation of these minerals.

7.3 Shallow burial

7.3.1 Meteoric water flushing

If there is a significant flux of meteoric water, the easier to remove minerals as K-feldspar and mica are assumed to be removed or severely leached. Shallow burial diagenesis can severely affect the reservoir quality as it has the ability to change the bulk composition in a geochemically open system. As the leaching of K-feldspar grains is assumed to correspond to the amount of kaolinite precipitated the initial amount of K-feldspar in the sediments will control the amount of kaolinite formed assuming the existence of a meteoric water flow.

The overall feldspar content of the samples were low, and overall less than ~2-3%, but there was quite a significant amount of kaolinite seen in the samples, with the most kaolinite being present in the upper parts of the formation in well 7120/2-3S and the uppermost and lowermost parts of the formation in well 7120/12-2. It should be noted that the higher kaolinite to feldspar ratio in these areas are not explicitly quantified as some kaolinite probably was not identified during point counting and are instead inferred from the visual appearances in the electron microscope.

Figure 7-4 shows the amount of K-feldspar, mica and total clay content counted in the samples. There seem to be a correlation between higher amounts of total clay content and detrital K-feldspar and mica. The correlation is consistent with the assumption that more clay rich intervals have been deposited in lower energy environments, thus also preserving more of the initial K-feldspar and micas due to a lower degree of reworking and possibly less influx of meteoric water, reducing the formation of authigenic kaolinite. Consistent with this is the observation from SEM that the samples from unit 2B showed K-feldspar grains with the least amount of leaching.

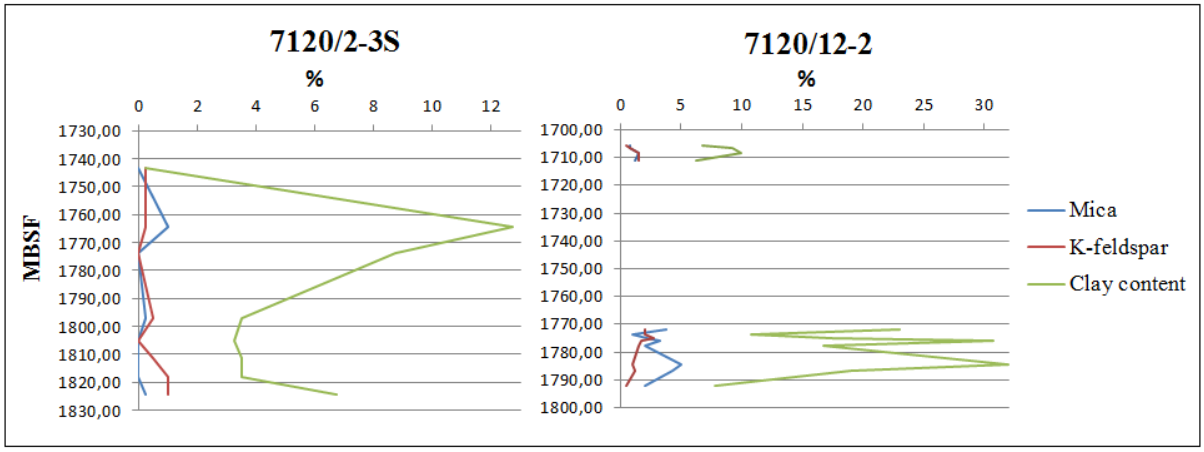

Figure 7-4. Mica, K-feldspar and total clay content in the point counted samples. There appears to be some correlation between the amount clay in the sediments and Preserved detrital K-feldspar and mica.

7.3.2 Allogenic clay

The presence of allogenic clay was highly polarized between the samples and between different parts of the formation. Most of the allogenic clay occurred as dispersed, intercalated laminae or infiltration residues. There were also areas with clay drapes existing only in samples from the 7120/12-2 well corresponding to unit 2B. The presence of clay in the Stø formation seem to follow a somewhat rhythmic pattern especially in well 7120/12-2 and the upper parts of the formation in well 7120/2-3S, with variations over short vertical distances seen also in the core logs available from npd (fig, 7-2). The presence of clay drapes in unit 2B may have interfered with the determination of IGV and the point counting in general as clay drapes may have been counted as matrix when in fact the areas might not have been grain supported. The relative presence of allogenic vs. authigenic clay is also much larger in the samples from well 7120/12-2 with some of the samples especially from unit 2B causing the high average clay content. Some samples from this unit where fairly clean, even though the unit on average had a higher content of clay and clay matrix. The major overall influence on the amount of clay in the samples is thought to be due to the relative proximity of the area of deposition, seen in unit 2B as it is interpreted as having been deposited in the most distal setting of the intervals in the Stø formation, The fluctuation of matrix content in the more proximal deposits can be due to tidal influences or rate of sediment discharge.

7.3.3 Carbonate cementation

Overall there was little carbonate cement in the samples analyzed, with the point counted observations being carbonate concretions or pore filling infiltration layers. Overall the Stø formation in well 7120/12-2 contained more carbonates than in 7120/2-3S, with the highest abundance in unit 2B, Some carbonates where identified in well 7120/2-3S, but only in unit 1A. From the wells analyzed with the electron microscope it was seen that the carbonates present where either dolomite or ankerite, most likely formed from calcite (Saigal et al., 1987). More heavily carbonate cemented intervals of the Stø formation are reported from e.g. Olaussen et al. (1984) and Bergan and Knarud (1993), and in cases where there is extensive carbonate cementation, it can significantly affect the reservoir quality. No significant amount was observed in the samples from the two wells investigated in this thesis.

7.4 Uplift estimation, burial depths and temperature

The bottom hole temperatures available from NPD for well 7120/12-2 gave a calculated geothermal gradient of 24.8 ºC (table 5-1), and the estimated uplift was determined to be approximately 900m, giving a maximum burial depth of 2603-2689m.When using the estimated present day geothermal gradient the highest temperatures that the Stø formation has been exposed to in this well would then be 69.2 – 71.4 ºC, a value assumed to be too low for any significant quartz cement to form (Bjørlykke and Egeberg, 1993), however a noticeable growth of quartz cement where observed in the samples from this well.

The expected present day geothermal gradient for the southwestern Barents Sea is on average 31-38 ºC (Smelror et al., 2009). In any casesthe paleo temperature gradient can be assumed to have been higher than the one calculated from the available bottom hole temperature due to the quartz cement observed.

Assuming instead a possible paleo geothermal gradient in the range of 31 – 38 ºC gives the temperatures at maximum burial for the Stø formation in well 7120/12-2 to be in the range of ~84-102 ºC temperatures high enough to account for the quartz cement observed (table 7-1).

The Stø formation in well 7120/2-3S, assuming the bottom hole temperature is correct and relatable to the paleo temperature gradient, have been subjected to higher maximum

temperatures than the formation in well 7120/12-2 . The Stø formation is also currently in the temperature range where quartz cementation can occur in this area, although in the lowermost ranges where the precipitation rates for quartz is expected to be low (Bjørlykke and Egeberg, 1993) (table 7-1).

The bottom hole temperatures measured from wells have a tendency to be biased to lower temperatures even after being corrected (Smelror et al., 2009), and there is no reason to believe that the estimated geothermal gradient is too high. For well 7120/12-2 even at the highest range of proposed geothermal gradients the current temperatures are just barely permitting the precipitation of quartz cement, and if a more cautious estimation of geothermal gradient is applied the Stø formation is currently experiencing temperatures not consistent with the precipitation of quartz cement.

Quartz cement is highly dependent on the time-temperature integral and at temperatures above that of quartz cement initiation further increase in temperature will significantly increase the precipitation rates (fig. 7-5).

Since the formations are of similar age, and the sediments in the 7120/2-3S well were exposed to higher temperatures the sandstones will here have experienced an ever increasingly amount of quartz cement compared to the sediments exposed to lower temperatures assuming no mechanisms were in place to prevent the formation of quartz cement. This correlates well to the observations in the samples where the samples from well 7120/2-3S showed significantly more quartz cement as discussed in section 7.6.

When sediments are exposed to temperatures above those enabling the precipitation of quartz cement this process will continue even through uplift until the sediments potentially gets uplifted to burial depths corresponding to temperatures below~65 °C as it appears is the case for the formation in well 7120/12-2. However, since the most significant amount of uplift is believed to have occurred in recent times from maximum burial depths in Eocene – or Oligocene (Baig et al., 2016) with at least parts of it occurring as late as Late Pliocene-Pleistocene due to the scouring of massive ice sheets (Cavanagh et al., 2006), the eventual time spent above the temperatures enabling quartz precipitation even for the Stø formation in well 7120/12-2 are deemed as low.

Table 7-1. Estimated maximum burial depths and temperatures of the Stø formation in the two wells, for well 7120/12-2 this table also shows the geothermal gradient and maximum burial temperatures assuming a higher geothermal gradient.

Well	Present depth of the Stø Fm. (MD)	Geothermal gradient calculated from BHT (°C)	Possible paleo temperature gradient (°C)*	Present temperature at current burial depth (°C)	Estimated maximum burial depth of the Stø Fm. (MD)	Temperature at maximum burial depth (°C)
7120/2-3S	1735.5-1885.5	39	N/A	67.7 – 73.5	2985.5 – 3135.5	116.4-122.3
7120/12-2	1703 - 1789	24.8 (?)	31* - 38*	42.2 – 44.4 (?) 52.8 – 55.5* 64.7 – 68*	2603-2689	64.6-66.7 (?) 80.7 – 83.4* 98.9– 102.2*

7.5 Intermediate burial

7.5.1 Mechanical compaction

The main method used to evaluate the influence of mechanical compaction is the intergranular volume of the sediments as this is assumed to remain mostly the same after onset of chemical compaction. Difference in IGV in sediments exposed to the same effective pressures is assumed to be caused by the textural and mineralogical composition of the sediments as determined at deposition e.g. (Fawad et al., 2011).

The IGV in well 7120/2-3S is estimated to be just under 25% in unit 1A corresponding to the upper parts of the formation and around 22,5% in unit 1B corresponding to the lower unit.

Unit 1A consists on average of somewhat finer grain sizes than unit 1B with the majority of grains being very fine and up to silt size, whereas unit 1B has majority of fine sized grains. The sorting is slightly better in unit 1B being well sorted whereas unit 1A is moderately well

sorted. The matrix content is higher in unit 1A with an average of 8% matrix content in this unit versus 5% in unit 1B. Finer grain sizes and better sorting is expected to preserve IGV better then coarser grained poorly sorted sediments, higher content of ductile grains, such as clay minerals, will often cause somewhat poorer IGV. From these results the major influence on preservation of IGV in this case is the grain size.

The IGV in well 7120/12-2 ranges from just above 20 % in units 2 A&B to 27.5 % in unit 2B. The average grain size where that of very fine sand in both unit 2 A&B and that of fine sand in unit 2C. Unit 2A were well sorted whereas 2 B&A where moderately well sorted. The matrix content was fairly similar in units 2 A&B at just below 10 % and significantly higher in unit 2B at over 20 %. This would indicate that the preservation of IGV relates to the increasing content of matrix, something that severely contradicts what is expected from experimental compaction of different sands e.g. by Fawad et al. (2011).

This contradiction along with the low IGV estimates overall, except perhaps that in unit 2B, compared to what expected from similar sandstones subjected to mechanical compaction down to depths of around 2-2,5 kilometers, where quartz cementation is assumed to halt further mechanical compaction in the formation in these wells indicates strongly that the IGV estimates overall are too low.

Furthermore, if the IGV where in fact as low as the results show there would presumably be evidence of extensive grain crushing seen to nucleate from grain-grain contacts in the detrital mineral grains, but only a few fractures where seen when investigated with cathode luminescence.

The fact that the IGV estimations are so similar in all units, the erroneous values are probably caused by a similar error for all samples. The error is most likely that of the definition of what were to belong as the constituents of the IGV during point counting, and the estimation of quartz cement (as discussed below).

The fact that the IGV estimates most likely are too low is unfortunate as it hampers the possibility to estimate the effect of mechanical compaction on the different lithologies. However, fortunately the textural appearance of the sediments in all units with respect to grain size and sorting were not vastly different, and the overall trend is a slightly higher IGV in the

7120/2-3S well which overall had the cleanest sedimentological composition. And somewhat of a correlation between higher IGV and finer grain sizes as seen in figure 6-12.

7.5.2 Authigenic illite and mineral alterations

Illite, mostly found to be pore filling was observed in all the samples investigated in the SEM, but were most often encountered in the sample from the upper parts of the formation in well 7120/2-3S and to a somewhat lesser extent in the sample from the cleaner lower parts.

In well 7120/12-2 the observation of illite often corresponded to the more clay rich intervals. In the samples from well 7120/2-3S the illite was predominantly found in association with kaolinite which could indicate that the kaolinite to illite reaction has been the source of the illite in these cases, this would require a slightly higher geothermal gradient than what is observed today. However, the kaolinite and illite could in several cases be seen to form the shape similar to that of a detrital grain or a mud clast, also microquartz was seen in association. It could in these cases be assumed that the illite, microquartz and kaolinite formed by replacement and re-precipitation of clay minerals in a mudstone rock fragment. This could explain the occurrence of microquartz in these confined areas as a result of the silica released in the smectite to illite reaction as explained in the paper by Thyberg et al. (2010), where the processes occurring in that exact area behaves more like in that of a shale.

The relatively large presence of kaolinite in the sediments and its unaltered appearance gives no direct evidence of illitization of kaolinite. This also favors smectite minerals as a source for the illite.

In deeply buried reservoirs where there has been an ample presence of K-feldspar, and or smectite in the initial sediments deposited, and large flux of meteoric water in the immediate subsurface causing early precipitation of kaolinite, illite can be detrimental to the permeability (Bjørlykke et al., 1995).

The burial depths most likely corresponding to temperatures below ~130 °C and the somewhat restricted source of K-feldspar in most areas means that this is not very relevant in these areas.

Several other observations of mineral alterations can to a certain degree be put into context with the smectite to illite reaction, and by extension the onset of quartz precipitation as the reduction in silica saturation is most likely what causes the smectite-illite reaction to occur (Abercrombie et al., 1994).

Some albite grains were observed in the SEM and most of which were seen in the samples from the lower parts of the formation in well 7120/12-2. The albite did in some places seem to replace K-feldspar grains. One of the causes of the formation of albite replacing K-feldspar grains may be that as dissolution of smecitite, and or kaolinite, and the precipitation of illite consumes potassium, the potassium concentration falls below that of equilibrium with K-feldspar (Bjørlykke et al., 1995).

Of the carbonates observed, although little overall, ankerite was the most prominent with only a minor amount of dolomite, the source for Fe^{2+} in the iron rich carbonate could come from the smectite to illite reaction (Ferry et al., 2015).

7.6 Quartz cement

An estimate of the amount of quartz cement was done from point counting and from the sonic log (P-wave). Figure 5-10 shows the estimated quartz cement over the Stø formation as calculated from the sonic log in the two wells, as well as amount of cement estimated in each sample by point counting. Figure 6-5 shows the amount of cement determined from point counting averaged for each unit.

The overall trend in both the petrographical and petrophysical result are a larger amount of quartz cement in well 7120/2-3S, with the lower section of the formation containing a higher amount of quartz cement than the upper parts. The amount of cement in well 7120/12-2 seems to, although with some fluctuations, be more consistent over the entire formation with somewhat lower values in the lowermost parts of the formation. An exception from the lower amount of quartz cement in the lowermost part is the area coinciding with the lowermost sample from this well. This sample was cleaner than most of the samples from this well and both the point count and sonic estimate of cement shows an increase in cement. The cement volume estimation from P-wave is done making several assumptions, it is based on the correlation between P-wave velocity increase with increasing amounts of quartz cement as

established for the Etive formation by Marcussen et al. (2010), and although this is also a mature shallow marine sandstone, the initial sonic velocity assumed to correlate to 0 % cement may differ due to differences in mechanical compaction related to differences in the initial composition. However, it appears that the estimation of quartz cement from the sonic log fits better with what was observed using cathode luminescence on a selection of samples (fig. 6-16,17,18,19 & 20) with the overall appearance being that of a larger amount of quartz cement in the samples from well 7120/2-3S. Although no quantitative measurements were done of the amount of quartz cement using CL, the overall impression fits more with the results seen from the sonic log estimate. This underestimation of quartz cement during point counting again relates to the low estimate of IGV seen above, where, if the amount of cement has been underestimated with as much as 10% or more and have been counted as detrital quartz grains, the IGV would then show values more as expected.

The reason for underestimating the amount of quartz cement during point counting most likely relates to the level of certainty set in identification of what was authigenic quartz cement, only when either a visible dust rim and/or the characteristic euhedral shape of the overgrowth where recognized was it determined to be quartz cement.

The trend in distribution of quartz cement is however similar in both the results from point counting, well log and cathode luminescence, meaning that the distribution can be compared with the mineralogical and textural composition of sediments as well as the burial history.

Overall the higher content of cement in well 7120/2-3S is in all likelihood the result of the higher temperatures that these sediments have been exposed to, as over time the large difference in precipitation rates for quartz with temperature will mean that the differences will become that much larger over time (fig. 7-5). So even though the depositional setting overall is quite different for the two wells especially between the lower parts of the formation in well 7120/2-3S with the continuous high energy proximal deposits, and the overall more shaly appearance of the formation in well 7120/12-2, it is hard to quantify the influence in initial composition with the differences in quartz cementation between the two wells. Within the formation in each well however the differences will greatly relate to the depositional setting as the sediments here will have been subjected to much more similar burial histories. When looking at the distribution of cement within the formation in well 7120/2-3S it is as mentioned more heavily cemented in the more continuous clean lower parts and somewhat less cemented

in the upper parts. The reason for this could be that some of the clay minerals deposited along with the sands in this area acted against the precipitation of cement by remaining in close contact with the detrital grains acting as grain coats (section 7.7).

When the neutron density porosity is plotted against the gamma ray values it further supports this argument as it is seen that higher porosities in the Stø formation in well 7120/2-3S correlates well with higher gamma ray values (fig. 7-6). When the calculate amount of cement is plotted against neutron porosity the trend is even more evident (fig. 7-8).

When the same parameters are plotted for the Stø formation in well 7120/12-2, there is no such clear correlation (fig. 7- 7&9). Instead a general trend of slightly decreasing porosities with increased gamma ray values can be seen.

At higher gamma ray values there is a large spread in both the estimated porosity and amount of cement. The clay rich intervals of the formation in this well were seen to contain a relatively larger amount of mica, as well as pyrite and dolomite/ankerite. Higher concentration of high density minerals will affect the density log and also sonic log, as these logs were used to calculate both porosity and volume of cement respectively, large variations in these intervals are not unexpected.

The clean intervals of well 7120/2-3S did still contain some mica and other clay minerals and although no core photos were available and stylolite spacing could not be resolved it is apparent that quartz precipitation has been able to proceed relatively unhindered in this section. The uppermost part contained less quartz cement and it is clear that there is some effect of the clay minerals present in the at least restricting cementation to some degree. Well 7120/12-2 poses more of a challenge when trying to compare the amount of quartz cement with the initial composition of the sediments. It is clear that the mineralogical composition in regards to mineralogical and textural features varies significantly over the Stø formation, and that the depositional setting has varied from that of a proximal beach/barrier bar setting to more open marine settings, but still the distribution of quartz cement seems to be surprisingly uniform. The samples from this well were however grouped into two “clusters” situated in the uppermost and lowermost parts of the formation and any estimates of quartz cement in-between only comes from the sonic log, a further cause of uncertainty is the highly varying shaliness of the formation in this well, and the fact that the sonic log/cement volume

correlation is based on a lithology that will be varyingly different from the Stø formation in this well, the uncertainty of this may be large, and hard to quantify.

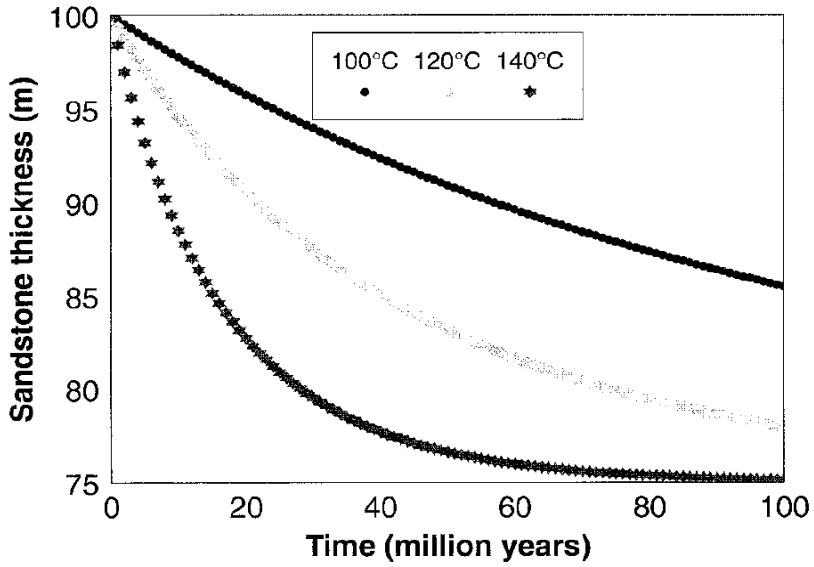

Figure 7-5. The reduction in thickness of an initial 100m thick sandstone body over time as a result of quartz cementation occurring under different temperatures (Walderhaug et al., 2001).

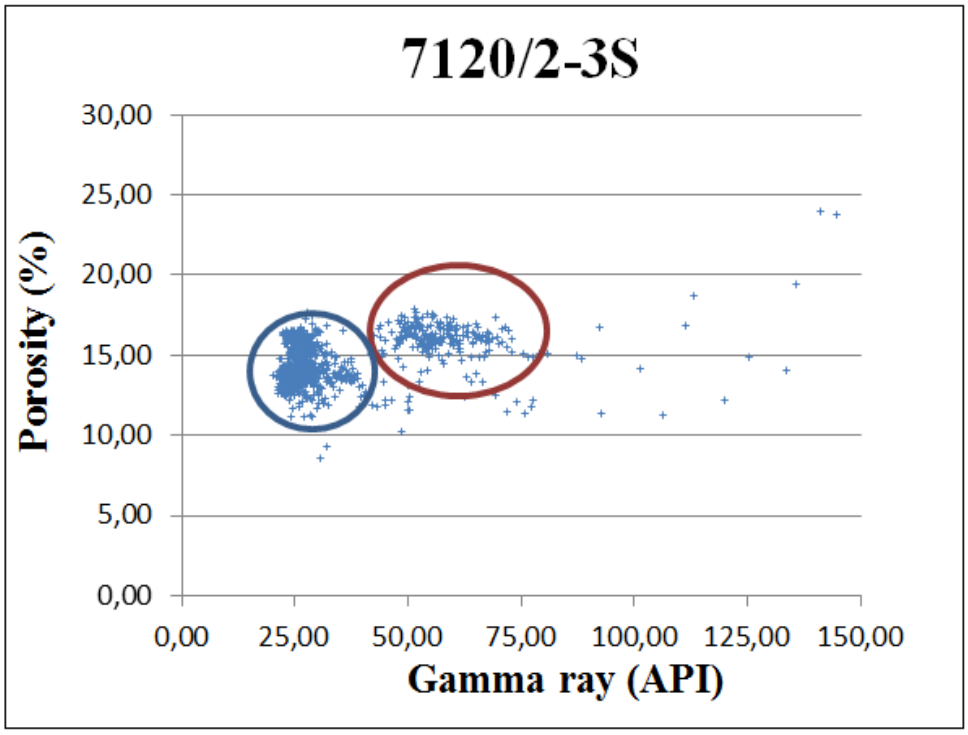

Figure 7-6. Porosity from neutron porosity plotted versus gamma ray. It appears that the higher gamma ray readings, corresponding to the upper parts of the Stø formation, have preserved slightly higher porosities.

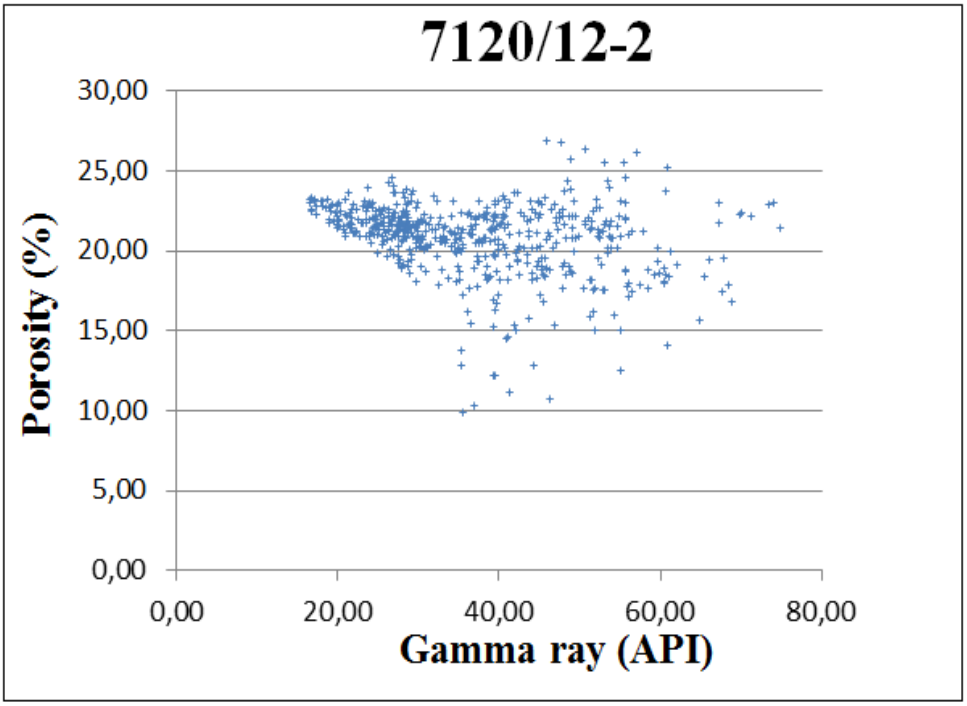

Figure 7-7. Porosity from neutron porosity plotted versus gamma ray. There seems to be no significant division between specific intervals, instead a trend as commonly expected is seen with a decreasing porosity with increasing gamma ray readings. At higher gamma ray readings the porosities shows a much larger spread than for the cleaner intervals.

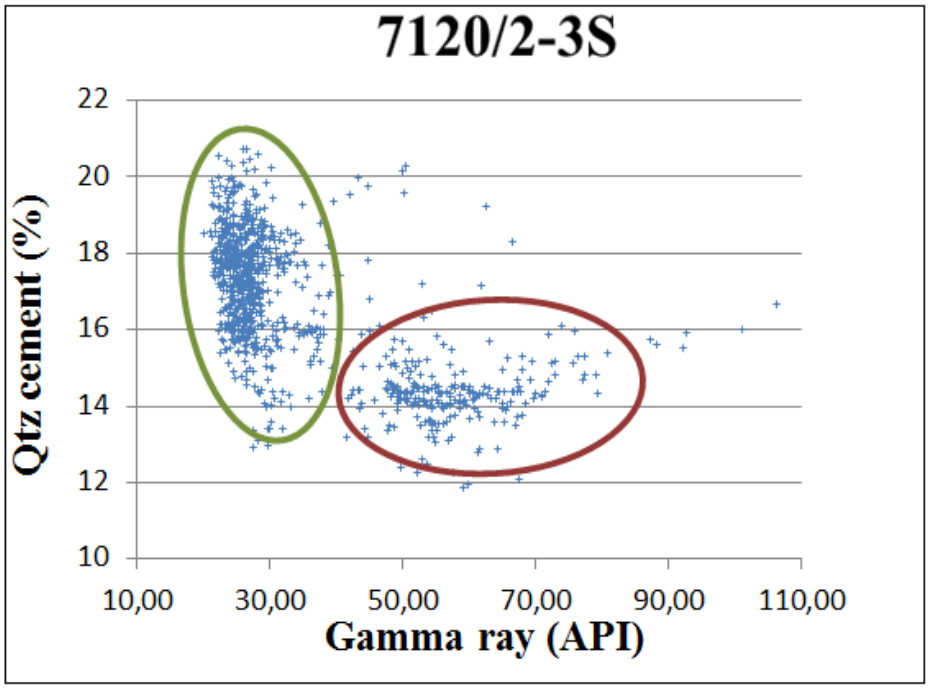

Figure 7-8. Cement calculated from P-wave plotted versus the gamma ray values. As seen in figure 7-3 there seem to be a significant difference in cement for the clean and more shaly interval.

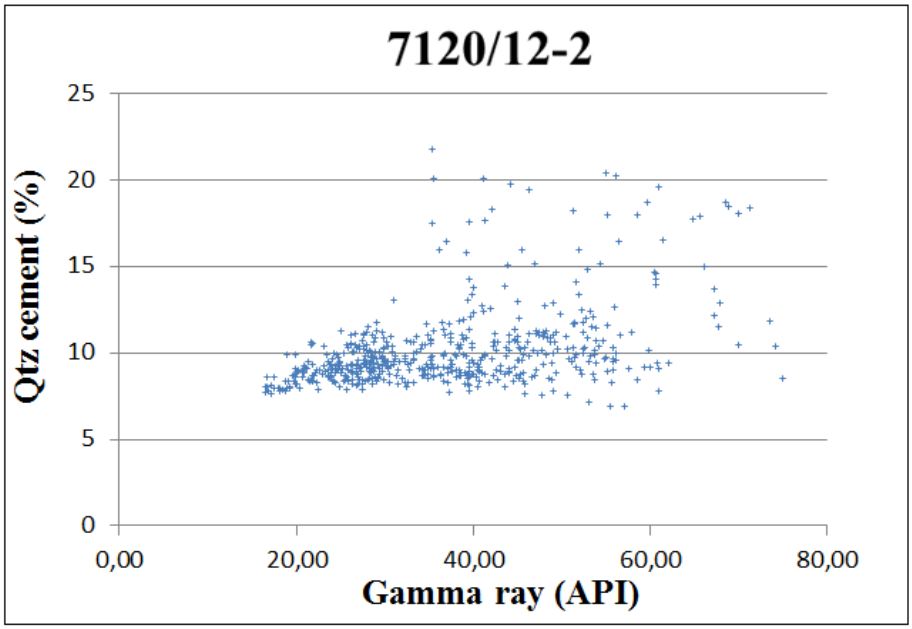

Figure 7-9. Cement calculated from P-wave plotted versus gamma ray values. Shows the same trend as figure 7-4 with larger variations in calculated cement content with higher gamma ray values.

7.7 Grain coats

Except for a very few observations in the samples from the uppermost parts of the formation in well 7120/12-2 (fig. 6-19), no significant grain coats where observed, illite where in some cases appearing to cover grains but where in fact not in any significant contact with the grains, and quartz cement could still be seen to have grown. In the few observations of grain coating appearing to hinder cement that were made, the coating most often appeared as a mix of authigenic illite and detrital clay.

In the less cemented upper parts of the formation in well 7120/2-3S grain coats could, as mentioned above be present. There is a significant decrease in quartz cement corresponding to the more clay rich interval in the upper parts of the Stø formation in well 7120/2-3S observed both in the petrographical and point counting analyses. Wilson (1992) reported inherited clay rims to be common in marine sediments in the shelf-offshore transition zone. Inherited clay rims are coating detrital grains prior to deposition. Bloch et al. (2002) used the term grain rim as these could also form during deposition. Grain rims consisting of detrital clay will act against quartz precipitation and preserve porosity and also permeability when they are thin and oriented subparallel to the detrital quartz grains (Wilson, 1992). Detrital clay grain rims

could quite possibly be the cause of the higher porosities and lower amount of quartz cement seen in the upper parts of the Stø formation, believed to have been deposited in a more distal setting.

7.8 Porosity distribution

As expected from the burial history of the sediments, the neutron-density porosity log shows higher porosity values in the less cemented rocks in well 7120/12-2, with an average porosity of ~21 % versus ~14 % in well 7120/2-3S. (fig. 5- 6&7).

The uppermost parts of the formation in well 7120/2-3S have higher porosities than the lower parts consistent with less quartz cementation. The porosity distribution of the formation in well 7120/2/12 is more skewed than the distribution seen in well 7120/2-3S, however when looking and the neutron density log it is seen to have several “stringers” or sharp intervals of significantly lower porosities, these sharp drops in porosity correlates to the spikes seen in the gamma ray readings, and are probably caused by more shale dominated intervals.

When comparing the porosity determined from point counting, with the porosity determined from neutron-density, they show a good correlation in well 7120/2-3S, and poor correlation in well 7120/12-2. In well 7120/12-2 the porosity determined from point counting are consistently lower than the readings from the neutron- density log, especially samples from the lower parts of the formation show vastly lower porosity values than that estimated from the well logs.

There might be several reasons for this large discrepancy between the two porosity estimations, first and foremost several of the thin section samples from this well especially those of the lower parts consisting of unit 2B contained a large amount of clay minerals, both clay drapes, various occurrences of detrital clay and pore filling kaolinite and some illite something that might yield lower values when porosity is determined from point counting than what is calculated from the well logs. Some samples contained a large amount of clay drapes and showed exceedingly small amount of porosities when point counted e.g. image 5 in figure 6-6 and image 4 in figure 6-22. Furthermore, the Stø formation in well 7120/12-2 have large vertical variations in the amount of matrix and clay minerals.

Although there were 12 samples available the samples from well 7120/12-2 represents only a small interval of the formation and although they showed a large presence of clay matrix, it is clear from the gamma ray log and from the core photos that especially the interval corresponding to unit 2B have large vertical variations and the results may not reflect the entire formation.

7.9 Reservoir quality

The reservoir quality of the various units relates mainly to the burial history of the sediments and the depositional setting, causing a varying amount of clay content. The amount of clay can be destructive when as substantial as that seen in unit 2B, or have a porosity preserving effect as seen in unit 1A. Table 7-2 on the following page summarizes the main lithological features and the interpreted reservoir quality.

Table 7-2. A brief summary of the main features relating to the reservoir quality of the different units.

Unit	Approx. maximum burial depth(m)	Main lithological features	Qtz cement from point counting, sonic log and CL appearance	Neutron -density porosity	Permeability (inferred)	Reservoir quality
1A	2985-3030	Very fine to fine sandstone, some clay	Intermediate 5-15%	~15-18%	Good to intermediate	good
1B	3030-3130	Consistently clean homogenous sandstone	Intermediate to extensive 10-20%	~12-15%	Intermediate	intermediate
2A	2600-2630	Overall homogenous clean sandstone, increasing clay content with depth	Varying amount, not extensive ~5%	20-25 %	good	good
2B	2630-2680	Argillaceous sandstone, frequent shale laminated horizons, increasingly micaceous	Varying amount, not extensive ~5%	20-22 %	Poor to intermediate. poorest vertical	Intermediate
2C	2690m	Clean sandstone, micaceous	Varying amount, not extensive ~5%	~20%	Intermediate to good	good

Chapter 8: Conclusion

- The different units of the Stø formation have similar textural parameters, with grain sizes being fine to very fine, and well to moderately well sorted. The main variation in the initial composition between units is the amount of detrital clay preserved at deposition. The clay content preserved in the sediments being controlled by the energy of the depositional environment. The lateral and temporal variations of clay content in the units within the Stø formation is mostly due to the relative proximity to shoreline at time of deposition.
- The depositional environment of the Stø formation in well 7120/2-3S is overall more proximal than in well 7120/12-2. Ranging from shallow marine beach/barrier bar deposits in unit 1B to lower shoreface/transition zone in the lower parts of unit 1A. The Stø formation in well 7120/12-2 is interpreted as being deposited in an offshore to upper shoreface setting over two cycles. With the more distal deposits consisting of argillaceous sandstone with frequent clay laminated horizons.
- The IGV of the sediments were similar, however the highest correlation was seen with respect to grain size. Finer grain sizes appeared to preserve higher IGV's. however the grain size and sorting did not vary significantly between the different units.
- The Stø formations in both wells have experienced Cenozoic uplift and are presently not located at their maximum burial depth. An uplift of 1250m is calculated for well 7120/2-3S, and 900m for well 7120/12-2. The more extensive burial and higher temperatures being the main reason for the higher amount of quartz cement seen in well 7120/2-3S.
- Higher porosities are preserved in well 7120/12-2 however the significant amount of clay laminated horizons probably poses severe restrictions on the permeability in large parts of the formation. The clean intervals at the upper – and lowermost parts show good reservoir properties.
- Indications of processes acting against precipitation of quartz was found in well 7120/2-3S where lower amounts of quartz cement correlated with higher clay contents, indicating depositional conditions favorable for infiltration and preservation of detrital clay rims.

References

Aagaard, P., Jahren, J., Harstad, A. O., Nilsen, O. & Ramm, M. 2000. Formation of grain-coating chlorite in sandstones. Laboratory synthesized vs. natural occurrences. *Clay Minerals,* 35**,** 261-269.

Abercrombie, H. J., Hutcheon, I. E., Bloch, J. D. & De Caritat, P. 1994. Silica activity and the smectite-illite reaction. *Geology,* 22**,** 539-542.

Asquith, G. B. & Krygowski, D. 2004. *Basic well log analysis,* Tulsa, OK, AAPG.

Baig, I., Faleide, J. I., Jahren, J. & Mondol, N. H. 2016. Cenozoic exhumation on the southwestern Barents Shelf: Estimates and uncertainties constrained from compaction and thermal maturity analyses. *Marine and Petroleum Geology,* 73**,** 105-130.

Bergan, M. & Knarud, R. 1993. Apparent changes in clastic mineralogy of the Triassic-Jurassic succession, Norwegian Barents Sea; possible implications for palaeodrainage and subsidence. *Norwegian Petroleum Society conference on Arctic geology and petroleum potential,* 2**,** 481-493.

Bjørkum, P. A. 1996. How important is pressure in causing dissolution of quartz in sandstones? *Journal of Sedimentary Research,* 66**,** 147-154.

Bjørkum, P. A., Oelkers, E. H., Nadeau, P. H., Walderhaug, O. & Murphy, W. M. 1998. Porosity prediction in quartzose sandstones as a function of time, temperature, depth, stylolite frequency, and hydrocarbon saturation. *AAPG Bulletin,* 82**,** 637-648.

Bjørlykke, K. 1994. Fluid-flow processes and diagenesis in sedimentary basins. *Geological Society Special Publication,* 78**,** 127-140.

Bjørlykke, K. 1999. Principal aspects of compaction and fluid flow in mudstones. *Geological Society Special Publication,* 158**,** 73-78.

Bjørlykke, K. 2014. Relationships between depositional environments, burial history and rock properties. Some principal aspects of diagenetic process in sedimentary basins. *Sedimentary Geology,* 301**,** 1.

Bjørlykke, K., Aagaard, P., Simmons, S. P. & Egeberg, P. K. 1995. Geochemical constraints from formation water analyses from the North Sea and the Gulf Coast Basins on quartz, feldspar and illite precipitation in reservoir rocks. *Geological Society Special Publication,* 86**,** 33-50.

Bjørlykke, K. & Egeberg, P. K. 1993. Quartz cementation in sedimentary basins. *AAPG Bulletin,* 77.

Bjørlykke, K. & Jahren, J. 2012. Open or closed geochemical systems during diagenesis in sedimentary basins: Constraints on mass transfer during diagenesis and the prediction of porosity in sandstone and carbonate reservoirs. *AAPG Bulletin,* 96**,** 2193-2214.

Bjørlykke, K. & Jahren, J. 2015. Sandstones and sandstone reservoirs. *In:* BJØRLYKKE, K. (ed.) *Petroleum Geoscience.* Springer.

Bjørlykke, K., Ramm, M. & Saigal, G. 1989. Sandstone diagenesis and porosity modification during basin evolution. *Geologische Rundschau,* 78**,** 243-268.

Bloch, S., Lander, R. H. & Bonnell, L. 2002. Anomalously high porosity and permeability in deeply buried sandstone reservoirs: Origin and predictability. *AAPG Bull.*

Cavanagh, A. J., Di Primio, R., Scheck-Wenderoth, M. & Horsfield, B. 2006. Severity and timing of Cenozoic exhumation in the southwestern Barents Sea. *Journal of the Geological Society,* 163**,** 761-774.

Chuhan, F. A., Bjørlykke, K. & Lowrey, C. 2000. The role of provenance in illitization of deeply buried reservoir sandstones from Haltenbanken and north Viking Graben, offshore Norway. *Marine and Petroleum Geology,* 17**,** 673-689.

Chuhan, F. A., Kjeldstad, A., Bjørlykke, K. & Høeg, K. 2002. Porosity loss in sand by grain crushing—experimental evidence and relevance to reservoir quality. *Marine and Petroleum Geology,* 19**,** 39-53.

Dimakis, P., Braathen, B. I., Faleide, J. I., Elverhøi, A. & Gudlaugsson, S. T. 1998. Cenozoic erosion and the preglacial uplift of the Svalbard–Barents Sea region. *Tectonophysics,* 300**,** 311-327.

Dott, R. H. 1964. Wacke, Graywacke and Matrix--What Approach to Immature Sandstone Classification? *Journal of Sedimentary Research,* 34.

Ehrenberg, S. N. 1993. Preservation of anomalously high porosity in deeply buried sandstones by grain-coating chlorite: Examples from the Norwegian Continental Shelf. *AAPG Bulletin,* 77.

Ellis, D. V. & Singer, J. M. 2008. *Well Logging for Earth Scientists,* Dordrecht, The Netherlands, Springer Science.

Faleide, J. I., Bjørlykke, K. & Gabrielsen, R. H. 2015. Geology of the norwegian continental shelf. *In:* BJØRLYKKE, K. (ed.) *Petroleum Geoscience.*

Faleide, J. I., Gudlaugsson, S. T. & Jacquart, G. 1984. Evolution of the western Barents Sea. *Marine and Petroleum Geology,* 1**,** 123-150.

Fawad, M., Mondol, N. H., Jahren, J. & Bjørlykke, K. 2011. Mechanical compaction and ultrasonic velocity of sands with different texture and mineralogical composition. *Geophysical Prospecting,* 59**,** 697-720.

Ferry, J. M., Stubbs, J. E., Xu, H., Guan, Y. & Eiler, J. M. 2015. Ankerite grains with dolomite cores: a diffusion chronometer for low- to medium-grade regionally metamorphosed clastic sediments. *American Mineralogist,* 100**,** 2443-2457.

Folk, R. L. 1974. *Petrology of Sedimentary Rocks,* Austin, Texas, Hemphill Publishing Company.

Folk, R. L. & Ward, W. C. 1957. brazos river bar: a study in the significance of grain size parameters. *Journal of Sedimentary Research,* 27.

Gabrielsen, R. H., Færseth, R. B., Jensen, L. N., Kalheim, J. E., Riis, F. & Norge, O. 1990. *Structural elements of the Norwegian continental shelf : 6 : The Barents sea region,* Stavanger, Oljedirektoratet.

Glørstad-Clark, E., Faleide, J. I., Lundschien, B. A. & Nystuen, J. P. 2010. Triassic seismic sequence stratigraphy and paleogeography of the western Barents Sea area. *Marine and Petroleum Geology,* 27**,** 1448-1475.

Gudlaugsson, S. T., Faleide, J. I., Johansen, S. E. & Breivik, A. J. 1998. Late Palaeozoic structural development of the south-western Barents Sea. *Marine and Petroleum Geology,* 15**,** 73-102.

Halland, E., Bjørnestad, A., Magnus, C., Riis, F., Meling, I. M., Gjeldvik, I. T., Tappel, I. M., Mujezinovic, J., Bjørheim, M., Rød, R. S. & Pham, V. T. H. 2014. Compiled CO2 atlas for the Norwegian Continental Shelf *Norwegian Petroleum Directorate*.

Halland, E. K., Mujezinovic, J., Riis, F. & Norge, O. 2013. *CO_2 storage atlas : Barents Sea,* Stavanger, Norwegian Petroleum Directorate.

Hendry, J. P. & Trewin, N. H. 1995. Authigenic quartz microfabrics in Cretaceous turbidites: Evidence for silica transformation processes in sandstones. *Journal of Sedimentary Research, Section A: Sedimentary Petrology and Processes,* 65**,** 380-392.

Henriksen, E., Ryseth, A. E., Larssen, G. B., Heide, T., Ronning, K., Sollid, K., Stoupakova, A. V., Spencer, A. M., Embry, A. F., Gautier, D. L., Stoupakova, A. V. & Sorensen, K. 2011. Tectonostratigraphy of the greater Barents Sea; implications for petroleum systems. London: London, United Kingdom: Geological Society of London.

Larionov, W. W. 1969. Radiometrija Skwaschin. *Nedra Verlag, Moscow*.

Larssen, G., Elvebakk, G., Henriksen, L. B., Kristensen, S., Nilsson, I., Samuelsberg, T., Svånå, T., Stemmerik, L. & Worsley, D. 2002. Upper Palaeozoic lithostratigraphy of the Southern Norwegian Barents Sea. *Norwegian Petroleum Directorate Bulletin,* 9**,** 76.

Marcussen, Ø., Maast, T. E., Mondol, N. H., Jahren, J. & Bjørlykke, K. 2010. Changes in physical properties of a reservoir sandstone as a function of burial depth – The Etive Formation, northern North Sea. *Marine and Petroleum Geology,* 27**,** 1725-1735.

Mondol, N. H. 2015. *Well logging: Principles, applications and uncertainties*, Springer.

Oelkers, E. H., Bjørkum, P. A., Walderhaug, O., Nadeau, P. H. & Murphy, W. M. 2000. Making diagenesis obey thermodynamics and kinetics: the case of quartz cementation in sandstones from offshore mid-Norway. *Applied Geochemistry,* 15**,** 295-309.

Ohm, S. E., Karlsen, D. A. & Austin, T. J. F. 2008. Geochemically driven exploration models in uplifted areas; examples from the Norwegian Barents Sea. *AAPG Bulletin,* 92**,** 1191-1223.

Olaussen, S., Dalland, A., Gloppen, T. G. & Johannessen, E. 1984. Depositional environment and diagenesis of Jurassic reservoir sandstones in the eastern part of Troms I area. *In:* SPENCER,

A. M. (ed.) *Petroleum Geology of the North European Margin: Proceedings of the North European Margin Symposium (NEMS '83), organized by the Norwegian Petroleum Society and held at the Norwegian Institute of Technology (NTH) in Trondheim 9–11 May, 1983.* Dordrecht: Springer Netherlands.

Paxton, S. T., Szabo, J. O. & Ajdukiewicz, J. M. 2002. Construction of an intergranular volume compaction curve for evaluating and predicting compaction and porosity loss in rigid-grain sandstone reservoirs. *AAPG Bulletin,* 86**,** 2047-2065.

Peters, S. E. & Loss, D. P. 2012. Storm and fair-weather wave base: A relevant distinction? *Geology,* 40**,** 511-514.

Powers, M. C. 1953. a new roundness scale for sedimentary particles. *Journal of Sedimentary Petrology,* 23**,** 3.

Ramm, M., Forsberg, A. W. & Jahren, J. S. 1997. Porosity-depth trends in deeply buried upper jurassic reservoirs in the norwegian central graben: an example of porosity preservation beneath the normal economic basement by grain-coating microquartz. *In:* KUPECZ, J. A., GLUYAS, J. & BLOCH, S. (eds.) *Reservoir quality prediction in sandstones and carbonates.* AAPG Memoir, v. 69, p. 177-199.

Rodrigues Duran, E., Di Primio, R., Anka, Z., Stoddart, D. & Horsfield, B. 2013. Petroleum system analysis of the Hammerfest Basin (southwestern Barents Sea): Comparison of basin modelling and geochemical data. *Organic Geochemistry,* 63**,** 105-121.

Saigal, G., Morad, S., Bjørlykke, K., Egeberg, P. & Aagaard, P. 1988. Diagenetic albitization of detrital K-feldspar in Jurassic, Lower Cretaceous, and Tertiary clastic reservoir rocks from offshore Norway, 1. Textures and origin. *Journal of Sedimentary Petrology,* 58**,** 1003-1013.

Saigal, G. C., Bjørlykke, K. & Marshall, J. D. 1987. Carbonate cements in clastic reservoir rocks from offshore Norway; relationships between isotopic composition, textural development and burial depth. *Geological Society Special Publications,* 36**,** 313-324.

Santin, C. E., Abel, M., Goldberg, K. & De Ros, L. F. 2009. Automatic Detection of the Degree of Compaction in Reservoir Rocks Based on Visual Knowledge. *AAPG Annual Convention and Exhibition.* Denver, Colorado, USA.

Smelror, M., Petrov, O. V., Larsen, G. B. & Werner, S. C. 2009. *Atlas : Geological History of the Barents Sea,* Trondheim, Geological Survey of Norway.

Storvoll, V., Bjørlykke, K., Karlsen, D. & Saigal, G. 2002. Porosity preservation in reservoir sandstones due to grain-coating illite: a study of the Jurassic Garn Formation from the Kristin and Lavrans fields, offshore Mid-Norway. *Marine and Petroleum Geology,* 19**,** 767-781.

Storvoll, V., Bjørlykke, K. & Mondol, N. 2005. Velocity-depth trends in mesozoic and cenozoic sediments from the Norwegian shelf. *AAPG Bull.*

Thyberg, B., Jahren, J., Winje, T., Bjørlykke, K., Faleide, J. I. & Marcussen, Ø. 2010. Quartz cementation in Late Cretaceous mudstones, northern North Sea: Changes in rock properties due to dissolution of smectite and precipitation of micro-quartz crystals. *Marine and Petroleum Geology,* 27**,** 1752-1764.

Walderhaug, O. 1990. A fluid inclusion study of quartz-cemented sandstones from offshore mid-Norway--possible evidence for continued quartz cementation during oil emplacement. *Journal of Sedimentary Petrology,* 60**,** 203-210.

Walderhaug, O. 1994. Precipitation rates for quartz cement in sandstones determined by fluid-inclusion microthermometry and temperature-history modeling. *Journal of Sedimentary Research, Section A: Sedimentary Petrology and Processes,* 64**,** 324-333.

Walderhaug, O. 1996. Kinetic modeling of quartz cementation and porosity loss in deeply buried sandstone reservoirs. *AAPG Bulletin,* 80**,** 731-745.

Walderhaug, O., Bjorkum, P. A., Nadeau, P. H. & Langnes, O. 2001. Quantitative modelling of basin subsidence caused by temperature-driven silica dissolution and reprecipitation. *Petroleum Geoscience,* 7**,** 107-113.

Walderhaug, O. & Bjørkum, P. 2003. The effect of stylolite spacing on quartz cementation in the lower Jurassic Stoe formation, southern Barents Sea. *Journal of Sedimentary Research,* 73.

Welton, J. E. 1984. *SEM petrology atlas,* Tulsa, Oklahoma, American Association of Petroleum Geologists.

Wilson, M. D. 1992. Inherited grain-rimming clays in sandstones from eolian and shelf enviroments: their origin and control on reservoir properties. *In:* HOUSEKNECHT, D. W. & PITTMAN, E. D. (eds.) *Origin, diagenesis and petrophysics of clay minerals in sandstones, p. 209-225.*

Wilson, M. D. & Pittman, E. D. 1977. Authigenic clays in sandstones; recognition and influence on reservoir properties and paleoenvironmental analysis. *Journal of Sedimentary Petrology,* 47**,** 3-31.

Worsley, D. 2008. The post-Caledonian development of Svalbard and the western Barents Sea. *Polar Research,* 27**,** 298-317.

Worsley, D., Ofstad, K. & Kristensen, S. E. 1988. The Mesozoic and Cenozoic succesion of Tromsøflaket. *In:* DALLAND, A., WORSLEY, D. & OFSTAD, K. (eds.) *A Lithostrategraphic scheme for the Mesozoic and Cenozoic succession offshore mid- and northern Norway.* Norwegian Petroleum Directorate Bulletin 4, 42-65.

Appendix

Appendix A: Well description

Table A1. Well data acquired from NPD factpages. (factpages.npd.no)

Well	Coordinates	UTM coordinates	Location
7120/2-3S	71° 47’ 20.97’’ N 20° 21’ 44.23’’ E	7965749.13 NS 477755.39 EW	Hammerfest basin
7120/12-2	71° 7’ 30.3’’ N 20° 48’ 19’’ E	7891571.43 NS 492968.97 EW	Hammerfest basin
Well	**Type**	**Discovery wellbore**	**HC content**
7120/2-3S	Exploration	Yes	Gas
7120/12-2	Exploration	Yes	Gas/Condensate

Table A2. Zones containing hydrocarbons. Well 7120/2-3S contained gas, well 7120/12-2 contained gas/condensate. (factages.npd.no)

Levels with HC			
7120/2-3S		**7120/12-2**	
Formation	*HC interval (MBSF)*	*Formation*	*HC interval (MBSF)*
Kolmule Fm.	1240.5 - 1303.9	Stø Fm.	1699 – 1792.5
Stø Fm.	1735.5 - 1760.4	Snadd Fm.	2358 - 2385
Knurr Fm.	Situational ~5m thick		

Table A3 - Geothermal gradient for each well, calculated from bottom hole temperature, and assuming a temperature of 4°C at the sea floor. Acquired from NPD factpages (factpages.npd.no)

Well	KB elevation (m)	Water Depth (m)	Total depth (MD)	Total vertical depth	Bottom hole temperature (°C)	Geothermal gradient (°C/Km)
7120/12-2	25	164	4680	4667	115 (?)	24,8 (?)
7120/2-3S	23,5	312	2625	2620	93	39

Appendix B: Petrophysical dataset

Table B1. Well logs and intervals where these were available for the two wells.

Logs and depth range available for each well (meters below KB)		
Log	*Well 7120/2-3S*	*Well 7120/12-2*
Caliper	1514 - 2614	302 - 4680
Bit size	390 - 2625	X
Bulk density	1520 - 2614	302 - 4680
Density correction	1514 - 2614	302 - 4680
Gamma ray	390 - 2624	189 - 4682
Spectral gamma (Th, P and U)	1506 - 2604	X
Neutron porosity	1520 - 2617	470 - 4680
P-wave	643 - 2616	189 - 4682
S-wave	978 - 2610	X
Resistivity deep	398 - 2624	189 - 4682
Resistivity medium	398 - 2624	X
Resistivity shallow	1543 - 2615	1849 - 3908
Resistivity mud	X	189 - 4682
Photoelectric	1520 - 2614	X
Rate of penetration	390 - 2625	X

Appendix C: Petrographical dataset

Table C1. Overview of thin section samples available for petrographical analyses, and designated units.

Well	Depth of sample (MDRKB)	Depth of sample (MBSF)	Unit
7120/2-3S	2078.70	1743.20	1A
“	2099.72	1764.22	“
“	2109.33	1773.83	“
“	2132.62	1797.12	1B
“	2140.60	1805.10	“
“	2146.80	1811.30	“
“	2153.36	1817.86	“
“	2159.75	1824.25	“
7120/12-2	1894.45	1705.45	2A
“	1895.70	1706.70	“
“	1897.40	1708.40	“
“	1900.15	1711.15	“
“	1960.70	1771.70	2B
“	1962.80	1773.80	“
“	1963.90	1774.90	“
“	1964.72	1775.72	“
“	1966.80	1777.80	“
“	1973.31	1784.31	“
“	1975.78	1786.78	“
“	1981.03	1792.03	2C

Table C2 – Thin section samples selected for SEM analysis.

Well	Depth of sample (MBSF)	Unit
7120/2-3S	1743.20	1A
”	1824.25	1B
7120/12-2	1711.15	2A
”	1773.70	2B
”	1784.31	2B

Appendix D: Petrographical data

Table D1. The results of point counting, 400 sample points in each sample.

			Matrix																		
			Allogenic				Authigenic														
Well 7120/2-3S	Unit 1A	Depth:	Dispersed	Flocule?	Mudstone rock frag.?	intercalated	Pore filling	Replacement	pore lining	Kaolonite	Total matrix	Matrix (%)	Quartz	Qtz cem.	Feldspar	lith. Frag.	Mica	Carbonates	Unknown	Porecount	IGV (%)
		1743,20					1			0	1	0,25	295	6	1	6	0	0	2	89	24
		1764,22	23				18	10		0	51	12,75	270	6	1	10	4	0	2	56	28,25
		1773,83	12				11	12		0	35	8,75	299	6	0	3	0	8	2	47	22
	Unit 1B	1797,12	6				8			0	14	3,5	282	25	2	7	1	0	1	68	26,75
		1805,10	3				7	3		2	13	3,25	313	19	0	0	0	0	0	53	21,25
		1811,30	6				2	6		2	14	3,5	301	15	2	0	0	0	0	66	23,75
		1817,86	7				2	5		0	14	3,5	317	15	4	1	0	0	0	49	19,5
		1824,25	15				9	3		1	27	6,75	309	22	4	0	1	0	0	36	21,25
Well 7120/12-2	Unit 2A	1705,45	9		1		6	11		1	27	6,75	310	10	2	2	3	3	0	42	19,75
		1706,70	17	6			7	7		1	37	9,25	294	8	3	2	3	8	0	44	22,25
		1708,40	6	2	1	4	16	8	3	1	40	10	301	16	6	1	6	6	0	23	19,75
		1711,15	3		2		6	14		0	25	6,25	303	10	6	0	5	9	0	42	19,25
	Unit 2B	1771,70	42	6	5	3	16	12	8	6	92	23	246	3	8	2	15	6	0	22	29,25
		1773,80	11	2			6	18	6	7	43	10,75	292	10	8	4	4	4	2	26	19,75
		1774,90	20	6	3		16	25		5	70	17,5	269	5	11	3	9	4	0	24	24,75
		1775,72	24	15		37	17	20	10	0	123	30,75	229	1	7	1	13	10	5	11	33,75
		1777,80	21				11	33	2	2	67	16,75	281	6	6	2	8	5	0	23	24
		1784,31	35			62	13	13	5	1	128	32	222	0	4	0	20	13	0	12	35
		1786,78	19	1		18	14	24		1	76	19	261	8	5	0	17	15	0	17	25,25
	Unit 2C	1792,03	14	1		2	8	6		3	31	7,75	301	5	2	0	8	5	0	45	20,25

Table D2. Textural analysis of 100 grains in each sample.

		Depth (MBSF)	Sphericity		Grain Contacts							Roundness			
			High	Low	Floating gra.	point.	long cont.	concave/convex	sutured	Very angu	angular	sub angul.	sub round.	rounded	well round.
Well 7120/2-3	Unit 1A	1743,2	52	48	7	20	34	26	13	3	27	26	26	17	1
		1764,22	55	45	4	20	38	25	13	18	30	25	17	10	0
		1773,83	54	46	7	22	36	20	15	12	23	23	27	12	3
	Unit 1B	1797,15	53	47	4	17	36	24	19	18	38	21	14	9	0
		1805,1	62	42	5	22	35	18	20	2	21	26	24	30	0
		1811,3	56	44	5	20	33	21	21	5	22	25	26	21	1
		1817,86	58	42	5	20	35	23	17	5	19	26	30	20	2
		1824,25	49	51	7	18	39	20	16	1	24	26	30	19	0
Well 7120/12-2	Unit 2A	1705,45	49	51	9	27	26	28	10	4	29	33	29	5	0
		1706,7	53	47	15	28	26	20	11	7	29	30	26	8	0
		1708,4	37	63	7	24	30	25	14	10	31	29	24	6	0
		1711,15	49	51	7	26	33	26	8	3	25	32	29	11	0
	Unit 2B	1771,7	53	47	6	28	31	24	11	10	37	37	14	1	0
		1773,8	48	52	4	28	33	22	13	7	38	34	17	4	0
		1774,9	53	47	4	26	30	26	14	3	27	45	20	5	0
		1775,72	53	47	10	27	26	21	16	10	34	38	14	4	0
		1777,8	59	41	8	28	27	25	12	13	23	38	20	6	0
		1784,31	55	45	12	24	26	24	14	11	32	37	15	5	0
		1786,78	52	48	6	28	32	23	11	4	18	41	34	3	0
	Unit 2C	1792,03	44	56	7	30	25	22	16	4	26	43	27	0	0

Table D3. Frequency of grain sizes for each sample.

	Frequency of grain sizes (φ)				
Depth (MBSF)	1	2	3	4	5
1743,2	0	0	57	44	1
1764,22	0	0	2	76	24
1773,83	0	0	18	78	11
1797,12	0	8	79	11	1
1805,1	0	12	74	12	0
1811,3	0	0	82	32	2
1817,86	0	15	65	19	0
1824,25	0	5	68	32	0
1705,45	0	0	8	87	11
1706,7	0	0	14	85	9
1708,4	0	0	12	85	10
1711,15	0	0	27	90	8
1771,7	0	0	35	63	11
1773,8	0	0	32	71	5
1774,9	0	0	35	73	5
1775,72	0	1	11	62	25
1777,8	0	0	4	90	30
1784,31	0	0	17	50	27
1786,78	0	0	2	55	43
1792,03	0	6	73	28	2